CHARACTERIZATION OF THE ACCURACY IN A REVERSE ENGINEERING PROCESS EMPLOYING WHITE LIGHT SCANNED DATA TO DEVELOP CONSTRAINT-BASED THREE DIMENSIONAL COMPUTER MODELS

By

Christopher W. Rhoades

A Thesis
Submitted to the
Faculty of the Graduate School
of
Western Carolina University
in Partial Fulfillment of the
Requirements for the Degree
of
Master of Science in Technology

Committee:

_____ Director

_____

_____

_____ Dean of the Graduate School

Date: _____

Spring 2011
Western Carolina
University
Cullowhee, North Carolina

CHARACTERIZATION OF THE ACCURACY IN A REVERSE ENGINEERING PROCESS EMPLOYING WHITE LIGHT SCANNED DATA TO DEVELOP CONSTRAINT-BASED THREE DIMENSIONAL COMPUTER MODELS

A thesis presented to the faculty of the Graduate School of Western Carolina University in partial fulfillment of the requirements for the degree of Master of Science in Technology

By

Christopher W. Rhoades

Director: Dr. Chip Ferguson
Associate Professor
Department of Engineering Technology

Committee Members:
Dr Wesley Stone, Engineering Technology
Dr. Aaron Ball, Engineering Technology

March 2011

Acknowledgements

I would like to thank my committee members, Dr. Chip Ferguson, Dr. Aaron Ball, and Dr. Wes Stone for their guidance and assistance during the time of my research. I would also like to t show appreciation to my fellow graduate students Jason Proffitt, Josh Ellis, Tyler Bennett, Andrew J. Punch, and Matthew Proffitt for their support and encouragement throughout my graduate studies. I would also like to express thanks to my sister Andrea Still for her help and suggestions while writing my thesis, and the rest of my family for their help and support during my research.

TABLE OF CONTENTS

LIST OF FIGURES

LIST OF TABLES

ABSTRACT

The statistical accuracy of constraint-based three-dimensional (3D) models created using reverse engineering software to post process scan data collected by an Advanced Topometric Sensor (ATOS) system is currently unpublished information useful to the end-user. Throughout the process of scanning an object and converting the scanned data into a constraint-based 3D model, error can be introduced into the final model. The error introduced into the constraint-based 3D model is difficult to calculate due to a large number of variables and factors. The current study sought to characterize the accuracy of this process based on different measurement volumes and object sizes.

Optical 3D metrology techniques have become an accepted method in the field of reverse engineering. The popularity of optical 3D metrology is due in large part to the non-contact approach, which can quickly produce a dense point cloud. Using post-processing software, these point clouds can be converted into a constraint-based 3D model and used in much the same manners as 3D models created using CAD software.

To simulate a variety of measurement conditions, four measurement volumes and three object sizes were selected generating a total of 36-point clouds. The 36-point clouds were converted into constraint-based 3D models. Four measurements were collected from each 3D model. To analyze the data collected, hypothesis testing was conducted to compare the data and inferential statistics were applied. The statistical tests include one-sample t-tests, two-sample t-tests, a General Linear Model (GLM), and multiple 1-way ANOVA. The statistical test found that a difference existed between the measured values and the actual values for both the object size and measurement volume.

CHAPTER 1: INTRODUCTION

The purpose of the current thesis was to characterize the accuracy of a reverse engineering process to develop constraint-based three-dimensional (3D) models. These 3D models were created using scan data collected by an Advanced Topometric Sensor (ATOS) system and Geomagic Studio reverse engineering software. Throughout the process of scanning an object and converting the scanned data into a constraint-based 3D model, error was introduced into the final 3D model. Error within the reverse engineering process is difficult to calculate due to a large number of variables. The current study seeks to characterize the accuracy of the reverse engineering process contingent on varying measurement volumes and object sizes. With the growing popularity in commercial scanners used for applications such as reverse engineering and industrial inspection, the demand for a greater understanding of the accuracy and precision of reverse engineered 3D models is increasing.

Purpose and Objective

Optical 3D metrology using structured light scanning techniques has become an accepted method in the field of reverse engineering, due in large part to the non-contact approach, which can quickly produce a dense point cloud (Gesellschaft für Optische Messtechnik [GOM mbH], 2006). Optical 3D measurement devices, such as the ATOS system, generate 3D computer models that contain dimensional measurement information of real world objects. According to V. Raja (2008), the ATOS system and other similar systems convert the geometry of a physical object into a digital 3D point cloud for use in computer-aided design (CAD) and computer-aided manufacturing (CAM) software

packages. Using post post-processing software, the point cloud can be transformed into a constraint-based parametric 3D CAD model with features that can be quickly edited.

Industries spanning multiple disciplines use non-contact 3D scanning to generate 3D computer models of objects that do not have dimensional data. The medical industry uses structured light scanning to create prostatic limbs that are custom fit for amputees (S. Summit 2011). Marc Levoy (2000) used non-contact reverse engineering in the field of archeology; Levoy used a 3D scanner to in order to generate 3D models of statues carved by Michelangelo. Within the automotive industry, 3D scanners have been used to transform a hand sculpted clay model into a working CAD model (G. S. Vasilash, 2009).

Problem Statement

Throughout the reverse engineering process, error is introduced into the final 3D model. The error from the reverse engineering process can be difficult to calculate due to a large number of variables. According to Sansoni (1997), the measurement resolution of scanners similar to the ATOS system depends on the configurations of distance and angle between the camera(s) and the projector, and the distance of the projector and camera(s) from the surface being measured. F. Chen (2000) observed that when point clouds between multiple scans were combined into a global point cloud, error was introduced into the 3D solid models. Chen also noticed that the lens distortion and aberrations were sources of error. Carsten Reich (1996) found that errors were introduced by the geometries of the measured objects. Reich (2000) also noted errors were introduced from the calibration process. Because of these inaccuracies, industries found it difficult to calculate the amount of error introduced into constraint-based 3D models. The current study seeks to characterize the accuracy of a reverse engineering process using the ATOS

system and Geomagic Studio post-processing software. This characterization will give industries a reference to use when reverse engineering objects with the ATOS system.

Background

V. Raja (2008) defined reverse engineering as the basic concept of producing a part from an original or physical model without the use of an engineering drawing. Raja found that in recent years, the technology of reverse engineering has grown exponentially. With the introduction of 3D CAD software, it is now possible to capture the geometry of an object and display it in 3D. Reverse engineering technologies have been divided into two major sections: non-contact and contact. One of the most popular and oldest contact systems is the coordinate measuring machine (CMM) (V. Raja & K. Fernandes, 2008). According to G. Sansoni, the CMM uses a stylus and probe that contacts the object's surface. Once contact has been made, the location of the probe is recorded by a computer; the X, Y, and Z coordinates for multiple points are recorded to form the dimensions of the object. Sansoni argued that traditional inspection methods, such as the CMM, are slow and inadequate when generating models of objects with complex geometry, such as a turbine blade with its complex curved surface. Sansoni additionally argued that with the growing popularity of non-contact reverse engineering systems, measurement of complex surfaces is made easier. The technology of non-contact reverse engineering systems, such as the ATOS, are now a leading method for creating 3D CAD models based on a physical object with complex geometry.

The ATOS system.

The ATOS system was created by GOM in 1995. Today more than 1,500 companies use the system in the fields of product development, quality assurance,

material and component testing, and reverse engineering (GOM mbH, 2006). The ATOS system uses the structured light scanning technique in conjunction with photogrammetry to capture the geometry of an object (Reich 2000). Structured light scanning uses a fringe of gray-coded light with a phase-shifting pattern that is projected onto an object. Two charge-coupled device (CCD) cameras capture the structured light pattern that is projected onto the object (GOM mbH, 2006). GOM uses a computer to evaluate the triangulation and reconstructs the 3D coordinates from the images captured by the CCD cameras of the fringe projection. To combine multiple scans into one global point cloud, photogrammetry is used to detect target points secured to the surface of the object being measured.

The cameras and projector lenses could be changed to vary the focal length and measurement volume for the ATOS system. Using a lens with a higher focal length will decrease the measurement volume. Although the measurement volume changes with the different lenses, the image resolution will remain static. Because the measurement volume changes and image resolution remains unchanged, scans using the smaller volumes result in a denser point cloud and higher accuracies. For the current experiment, four measurement volumes will be analyzed ranging from 90mm x 80mm x 60mm (90mm measurement volume), 120mm x 108mm x 95mm (120mm measurement volume), 250mm x 200mm x 200mm (250mm measurement volume), and 500mm x 440mm x 440mm (500mm measurement volume) (GOM mbH, 2006).

Methodology

Through a series of processes and tests described in detail within Chapter III, the current thesis seeks to characterize the accuracy of a reverse engineering process

employing the ATOS system and Geomagic Studio's reverse engineering software to create a parametric constraint-based 3D model. The methodology and acquisition of data was divided into three stages: the measurement of National Institute of Standards and Technology (NIST) certified gage blocks with the ATOS system, the conversion of the scanned data into a constraint-based 3D model, and the analysis of the data collected while measuring the 3D model. The current study hypothesized that while taking multiple measurements of the same gage block, each measurement will statistically deviate from the nominal size of the gage block specified by NIST. The current study's aim was to characterize the accuracy for the reverse engineering processes of scanning a gage block using the ATOS system and converting the scanned data into a constraint-based 3D model. In the current study, both object size and measurement volume will be evaluated to determine the effect these parameters have on the accuracy of the reverse engineering process.

Overview of Measurement Procedure.

A series of gage blocks conforming to the ASME B89.1.9-2002 standard were scanned to cover four different measurement volumes supported by the ATOS system. The scanning of standard gage blocks produced a three dimensional array of points (point cloud) that closely matched the geometry of the gage blocks. The point clouds were converted into a surface model using Geomagic Studio© software. Geomagic Studio© was designed to transform 3D scan data and polygon meshes into accurate 3D digital models for reverse engineering, product design, and rapid prototyping by finding the best fit for each point in the cloud (Geomagic, Inc. 2009). The creation of surface models took the variance between points on a surface and converted them to a single distance to form a

smooth surface using best-fit analysis (Geomagic, Inc. 2009). The process of converting the point cloud's surfaces into a surface model was repeated for all six surfaces of a gage block's point cloud. The surface model was imported into the parametric three-dimensional CAD software, Pro/Engineer© (Pro/E). Within Pro/E, the program's measurement tool was used to virtually measure the length of the computer model. The constraint-based 3D models' lengths were measured to the millionth of an inch to establish the accuracy of the gage blocks.

Analysis of measurements.

The data collected from the ATOS system was compared to the known values from the NIST certified actual gage block size using a analysis of variance (ANOVA), one sample t-test, two sample t-test, and a general linear model. These tests compared the means of the data collected to determine if there were any statistically significant differences within the data in addition to looking at the effects of the gage block's size and measurement volume. Along with the test data, the measurements taken from the 3D models will be presented in Chapter IV and an analysis of the data will be presented in Chapter V.

Knowledge gained from the current study will be disseminated through reference tables that can be utilized when users desire a standardized setup procedure with known results. The tables may be referenced before measuring objects requiring precision tolerances and locational constraints; therefore, users of the ATOS will be able to determine if the accuracy and precision of their measurements during a reverse engineering project are within the desirable range.

Terms and Definitions

Metrology – a field of knowledge concerned with measurement.

Non-Contact Metrology – metrology using methods which do not fiscally touch the object, often using optical methods.

Structured Light Scanning – The non-contact metrology technique used by the ATOS system to calculate the 3D coordinates of a point. The structured light scanning technique uses a projector to project a light pattern onto the surface of an object and a camera to capture the light pattern.

Coded Light – the light pattern projected onto the object's surface. The light pattern contains a code, which allows each pixel to be identified individually.

Gray Coding – a type of coded light which involves projecting multiple patterns of light and dark stripes onto the surface of an object. Images of each stripe pattern are captured and a binary value assigned to the light and dark stripes. The binary values are combined to give each pixel a unique value.

3D CAD – computer aided drawings which can be viewed in 3D much like a real object.

Constraint-Based 3D Models – 3D CAD models which are defined by geometrical constraints, such as curvature, points, distance, or shape.

Point Cloud – A grouping of points within a Cartesian coordinate system; each point contains an X, Y, and Z location.

Measured Object – the object which is being scanned; for the current study, the measured objects were the three gage blocks.

Measurement Volume – the amount of volume which can be measured by the ATOS system without moving the projector or measured object.

Measurement Location – the four measurements which were gathered from each gage block; to keep the measurements constant throughout the test, each location was tracked by numbering the edges of the constraint-based 3D model.

Reference Point – the circular targets that were attached to the measured object's surface. These reference points allowed multiple point clouds of the same object to be combined.

Post-Processing – the process used to convert a point cloud into a constraint-based 3D model.

Limitations and Delimitations

The current accuracy characterization within this study was limited to the following specifications:

- Specified Reverse Engineering Process – The current study implements a detailed process to develop the constraint-based 3D models from which all measurements were taken. Within the current study, the reverse engineering processes detailed in Chapter III were followed. Other reverse engineering processes could have been utilized; however, results may differ depending on the specific process followed. Because the options for reverse engineering processes are almost limitless, the results of this study are delimited by the process outlined in Chapter III.
- Flat Surfaces – The current study has been limited to surfaces the reverse engineering process has determined to be flat. Although the ATOS system and reverse engineering software within the current study were capable of processing data from curved surfaces, the study was limited to flat surfaces due to added complications within the reverse engineering processes.

- Software – The post-processing of the point cloud was restricted to the ATOS software, and Geomagic Studios 12. The measurement of the constraint-based 3D model was conducted using Pro/Engineer 5.0. The use of different post-processing software may yield different results.
- Hardware – The current study was restricted to the ATOS II model number: XXX system using the 90mm, 120mm, 250mm, and 500mm measurement volumes and the SO and 400 camera supports configurations.
- Gage Blocks – The current study was limited to Mitutoyo square ceramic gage blocks which conform to the ANSI B89.1.9M – 2002 gage block standard. A two inch grade AS-1 gage block, a one inch grade 0 gage block, and a half inch grade AS-1 gage block were used. Using a different type, size, or grade of gage blocks may yield different results.

CHAPTER 2: LITERATURE REVIEW

The purpose of the current thesis was to characterize the accuracy of constraint-based 3D models. These 3D models were created using scan data collected by an ATOS system and Geomagic Studio® reverse engineering software. In Chapter II, the background for this study was presented. This background includes an explanation on metrology, reverse engineering, computer aided drawings, gage blocks, and post-processing software. Additionally, Chapter II contains alternative forms of contact and non-contact metrology and a comprehensive explanation on the technique the ATOS system utilizes to measure objects. Knowledge of the background will assist in the understanding of where and why error is introduced into the constraint-based 3D models.

Metrology & Reverse Engineering

The ATOS system was often used to generate measurements of objects that lack dimensional data. The acquisition of dimensional data falls under a broad field known as metrology. The Joint Committee for Guides in Metrology (2006) defined metrology as a field of knowledge concerned with measurement. This definition of metrology included all theoretical and practical aspects of measurement, whatever the measurement uncertainty and field of application may be. This definition was further defined by Swinton de Silva (2002) to a specific area of metrology, known as dimensional metrology. Silva described dimensional metrology as the process of measuring a distance or angle. Dimensional metrology was also defined by Francis Farago (1968) as a way to designate processes for determining the linear and angular magnitudes of technical parts for their specific features.

Although the ATOS system has been used for applications outside of reverse engineering, the focus of the current study was to characterize the accuracy and precision of an ATOS system for reverse engineering applications, where the objective was to create a solid computer aided design (CAD) model from an object with no dimensional data. Reverse engineering has been defined by Raja (2008) as the process of finding and analyzing the inner workings of a machine. To apply this definition to the process that the ATOS system uses, Motavalli and Shamsaasef (2006) have defined reverse engineering as the process of obtaining a geometric CAD model from 3D points acquired by scanning and digitizing existing parts and products. With the jump from 2D to 3D in effect, the challenge for reverse engineering has been to generate a constraint-based 3D model from an existing product (P. K. Venuvinod, and W. Ma, 2004). Many systems were developed that can capture the 3D geometry of an object. These systems have been divided into the categories of contact and non-contact 3D measurement. (V. Raja, and K. J. Fernandes, 2008).

Computer Aided Design (CAD)

To display dimensions in a simple and concise manner, technical drawings were used to describe the geometry of an object visually by adding dimensions to a drawing of the object (S. J. Schoonmaker, 2003). Schoonmaker has additionally argued that as computer technology advanced, technical drawings changed from being drawn on paper to CAD drawings. The transition to computer-aided design made editing and copying the drawings faster and easier. In the late 1980's and early 1990's, technical drawings underwent another change with the advances in technology. 2D CAD programs were replaced with 3D CAD systems. Much like the switch from hand drawn technical

drawing to 2D CAD drawings, 3D CAD presents benefits that previously were not available with 2D CAD. A 3D CAD model can be viewed like a real object without the need to study a 2D drawing (S. J. Schoonmaker 2003). According to Giesecke (2009), as technical drawings became the medium of choice to display technical information, standards were developed to regulate the way dimensional data were displayed. Modern technical drawings follow the standards set by the American National Standards Institute (ANSI), so the drawings can be easily interpreted. Schoonmaker found that 3D CAD drawings can take the form of four different types of models: point clouds, wireframe, surface models, and solid parametric models.

Solid models.

According to R. Toogood (2009), a solid model is a computer model that contains all of the information of a real object. Solid models are capable of having volume, density, mass, and inertia, and are often constructed as feature-based parametric models. Toogood explained feature-based models as models created based on higher level physically meaningful features. These higher level features include extrusions, sweeps, cuts, hole, slots, and rounds. Feature-based models were not created using lower level geometries such as lines and points. Additionally, Toogood explained parametric models as models whose physical geometry is driven by the features, attributes, and the values assigned to these attributes. With a parametric model, the attribute dimensions could be defined or modified at any time during the model's creation, and the changes would automatically propagate throughout the model. Designing and editing models was simplified with the advent of feature-based parametric 3D solid models, as opposed to the

complicated polygon meshes or surface models that contain less information about the model and take longer to create.

Contact Metrology

The term contact metrology is used to describe measuring dimensional measurement techniques that require the measured object to be physically contacted. Contact metrology techniques may include measuring using calipers, micrometers, and steel rules to measure between two points on an object. Contact metrology may also include coordinate measuring machines (CMM) to measure the dimensions on an object.

Coordinate measuring machine.

The CMM uses a contact probe to record the surface geometry of an object. Dimensional data was digitally recorded when the probe came in contact with the surface of an object. The probe was connected to a carriage that was capable of moving in the X, Y, and Z directions. Each carriage was fitted with a precision scale that could continually record the position data to a computer (Dotson, Harlow, & Thompson, 2002). Figure 2.1 displays a Ziess Contura bridge type CMM.

Figure 2.1: Coordinate Measuring Machine.

According to Dotson (2002) there are two types of probes: touch trigger probes and continuous analog scanning probes. The touch trigger probe records a point when a sensor detects a change in resistance from the deflection of the stylus. When a point is detected, most CMM machines will indicate that the point was recorded by an LED light or an audible signal. With touch trigger probes, a single point is captured to define features quickly. CMM software allows the operator to choose subroutines for measurements that are performed frequently such as circles, planes, and cones. These subroutines permit operators to choose a specific point around the feature. Once the minimum number of points has been captured, the software will automatically find the

best fit and construct the feature. The continuous analog scanning probe is dragged across the surface of the object being measured. As the probe is moved along the surface, the sensors constantly record data. The continuous collection of data makes the measurement of irregular or contoured surfaces possible in a short amount of time (Raja & Fernandes, 2008).

Non-Contact Metrology

For objects with no 3D computer data attributed to them, dimensional metrology must be used to convert the geometry of the object into a CAD drawing. Traditionally, CMMs have been used to collect dimensional data from objects (J. A. Bosch, 1995). Recently, optical methods have become popular due to their high speed, high accuracy, high spatial resolution, low cost, and full field easy implementation (X. Chen, J. Xi, Y. Jin, J. Sun, 2009). Many optical methods are used to digitally capture the 3D geometry of an object. Depending on the application, each method has advantages and disadvantages (F. Chen, G. Brown, and M. Song, 2000).

Interferometry.

Basic interferometry operates under the principle that two coherent light waves will interfere and cancel if out of phase and combine if in phase (D.A. Page, 2009). An interferometer is an instrument that can measure the intensity of a light wave. Two waves that are out of phase will result in a lower intensity, while two waves that are in phase will result in a higher intensity. A simple interferometer works by generating a beam of coherent light that is then split by a beam splitter. Part of the beam is retroreflected to a sensor, and the other part is reflected by the surface on an object. If the object has a varying height, then the wave lengths reflected back will be out of phase and the sensor

will detect a lower light intensity. Page argued that the result was a fringe pattern of high and low intensities showing the height variation in the object's surface. Figure 2.2 represents a diagram of an interferometer that works on the interference principle.

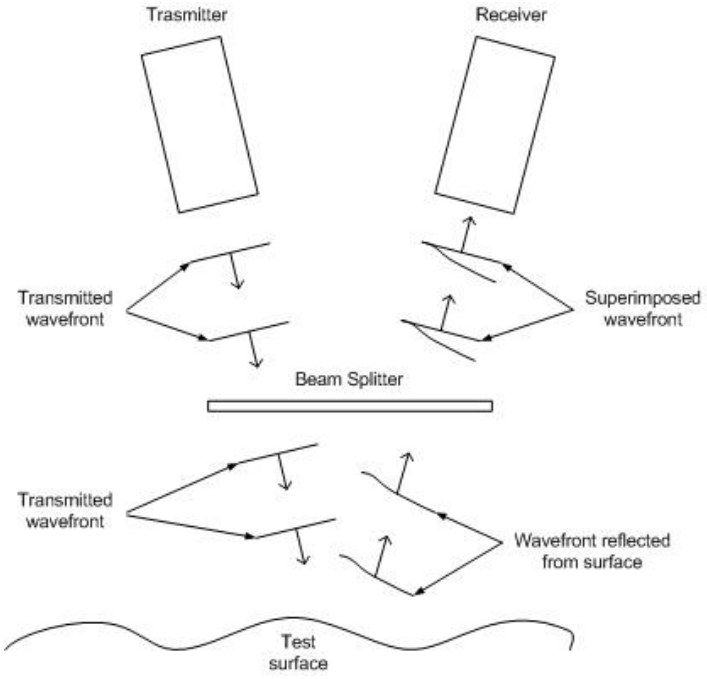

Figure 2.2: Simple diagram for interferometry. Adapted from "Interferometry" by Page, D. (2003). In T. Yoshuzawa (ed.), Handbook of Optical Metrology Principles and Applications (pp. 191-217). Boca Raton, FL.: CRC Press.

Photogrammetry.

Photogrammetry was first developed for cartography, using aerial images to generate 3D representations from 2D images of the earth surface. With the advances in digital cameras, close-range photogrammetry has been used for the measurement of large objects (H. Karara, 1979). Nobuo Kochi (2009) argued that with the advances in digital imaging, close range photogrammetry was used for archiving, transportation accident investigation, civil engineering, architecture construction, and industrial measurement.

Linder (2003) described the basic principle photogrammetry uses to construct 3D point clouds using digital images. The basic principle is based on photo image and center of projection of two or more photos of an object from multiple locations. *Figure 2.3* describes how the image center of projection principle was used to determine the 3D location (X, Y, and Z) of point P by setting up the equation for the rays $P \rightarrow P_1$ and $P \rightarrow P_2$ and calculating their intersection (W. Linder, 2003). According to Kochi, to determine the point's location, the interior orientation and exterior orientation need to be determined.

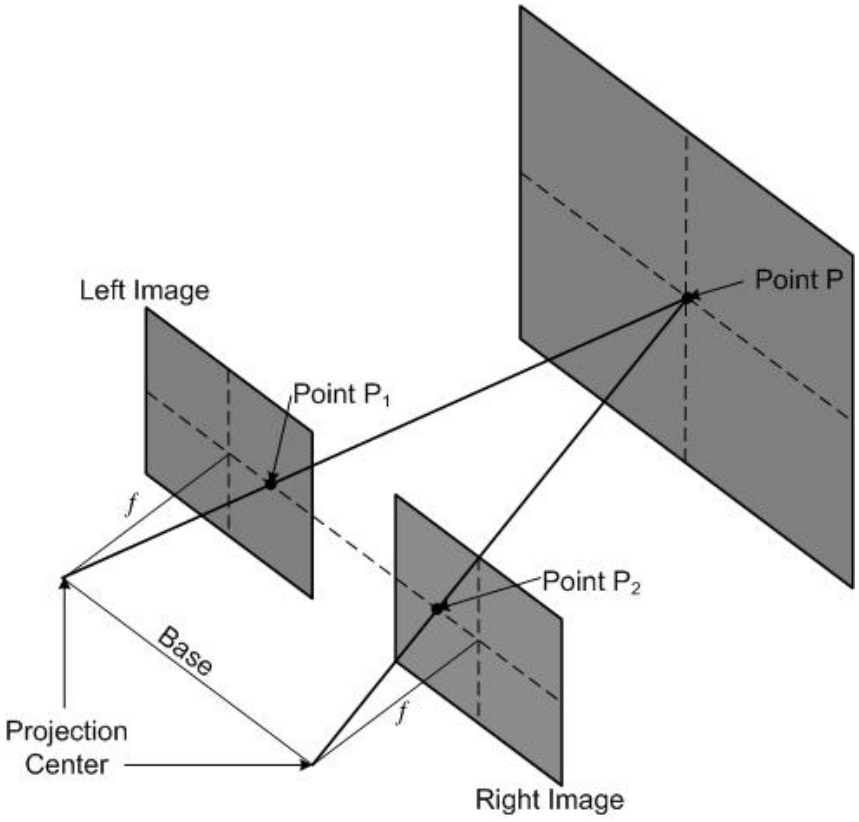

Figure 2.3: Diagram of photogrammetry center of projection principle. Adapted from "Photogrammetry," by Kochi, N. (2003). In T. Yoshuzawa (ed.), Handbook of Optical Metrology Principles and Applications (pp. 511-529). Boca Raton, FL.: CRC Press.

The interior orientation describes camera parameters such as focal distance. Camera calibration was used to find the interior orientation in photogrammetry. Z. Zhang (2000) has developed a camera calibration technique based on the pinhole camera model, in which a calibration object with known geometry is used to calculate the camera's position.

The exterior orientation describes the camera's location and direction. This has been achieved using the coded targets seen in *Figure 2.4*. According to Z. Zhang (2000), the exterior orientation can be calculated from six corresponding points from all the images. Each target has a white circle inside a black square for contrast. A partial ring of white area contains a code, which when viewed from more than one location can be distinguished from the other targets.

Figure 2.4: Coded target based from observed close range photogrammetry targets.

Moiré metrology.

Moiré is a word of French origin, meaning an irregular wavy pattern of a fabric. This term was applied to the pattern seen when two geometrically regular patterns, such

as the grid pattern from a screen, are superimposed on top of one another (L. Jin, 2009). *Figure 2.5* displays the moiré pattern that results from two identical line patterns superimposed at an angle. Jin found that two patterns, in-plane and out-of-plane, are typically used with moiré metrology. The in-plane moiré pattern is the resultant pattern of two gratings with parallel lines. Jin further explained these gratings can be the same frequency and superimposed at an angle, or have different frequencies and be superimposed at the same angle. An out-of-plane pattern is the result of two curved line patterns of different sizes that are superimposed. Examples of these patterns can be seen in *Figure 2.6.*

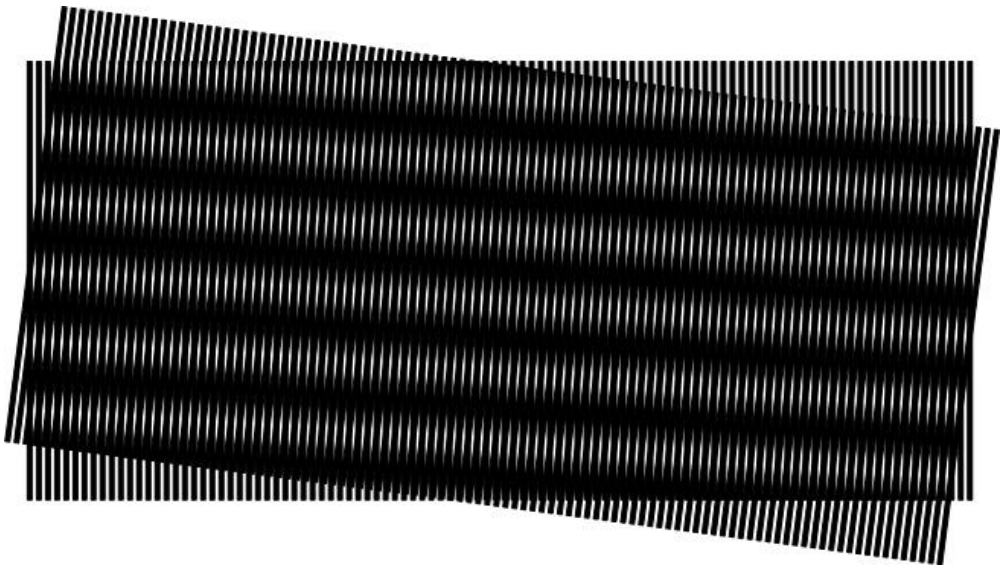

Figure 2.5: Moiré pattern of two identical line patterns superimposed at an angle on a flat surface. Adapted from "Moire Metrology," by Jin, L. (2003). In T. Yoshuzawa (ed.), Handbook of Optical Metrology Principles and Applications (pp. 263-280). Boca Raton, FL.: CRC Press.

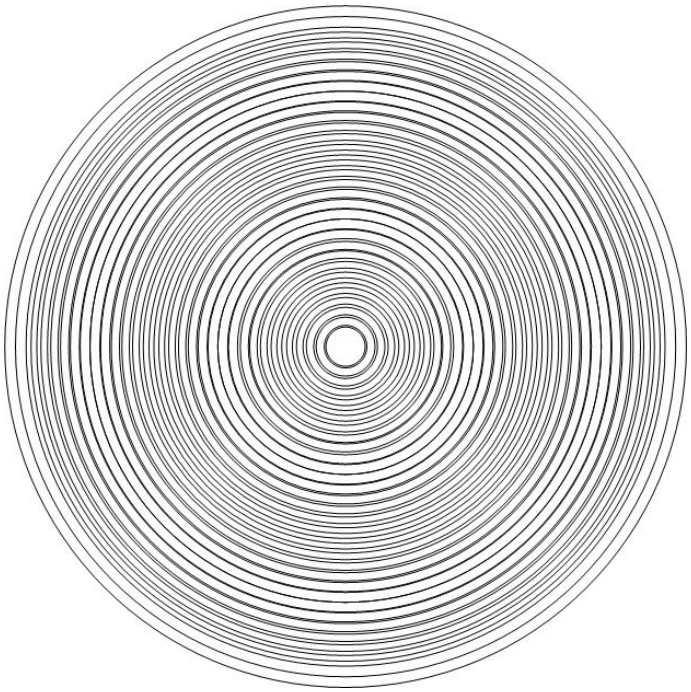

Figure 2.6: Out-of-plane moiré pattern. Adapted from "Moire Metrology," by Jin, L. (2003). In T. Yoshuzawa (ed.), Handbook of Optical Metrology Principles and Applications (pp. 263-280). Boca Raton, FL.: CRC Press.

According to James Wyant (2002), two types of moiré methods exist, shadow moiré and projection moiré. In shadow moiré, a grating is placed in front of an object so that a shadow of the grating is produced on the object. Wyant explained that a moiré pattern is produced when the object is viewed from a different direction through the grating. In projection moiré, a grating is projected onto the surface of the object and a moiré pattern is produced when the object is viewed through a second grating. This allows two different patterns to be used (J. Wyant, 2002).

According to Craig Scott (1998), two gratings were typically used for projection moiré metrology; the first grating was known as the projection grating, the other grating was known as a viewing grating. The projection grating cast shadows onto a curved

surface which appear distorted. When the distorted shadows were viewed through the viewing grating, the overlaid shadows produced a contour map of the object.

Structured Light Scanning

According to Toru Yoshizawa (2009), structured light scanning has become one of the leading optical methods used in the acquisition of dimensional data from an object. D. Bergmann (1995) found that a structured light scanning method that implements both a camera and projector has captured dimensional data from an object by projecting a line onto the surface of the object. When viewed from different angles, the line appeared distorted. To increase the speed of measurement, a coded pattern was projected instead of a line. With projected coded light, each point was encoded to identify the point's coordinates within the projected area (J. Pagés, 2003). Different methods of coding structured light are discussed later in Chapter II. According to F. Chen (2000), when a coded light pattern was projected onto an object, the object's geometry distorted the pattern. *Figure 2.7* displays a coded pattern that has been distorted by an object.

Geometric data can be extracted from the coded light by use of triangulation. A triangle is formed between the projector, camera, and a point on the object's surface. If the angle and distance between the camera and projector is known, the coordinate of the surface point can be calculated. *Figure 2.8* illustrates triangulation: P is a point on the surface of an object, and the distance between the camera, projector, and angles α, β_1, and β_2 are all known through calibration. Using trigonometry, the length of the two unknown sides could be determined given the location of point P.

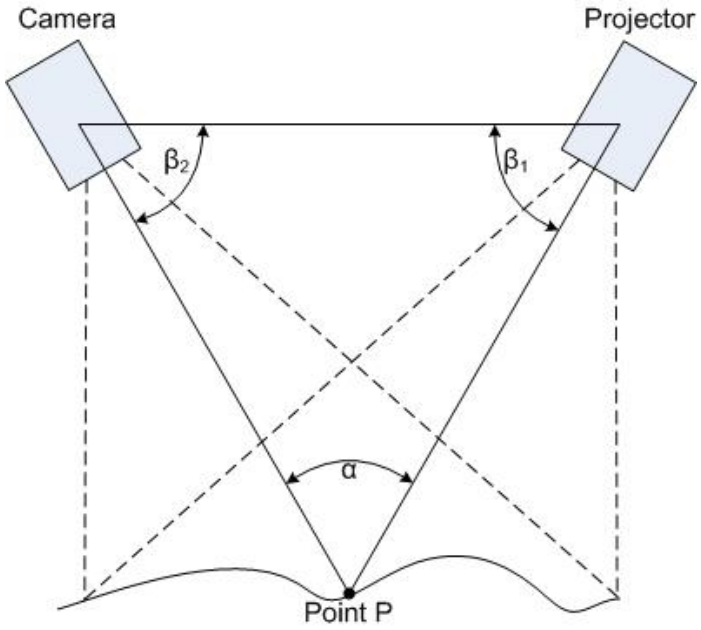

Figure 2.7: Distortion of coded light when projected onto an object. Image was taken using the ATOS white light scanner.

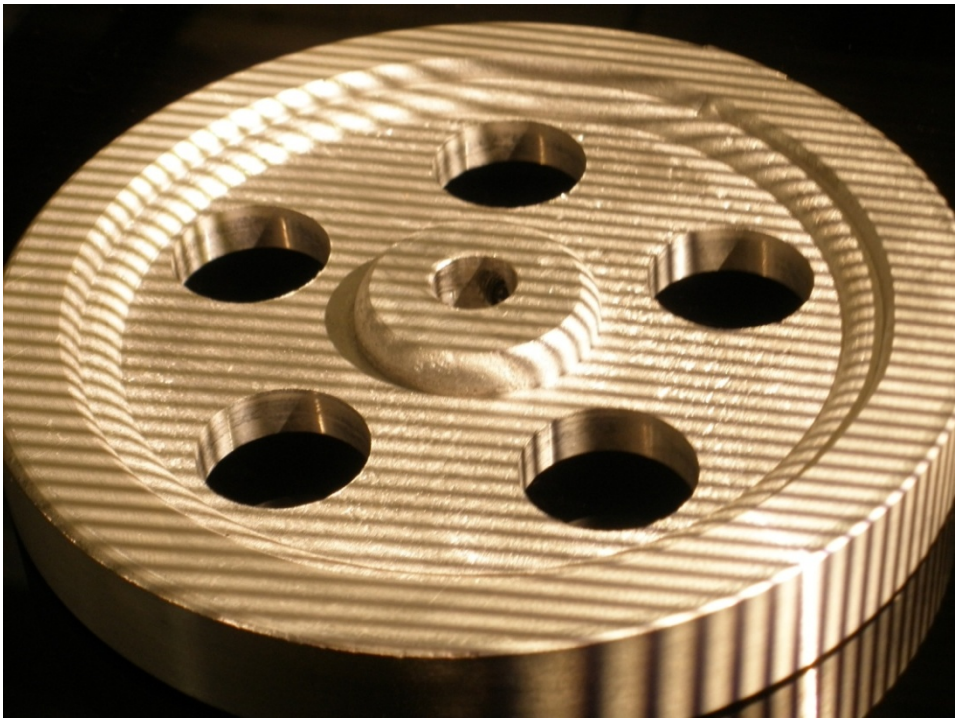

Figure 2.8: Triangulation of point P. Adapted from "New Approach for Automatic Surface Reconstruction with Coded Light," Bergmann, D. (1995). *SPIE*, 2572, 2-9

According to Sansoni (1997), the measurement resolution of scanners similar to the ATOS system depends on the configurations of distance and angle between the camera(s) and the projector, and the distance of the projector and camera(s) from the surface being measured. F. Chen (2000) noticed that when point clouds between multiple scans were combined into a global point cloud, error was introduced into the models. Chen also noticed that the lens distortion and aberrations were also a source or error. Carsten Reich (1996) found that errors were introduced by the geometries of the measured objects. Reich (2000) also noted that errors were introduced from the calibration process.

Projection patterns.

Several types of coded patterns have been proposed for use in structured light scanning (J. Pagés, J. Salvi, R. Garcia, and C. Maatabosch, 2003). The authors argued that although each pattern differed, they shared a common task of identifying points. Point identification was achieved by coding one or both axes of the projected pattern. Each coded pattern presents its own set of advantages and disadvantages. Some of these advantages are scanning moving objects, scanning colored objects, and whether or not the coding is repeated.

Joaquim Salvi (2004) found that to scan moving objects, a type of coding known as spatial neighborhoods can be used. According to Salvi, points were coded in the spatial neighborhoods method by coding the surrounding points. These codes often used intensity patterns or color patterns for codification. Pagés et. al. (2003) found that the decoding stage for the spatial neighborhoods coding to be more difficult, due to the requirement that the entire neighborhood be present in the image. Three techniques were

used to code spatial neighborhoods: non-formal codification, De Bruin sequences, and M-array patterns. Salvi also found that patterns classified as direct coding were used to measure moving objects. With direct coding, the entire code can be viewed with one image. The direct coding is often achieved using color coding or gray level coding.

Pagés et. al. (2003) discovered that the measurements with the highest accuracies came from a type of coding known as time-multiplexing. The authors found that time-multiplexing coded light was based on temporal coding, in which a set of patterns was projected successively onto an object's surface. J. Pagés also found that the coding for the individual pixel could be determined by the total illuminates value because each pixel was exposed to different levels of light intensity. Pages divided the time-multiplexing patterns into three types: binary codes, n-array codes, and gray coding with phase shifting.

Gray coding.

The gray coding method applies stripes of white light to illuminate a scene. By viewing the scene with a camera, each pixel can be assigned a binary value of 1 or 0 depending on whether or not the stripe is illuminated (C. Reich, R. Ritter, J. Thesing, 2000). For gray coding to work correctly, the image must be encoded so each pixel is assigned a unique value. To fully encode a scene, multiple images, each with a different stripe pattern, must be combined. D. Scharstein (2003) found that using a gray code pattern requires $\log_2(n)$ patterns to be projected where n is the width of a pixel. *Figure 2.9* illustrates a gray code using four projection patterns. E. Müller (1995) explained that as the amount of stripe patterns increase, the resolution of the coded image will also

increase. For high resolution images a large number of stripe patterns are required, causing the time of acquisition to increase.

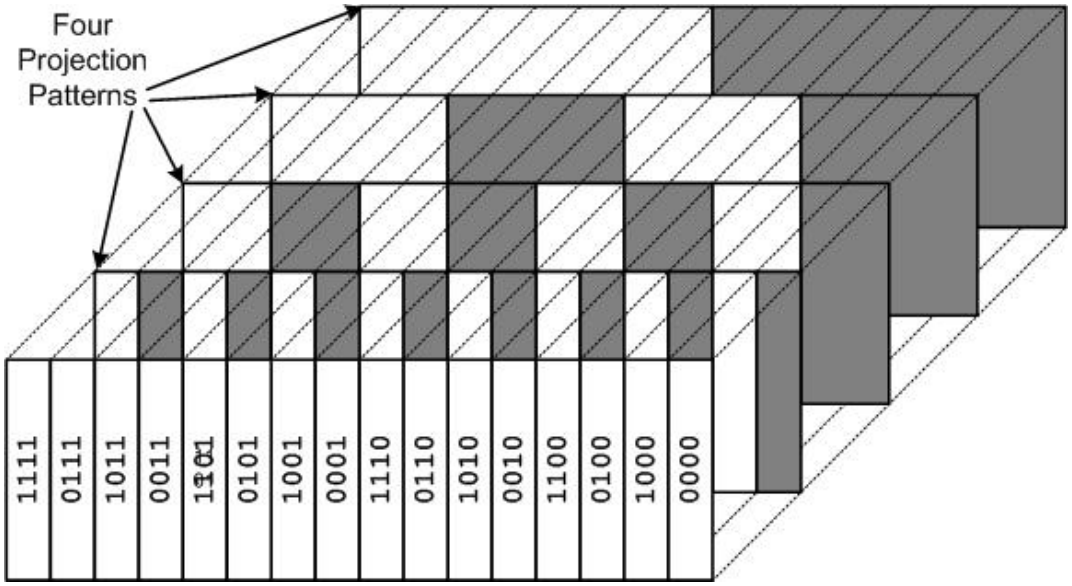

Figure 2.9: Gray code using four projection patterns. Addapted from "Photogrammetric Matching of Point Clouds for 3D-Measurement of Complex Objects," by Reich, C. (1998). *SPIE,* 3520, 100-110

D. Scharstein (2003) found that to reduce the amount of stripe patterns required to encode an image, the capability of an LCD projector can be utilized to project a continuous function. C. Reich (2000) found that a sinusoidal shape works best. When the phase of the sinusoidal pattern is shifted by a fixed phase step, the intensity will change for one pixel. X. Chen (2009) used a four step phase shift, shifting the phase by 90° each shift. Chen further argued that the phase shifting method results in an ambiguity problem. According to Scharstein, points at the same phase in the pattern cannot be distinguished. The phase shifting method is illustrated by *Figure 2.10.*

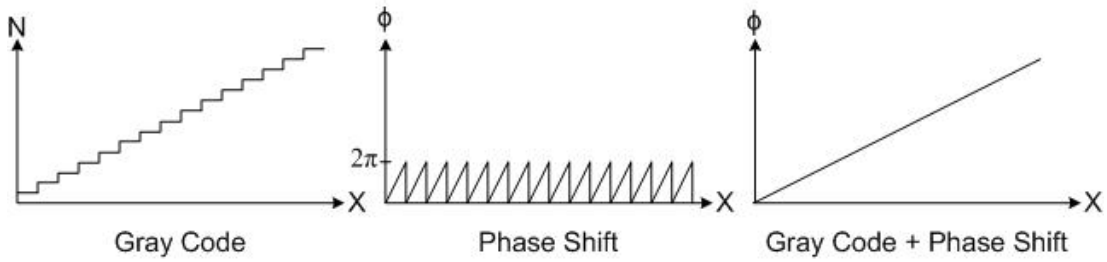

Figure 2.10: Gray code + phase shift. Adapted from "New Approach for Automatic Surface Reconstruction with Coded Light," by Bergmann, D. (1995). *SPIE*, 2572, 2-9

To overcome the issue of ambiguity, while keeping the acquisition time reasonable, a combination of gray coding and phase shifting was used to form an absolute phase (X. Chen, 2009). Chen used the combination of phase shifting to subdivide the gray coded pattern. With Chen's approach, the absolute phase is distributed linearly and spatial-continuously over the whole scene, allowing the light directions to be tracked by their absolute phase.

ATOS System

The Advanced Topometric Sensor (ATOS) system was created by GOM in 1995. Today, more than 1,500 companies use the ATOS system in the fields of product development, quality assurance, material and component testing, and reverse engineering (Gesellschaft für Optische Messtechnik [GOM mbH], 2006). GOM stated that the ATOS system is capable of measuring up to 1,400,000 points spaced between 0.02 mm and 1.0 mm in two seconds. The ATOS system has a measurement window of 90mm x 80mm x 60mm (90mm measurement volume), 120mm x 108mm x 95mm (120mm measurement volume), 250mm x 200mm x 200mm (250mm measurement volume), and 500mm x 440mm x 440mm (500mm measurement volume) (GOM mbH, 2006).

Reference points.

In order to generate a full 360° scan, the scanner must be located at different points around the object. A problem of ambiguity emerges when multiple scans, each containing its own coordinate system, need to be combined (F. Chen, G. Brown, and M. Song, 2000). According to Chen, to overcome the ambiguity problem, the coordinates of each sensor's location must be known and the multiple local point clouds combined into a global point cloud. If an error occurs during the detection of the sensor's location, the local point clouds will not match, causing the accuracy of the global point cloud to suffer. Dirk Bergmann (1995) developed a method that allows multiple local point clouds to be combined into one global point cloud by using a photogrammetric bundling adjustment to determine the sensor's position relative to the object being measured. Bergmann's bundle adjustment algorithm is shown in *equation 2.1.*

$$\begin{pmatrix} x - x_o - d_x \\ y - y_o - d_y \\ c \end{pmatrix} = s * R * \begin{pmatrix} X - X_o \\ Y - Y_o \\ Z - Z_o \end{pmatrix} \quad (2.1)$$

x,y	=	Image Coordinate
x_o, y_o	=	Principal Point
d_x, d_y	=	Lens Distortion
c	=	Camera Constant
R	=	Rotation Matrix
X_o, Y_o, Z_o	=	Projection Centre
X,Y,Z	=	Object Point

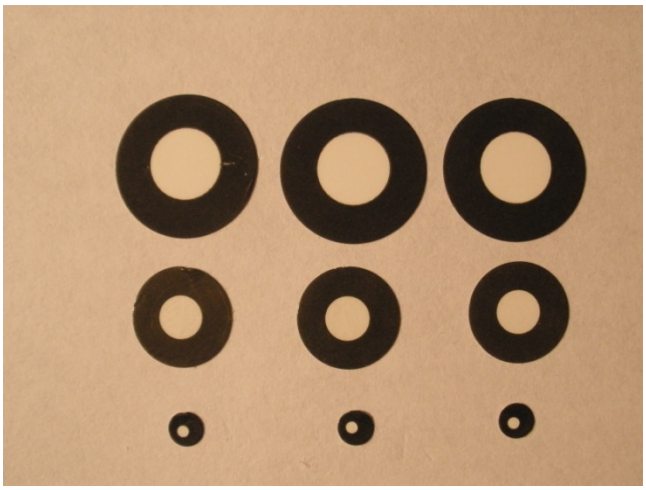

Figure 2.11: Reference points, 5mm on top, 3mm in the middle, and 0.8mm on the bottom

Photogrammetry is used to detect reference points attached on or around the object. The reference point's coordinates are determined in the first sensor position. Additional sensor positions require at least three reference points from the previous scan to be present in order to triangulate the sensor's position (C. Reich, 1996). The ATOS system completely automates the process of detecting, identifying, measuring, and computation of the reference points. The reference points used are black circles with a white dot in the center (*Figure 2.11*). The black circle is not recognized by the sensor, resulting in measured points that are separated from the measured object. Because the size of this point is known, the ATOS system will recognize the separated point as a reference. *Figure 2.12* provides an example of the measured point cloud around a reference point, the surface model of the reference point before filling the hole, and the surface model of the reference point after filling the hole.

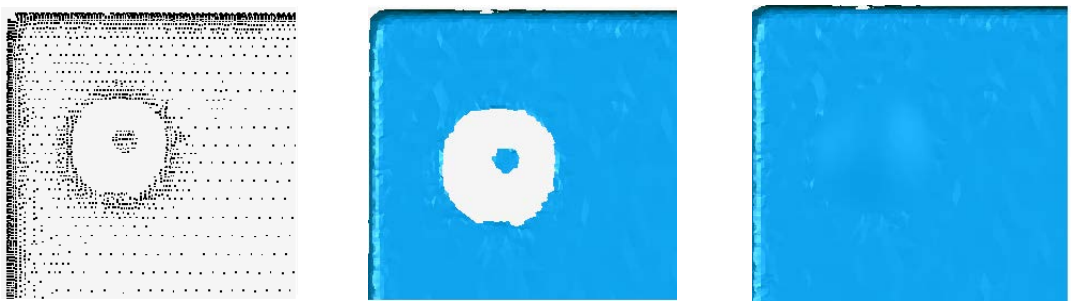

Figure 2.12: Measured point cloud around a reference point. Image created using scan data from a 1” gage block acquired using the ATOS system

Calibration.

According to C. Reich (2000), only the cameras need to be calibrated because the system is based on a passive stereo-photogrammetric setup with two cameras. Reich (1996) found the sensor’s accuracy depends on the quality of calibration and thus a higher quality calibration will lead to a more accurate measurement. Dirk Bergmann (1995) argued that the higher quality of a photogrammetric calibration would result in accuracies higher than those achieved by fringe projection, making photogrammetry an ideal method for the calibration of the ATOS system. C. Fraser (1992) proved that a photogrammetric bundle adjustment, similar to the algorithm used by Burgmann, could yield accuracies close to one part in a million.

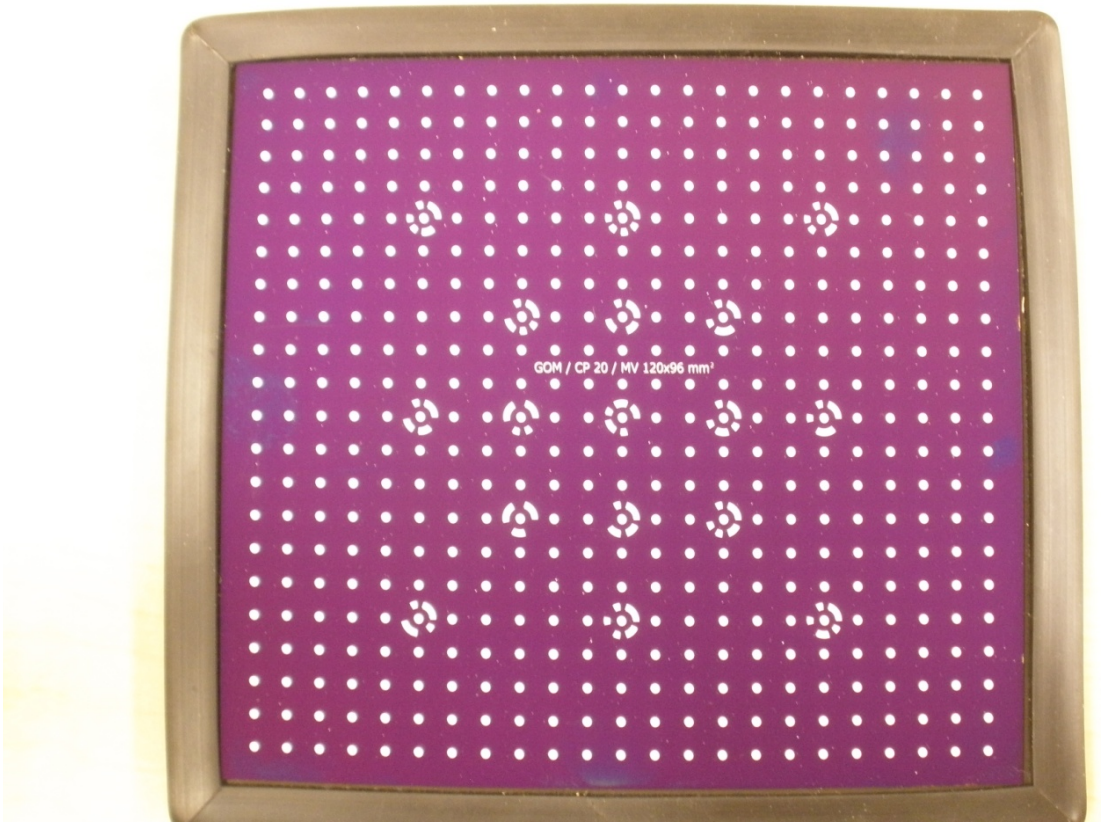

Figure 2.13: Calibration object for the 120mm measurement volume.

The photogrammetric bundle adjustment algorithm required multiple images taken of a calibration object (*Figure 2.13*). The calibration object was described by Burgmann (1995) as a plate with circular targets fixed to its surface. The targets used are similar to the coded targets seen in *Figure 2.4.* Bergmann found that only the distance of two points must be known prior to calibration. According to GOM, the calibration procedure needs to be performed every time the camera and projector lenses are changed.

Gage Blocks

A gage block is a length standard made from 52100 hardened steel, carbide, or ceramic that has flat and parallel opposing surfaces (Doiron & Beers, 2005). There are two main American standards for gage blocks: the Federal Specification GGG-G-15C

and the American National Standard ANSI/ASME B89.1.9M. The main differences between the two standards are organization of the material within the standard and the listing of standard sets of blocks given in the GGG-G-15C specification (Doiron & Beers, 2005). The ASME standard defines physical properties for the block's geometry (length, parallelism, flatness, and surface finish), standard nominal lengths, and a tolerance grade system for classifying the accuracy level of blocks (American Society of Mechanical Engineers [ASME], 2002). The B89.1.9M gage block standard also defines the parameters used to create a gage block: temperature = 20 ºC (68 ºF), barometric pressure = 101,325 Pa (1 atmosphere), water vapor pressure = 1,333 Pa (10 mm of mercury), CO_2 content of air = 0.03%. Of these four parameters, only temperature has an effect on the size of the gage block (Doiron & Beers, 2005). The grade system for the tolerances of gage blocks specifies four tolerance grades: 0.5, 1, 2, and 3. Grades 0.5 and 1 gage blocks have lengths very close to their nominal values. Grades 2 and 3 are of lower quality. As the size of the block rises, the accuracy will decrease. A grade 2 10mm block will have an accuracy of +0.10, -0.05 μm, whereas a 500mm block will be +1.00, -0.50 μm (Doiron & Beers, 2005).

Post-Processing

Reverse engineering software, such as Geomagic Studio®, was used to transform point cloud data into polygon meshes, non-uniform rational B-splines (NURBS), surface models, and solid parametric models (D. T. Pham and L. C. Hieu, 2008). *Figure 2.14* displays the evolution of a point cloud as it is converted to wire frame, and finally parametric models. William B. Thompson (1999) suggested the conversion of scanned data into feature based 3D models. Converting the data into feature based parametric 3D

models is often desirable for reverse engineering because it allows for the easy modification to the model, is more appropriate for manufactured components, and can reduce the noise and increase the accuracy of the 3D model.

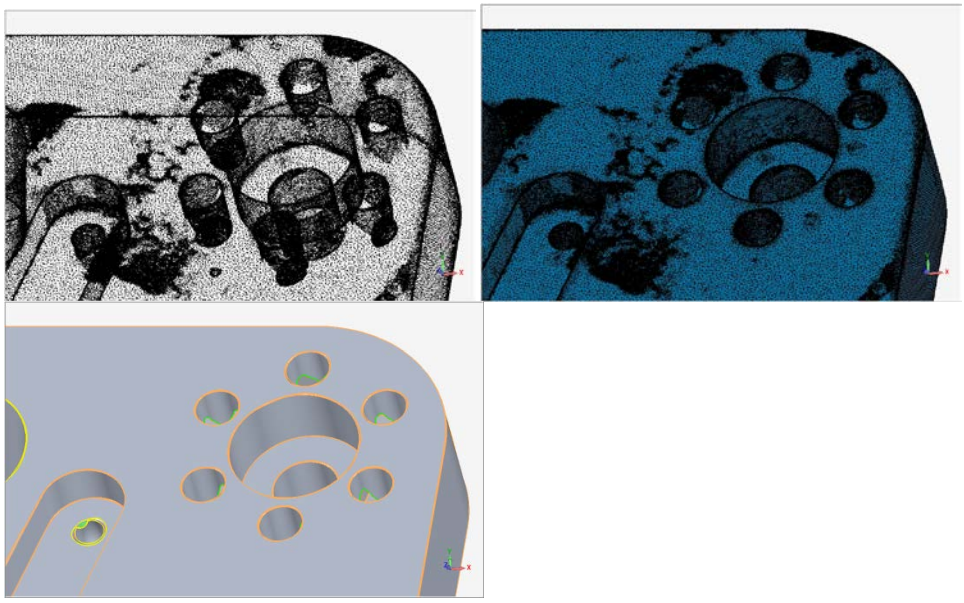

Figure 2.14: Transformation of a point cloud into a parametric solid model. Image created using scan data from an object acquired using the ATOS system.

Pham (2008) explained that to convert a point cloud into a geometric solid model, Geomagic and other similar software offers a variety of options and features to improve the quality of a polygon mesh. Some of the common features used when reverse engineering an object are polygon mesh optimizing, hole filling, defeaturing, primitive fitting, and edge detection. With these features slight abnormalities to the polygon mesh can be altered to conform to the surrounding polygon mesh. The software will automatically find the best fit plane for a group of data points using a least squares algorithm. Additionally, Pham explained that holes in the polygon mesh can be filled using the same least squares algorithm, and that edges can be smoothed out so all points

lie on the same line. *Figure 2.15* represents a polygon mesh containing a number of abnormalities, and *Figure 2.16* displays the same polygon mesh after post-processing.

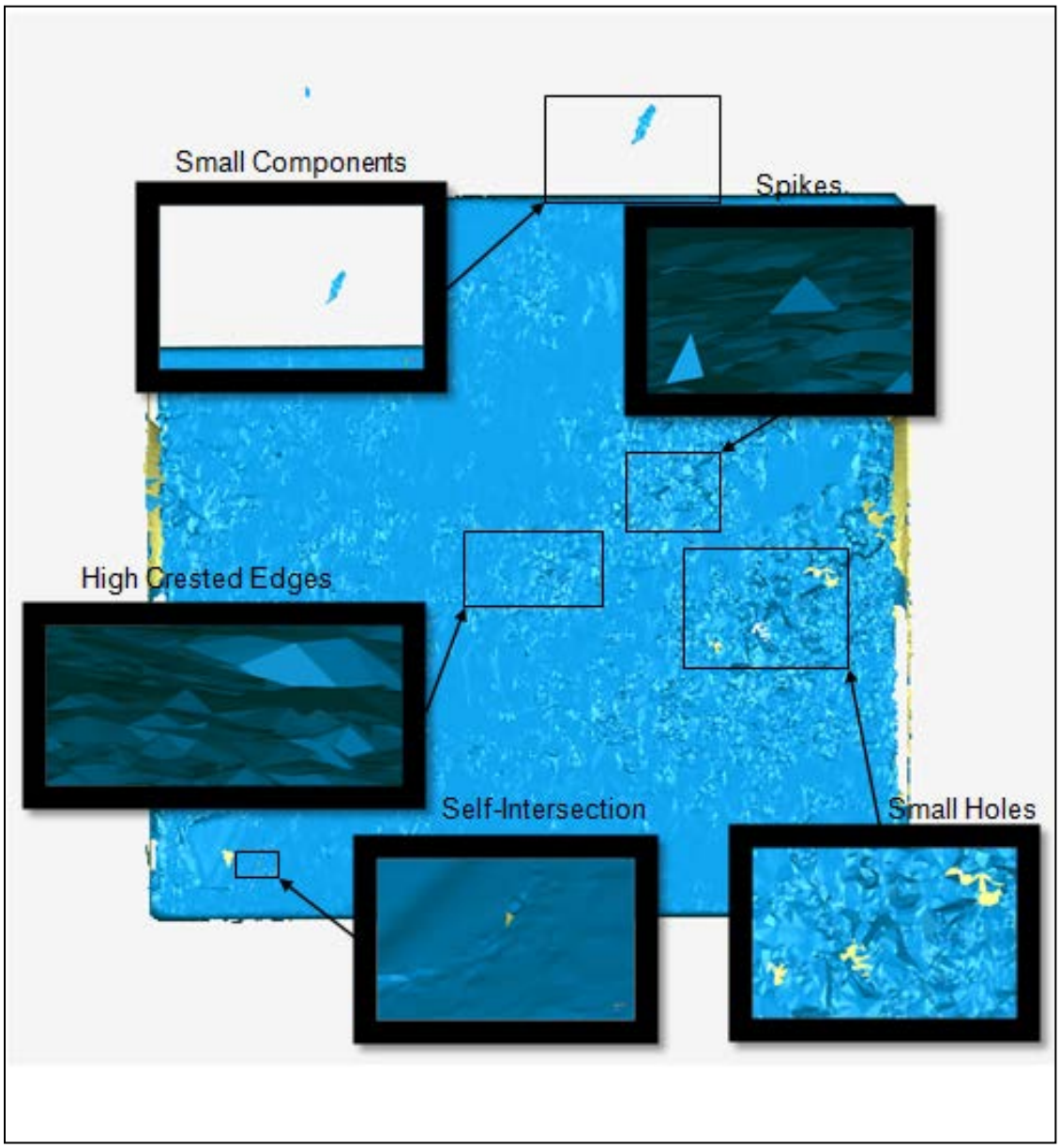

Figure 2.15: Polygon mesh abnormalities. Image created using scan data from a 1” gage block acquired using the ATOS system.

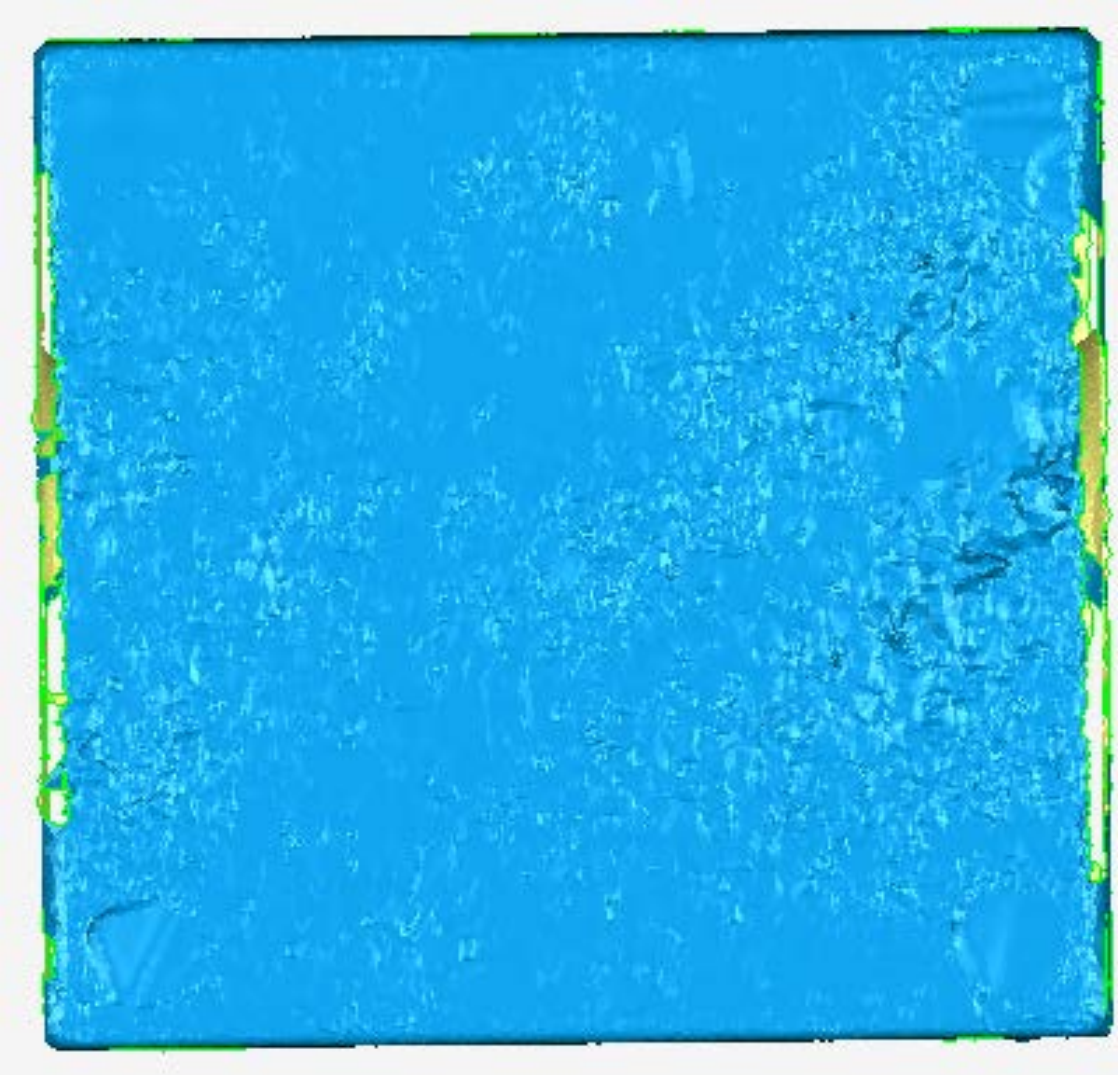

Figure 2.16: Repaired polygon mesh. Image created using scan data from a 1” gage block acquired using the ATOS system

The National Institute of Standards and Technology (NIST) has completed a report on the least squares algorithm, which Geomagic, Inc. uses for features such as lines, circles, planes, spheres, cylinders, and cones. This study was conducted to find the measurement uncertainty of Geomagic’s algorithm based on the ASME B89.4.10-2000 Standard Default Test. According to NIST, Geomagic’s algorithm was used to generate a data set simulating the range of test conditions. These data were compared to data

generated by NIST using the ASME B89.4.10-2000 Standard Default Test. NIST has found that the reported test results for each geometry type are the root mean square values. The results of the standard default test are displayed in *Table 2.1*.

Table 2.1

Measurement uncertainty of Geomagic's algorithm based on the ASME B89.4.10-2000 Standard Default Test

Geometry Type	**Maximum Observed Deviations**					
	Separation (μm)	Tilt (arc seconds)	Radius/dist under (μm)	Radius/dist over (μm)	Apex under (arc seconds)	Apex over (arc seconds)
Lines	$< 10^{-5}$	1.1×10^{-7} data set 4	———	———	———	———
Lines 2D	$< 10^{-5}$	$< 10^{-7}$	———	———	———	———
Planes	$< 10^{-5}$	7.7×10^{-6} data set 25	———	———	———	———
Circles	1.3×10^{-4} data set 26	1.3×10^{-5} data set 1	1.2×10^{-4} data set 26	$< 10^{-5}$	———	———
Circles 2D	1.2×10^{-4} data set 18	$< 10^{-7}$	1.1×10^{-4} data set 18	$< 10^{-5}$	———	———
Spheres	1.9×10^{-5} data set 10	———	1.5×10^{-5} data set 10	$< 10^{-5}$	———	———
Cylinders	$< 10^{-5}$	6.7×10^{-5} data set 8	$< 10^{-5}$	$< 10^{-5}$	———	———
Cones	3.7×10^{1} data set 10	1.5×10^{1} data set 27	1.9×10^{0} data set 10	3.9×10^{-1} data set 7	1.4×10^{1} data set 27	7.7×10^{0} data set 18

CHAPTER 3: METHODOLOGY

The purpose of the current study was to characterize the accuracy of a reverse engineering process to develop constraint-based 3D models. These 3D models were created using scan data collected by an ATOS system and Geomagic Studio reverse engineering software. Chapter III contains an overview of the method used during the testing process, a description of the equipment used during testing, and an explanation of the statistical testing that was conducted. The method implemented during testing is divided into sections, containing a detailed list of the procedures; the sections are presented in Chapter III.

Overview of Testing Procedure

The following procedure presents an overview of the process used when collecting data with the ATOS system and the post-processing of the data. Detailed procedures are presented throughout Chapter III under the appropriate heading.

- The ATOS system was set up for each measurement volume.
    - The sensor's offset distance was adjusted.
    - The cameras' apertures were adjusted.
    - The cameras were aligned.
    - The sensor was calibrated.
- The gage blocks were prepared for scanning.
    - 2-4 reference points were attached to each surface of the gage blocks.
- Scanning was conducted with the ATOS system.
    - The temperature and lighting conditions were checked prior to scanning.

    - The gage block was placed in the center of the measurement volume. (*Figure 3.7*)
    - Scan I was taken at 0°.
    - Scan II was taken at 90°.
    - Scan III was taken at 180°.
    - Scan IV was taken at 270°.
    - Scan V was taken at 360° with the gage block rotated 90°.
- Post-processing was conducted within the ATOS software.
    - Local point clouds were aligned.
    - Local point clouds were combined into a global point cloud using the polygonization process.
    - Global point cloud was saved as .g3d file and imported into Geomagic Studio.
- Further post-processing was conducted using Geomagic Studio® reverse engineering software to construct a constraint-based 3D model.
    - Coordinate axis was set.
    - Small abnormalities were repaired.
    - Large holes were filled.
    - Unwanted data were removed.
    - Surfaces were classified as planes.
    - Surfaces were created from the classified polygon mesh.
    - Surfaces were exported into Pro/Engineer.
- The 3D model was virtually measured using Pro/Engineer® solid modeling software.
- Statistical tests were performed to validate the data collected.

Equipment Used

Before detailed explanations of the procedure used in the current study could be presented, an understanding of the equipment used was needed for conducting the study properly. The "Equipment Used" section provides explanations on the ATOS system and the gage blocks used for measuring as well as the correct settings needed to conduct this study.

ATOS system.

According to the ATOS User Manual – Software (2008), the ATOS is a stand-alone system that is comprised of two CCD cameras, a projector, and a stand. The system is controlled by a Linux PC with specialized software for the operation of the sensor and the processing of data. Additionally, the ATOS system has the ability to switch camera lenses and camera frames to adjust for different sized measurement volumes (GOM mbH, 2008). The lenses for the 90mm, 500mm, and 250mm are shown in *Figure 3.1*. A set of three lenses, one for the projector and one for each camera, were used for each measurement volume.

Figure 3.1: The lenses for the 90mm, 500mm, and 250mm for the projector and left and right camera

Sensor configurations.

For the current study, two different sensor configurations were used to achieve the four measurement volumes tested. The two smaller measurement volumes, 90mm and 120mm, used the ATOS IIe SO configuration. The two larger measurement volumes, 250mm and 500mm, used the ATOS IIe 400 configuration. According to the ATOS User Manual – Software (2008), changing the camera support will change the distance between the two cameras and allow for a different measurement volume. For all four measurements, the same two cameras and projector were used and only the lenses were changed to adjust the measurement volumes. The two configurations can be seen in *Figure 3.2.* Details about both sensor configurations may be found in the ATOS IIe and ATOS IIe SO Hardware User Manual (2008).

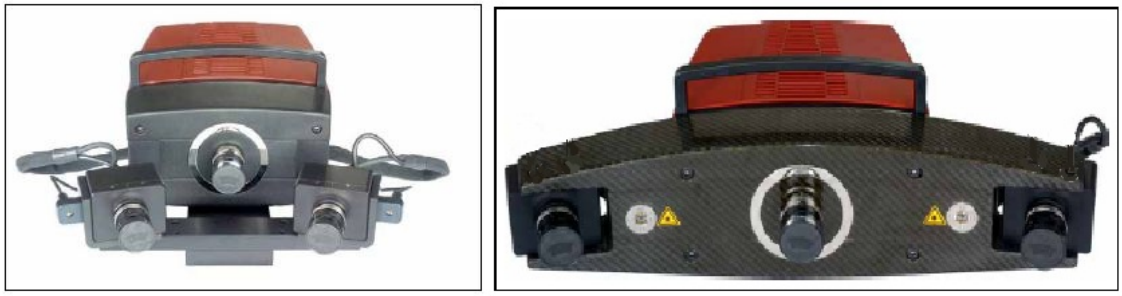

Figure 3.2: ATOS IIe SO (left) and ATOS IIe 400 (right)

The ATOS IIe and ATOS IIe SO Hardware User Manual (2008) described the process to follow when changing lenses. The lens changing process required the projector to be set to 25% light intensity and a white sheet of paper placed in the camera's view and the shutter time adjusted to optimum brightness. A tape measure was used to adjust the measurement distance between the camera support and the center of the measurement

volume. The apertures were adjusted for the projector to the parameters listed in the ATOS user manual, and the camera's positions were aligned with the projectors. To set the cameras' apertures, the shutter time was adjusted to the limits specified in the user manuals and the false color setting was used until the camera's images resembled *Figure 3.3*. The aperture adjustment procedure was followed each time the measurement volume changed prior to calibration.

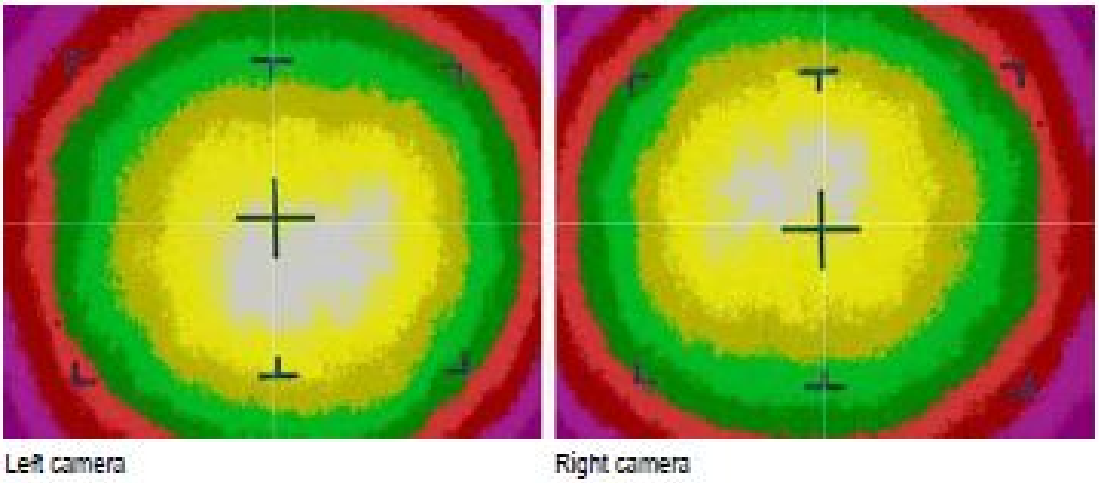

Figure 3.3: False color mode for left and right cameras during aperture adjustment.

Calibration.

The ATOS User Manual - Software (2008) specified the specific calibration procedure used for the photogrammetric calibration of the cameras. Calibration is achieved with a calibration object seen in *Figure 2.13*. For each measurement volume, a different calibration object was required. Although the calibration objects may differ slightly in appearance, all the objects are fitted with photogrammetric coded targets and follow the same calibration procedure. According to GOM, the ATOS system should be calibrated every time the measurement volume is changed or if the measurement

reference point's central value exceeds 0.1 pixels; exceeding 0.1 pixels may occur if the camera angle or cameras' lenses were changed. GOM found that a satisfactory calibration should yield deviation results of 0.01 to 0.04 pixels (ATOS User Manual - Software 2008). Additionally, a satisfactory calibration should yield a deviation of the adjusted calibration scale bar under 0.005%. Higher deviations suggest that the wrong calibration object was used or the scale parameter was incorrect.

Gage block selection & preparation.

Three NIST certified square ceramic gage blocks were selected to be the scanned objects for the current study. 52100 hardened steel gage blocks were rejected because of their polished finish, which would require the gage blocks to be coated with a white powder. The structured light pattern projected onto the steel gage blocks was not identified by the two CCD cameras, causing errors in the data collected. The ATOS User Manual (2008) suggested that for shiny and reflective surfaces, the gray levels detected by the two cameras will differ. If the difference in gray values detected exceeds the software's acceptable limits, measurement error could occur. To resolve the issue of the gage block's reflective surface, a ceramic gage block was used. The ceramic gage blocks are made from zirconia oxide (ZrO_2) and have a white finish, which can be easily recognized and recorded by the ATOS system. To cover a broad spectrum of object sizes, three Mitutoyo NIST certified square gage blocks were chosen. These gage blocks can be seen in *Figure 3.4*: a two inch grade AS-1 gage block, a one inch grade 0 gage block, and a half inch grade AS-1 gage block.

Figure 3.4: Mitutoyo ceramic square gage blocks, sizes 1 inch, 0.5 inch, and 2 inch, certified by NIST used during data collection.

For the ATOS system to combine multiple scans, reference points must be placed on the surface of the gage block. The reference points were paper targets with an adhesive backing; the adhesive backing will adhere to the object and secure the reference points in place. The reference targets were circular with black outside diameters. A white dot is located within the black target point. The white dot is recorded by the ATOS system while the black circle does not reflect the structured light pattern, so no data are recorded. *Figure 2.11* displayed the .8mm/3mm and the 2.5mm/5mm reference points used during the current study. Two different sized reference points were required when

collecting data; the ATOS IIe SO configuration utilizes the 0.8mm/3mm reference points, while the ATOS IIe 400 configuration required the use of the larger 3mm/5mm targets. *Figure 3.5* shows how the reference points were located on the gage block's surface, in addition to the text on the front of the gage block.

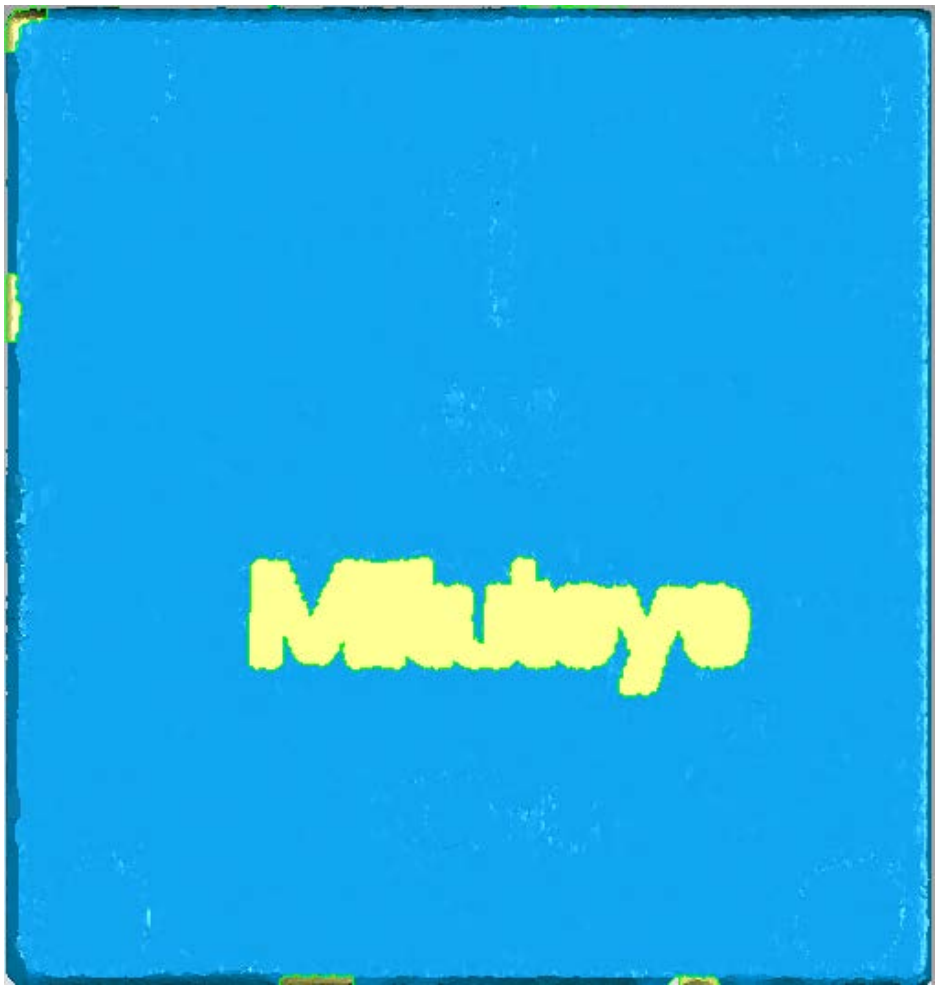

Figure 3.5: 3mm reference points placed on the surface of the three gage blocks.

To combine multiple scans, a minimum of three reference points from the previous scan must be visible on the current scan (ATOS User Manual - Software 2008). On each surface of the gage block, two to four reference points were randomly placed.

These randomly placed points were deleted from the final surface model, insuring that inaccurate data were not collected from the surface of the gage block. The front surface of the gage block had black text displaying the manufacturer, size, and model number of the gage block. This text was not recorded by the cameras due to the non-reflective nature of the text, leaving holes in the point cloud where the writing was located. *Figure 3.6* provides an example of the scanned data collected from the front surface of the gage block. This text was used to correctly orient the scan data during post-processing.

Figure 3.6: Front surface of polygon mesh, image created using scan data from a 1” gage block acquired using the ATOS system.

Point Cloud Acquisition

The procedure for collecting the point cloud data using the ATOS system is outlined below. The gage blocks and ATOS system were previously prepared for scanning. The procedure below was followed for the four measurement volumes:

- The temperature and lighting conditions were checked prior to scanning.
- The gage block was placed in the center of the measurement volume (*Figure 3.7*).
- Scan I was taken at 0°.
- Scan II was taken at 90°.
- Scan III was taken at 180°.
- Scan IV was taken at 270°.
- Scan V was taken at 360° with the gage block rotated 90°.

Each global point cloud was comprised of five local point clouds, taken from different locations around the gage block. These five locations were repeated for each scan in order to keep the scans consistent across all samples at gage block length and measurement volumes. The fringe projector's center of projection was aligned to the gage block's center. The gage block was scanned so the left surface was resting on the surface of the rotating table; this orientation allowed the two inch gage block to fit inside the 90 mm measurement volume. The gage block's position within the projector's measurement volume may be observed in *Figure 3.7.*

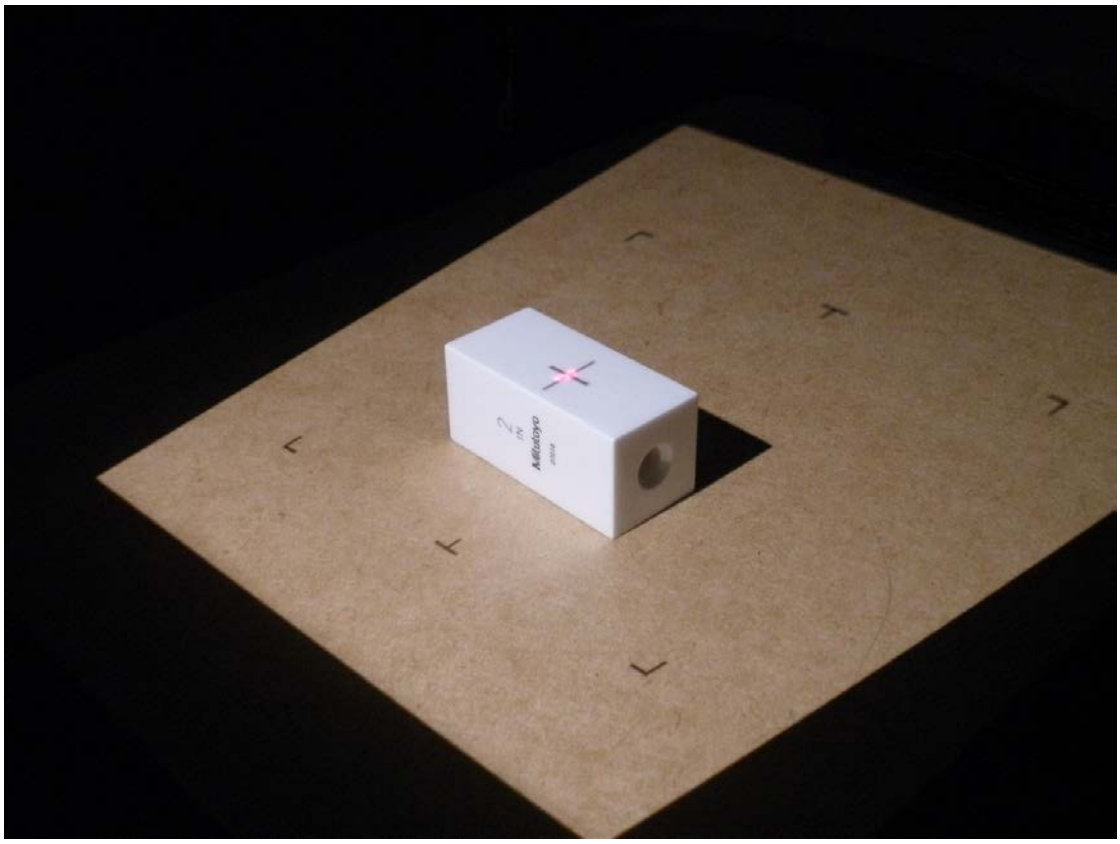

Figure 3.7: Two inch gage block inside the 120mm measurement volume.

The first scan was conducted with the front surface facing the fringe projector. The ATOS system was able to construct a point cloud of both the front surface and the right surface in one scan because the sensor was at a 40° angle from the measurement surface. *Figure 3.8* illustrates the gage block's position during the five scans, as well as the local point clouds generated by each scan.

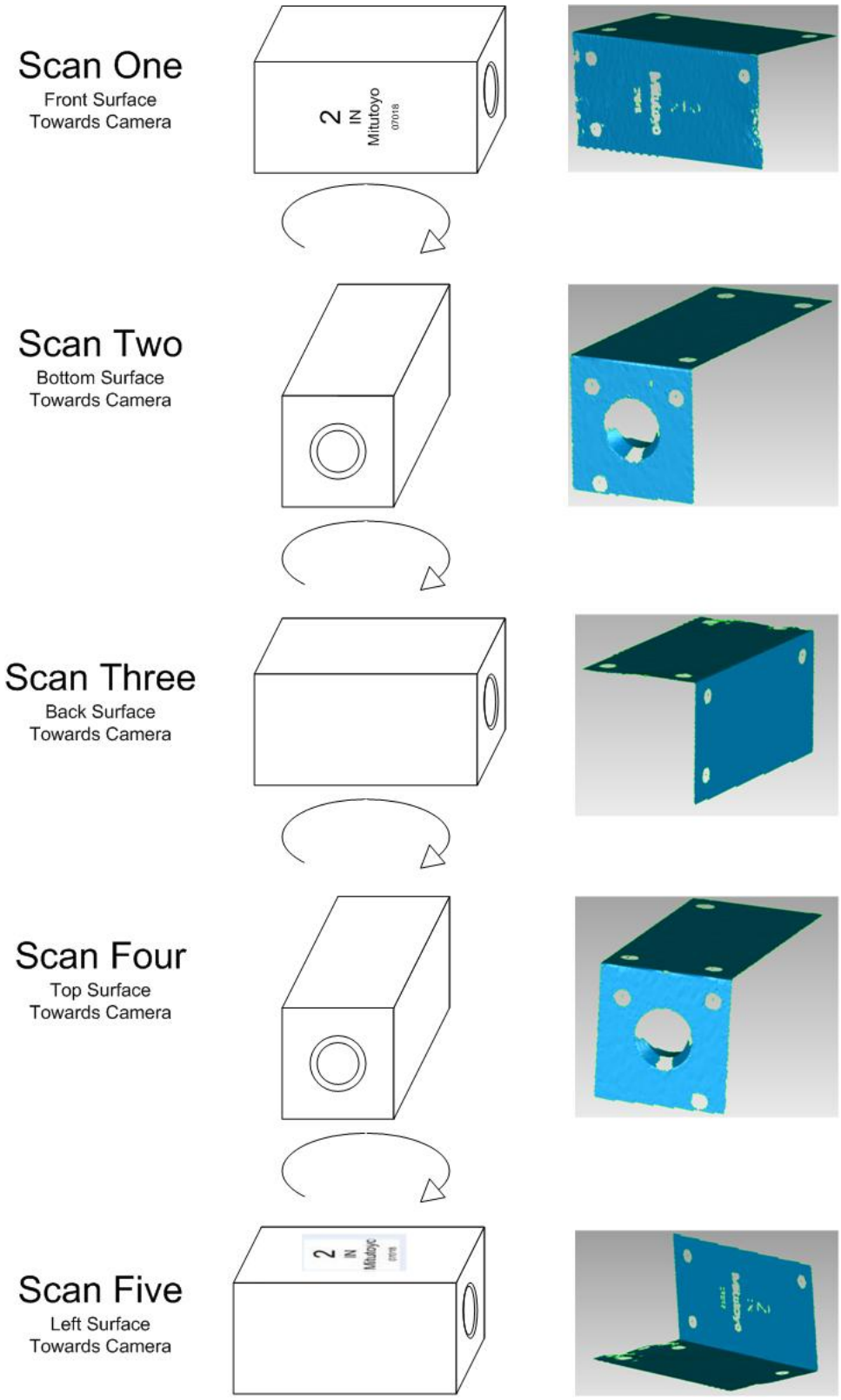

Figure 3.8: Gage block orientation for each scan (left) and local point clouds of the five corresponding scans (right).

For scan II, the table was rotated 90° so the bottom surface faced the fringe projector. The resulting local point cloud contained information for the right surface and the bottom surface. For scan III, the table was rotated an additional 90° facing the gage block's back surface, resulting in a local point cloud of both the right and back surfaces of the gage block. Scan IV was conducted after rotating the table 90° so the top surface of the gage block faced the fringe projector. The fourth scan produced a local point cloud of the right and top surfaces of the gage block. The table was rotated another 90° so the front surface of the gage block once again faced the fringe projector. To measure the gage block's left surface, the block was also rotated 90° so the left surface of the gage block faced the fringe projector and the gage block's back surface lay on the table. The fifth scan produced a local point cloud of the gage block's left and front surfaces. Three replicates for each scan were conducted to insure that the sample mean was representative of the mean for the entire population.

Post-Processing

The procedure for post-processing is outlined below. Post-processing was conducted using both the ATOS software and Geomagic Studio software. The input data into the post-processing process were the five point clouds captured during the point cloud acquisition stage.

- Local point clouds were aligned.
- Local point clouds were combined into a global point cloud using the polygonization process.
- Global point cloud was saved as .g3d file and imported into Geomagic Studio.
- Coordinate axis was set.

- Small abnormalities were repaired.
- Large holes were filled.
- Unwanted data was removed.
- Unwanted points were removed.
- Surfaces were classified as planes.
- Surfaces were created from the classified polygon mesh.
- Surfaces were exported into Pro/Engineer.

Polygonization using ATOS software.

The ATOS User Manual (2008) described polygonization as the process of transforming the point cloud into an editable polygon mesh. D. T. Pham (2008) suggested that polygonization is a required step in the creation of a parametric model. Pham explained that the options available to a polygon mesh, such as hole filling and noise reduction, were important features for downstream processes. Pham found that during the polygonization process, the point clouds are optimized to reduce point redundancy and local point clouds are combined into one global point cloud.

Chapter II explained how the ATOS system uses reference points and photogrammetry to accurately match local point clouds while scanning an object. According to the ATOS User Manual (2008), small systematic deviations still exist between the overlapping areas of local point clouds. The ATOS software's post-processing capabilities can correct these deviations using fine alignment. The fine alignment will allow each reference point to slightly shift to reduce the point cloud's deviation while restricting movement that might be dimension changing.

For each scanned gage block, five local point clouds were generated. These point clouds were closely matched using the reference point method, but a slight deviation remained. A list of the deviations can be found in Appendix A. For each point cloud, the deviations remained within the acceptable limits of the ATOS system that were programmed into the ATOS software. To adjust for the point cloud deviation, the five local point clouds were combined using the ATOS software's fine alignment process. The ATOS User Manual (2008) explained that even after the fine alignment is conducted, randomly distributed deviations in the point cloud still remain due to measuring noise. The randomly distributed deviations were calculated by the software and displayed in the form of intensity of the average measuring noise within the project. A list of the point cloud deviations can be found in Appendix A.

To convert the global point cloud into a polygon mesh, the polygonization process was implemented. The conversion process created triangles between the individual points in the point cloud and created a surface between the points. During the polygonization process, a 1:4 raster is typically used to reduce the number of unneeded triangles in flat areas. The ATOS User Manual (2008) explains the 1:4 raster. In high curvature areas, the initial point density is retained, for medium curvatures the point density is reduced by half, and for flat areas the point density is reduced by 1/4. The differences in mesh density for curved regions can be seen in *Figure 3.9*. To determine the difference between high curvature, medium curvature, and flat areas for the gage block scans, a value of 12 was entered as a surface tolerance. According to the User Manual, the software creates a 4x4 point raster. If the points are further apart than the surface tolerance, the raster is split in half, forming a second 2x2 raster. The 2x2 point raster was

then checked to determine if the points were further apart then the surface tolerance. If the software determined that a raster was within the tolerance, the combined point raster was used for polygonization.

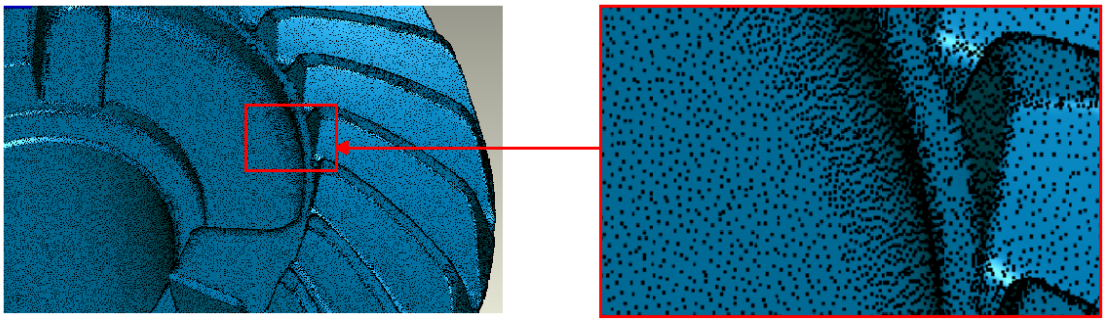

Figure 3.9: Change in point density in curved regions. Image created using scan data from a gear acquired using the ATOS system.

Although the polygonization process offers advanced features such as mesh smoothing, mesh thinning, and mesh regularization, these features are optional and were not performed for the current study. The created polygon mesh was saved as a GOM 3D file format (.g3d). According to GOM (2010), the .g3d file format is used by the ATOS system to store several types of 3D data. For polygon meshes, the .g3d file saved all the information for each point and triangle in the form of Cartesian coordinates.

Developing constraint based solid 3D models.

For the CAD application of reverse engineering, a feature-based parametric 3D model was desired. According to William B. Thompson (1999), feature-based parametric models allow for an accurate model that can be easily implemented into a 3D modeling package. To develop a parametric surface model, the polygon mesh was transferred from the ATOS software to a dedicated post-processing software package. Geomagic Studio® 12 was used to create the parametric model from the polygon meshes created during the

polygonization process from the scanned point clouds. For the current study, Geomagic Studio was used to set a coordinate axis, delete unwanted data, and create parametric surfaces for the scans of the gage block.

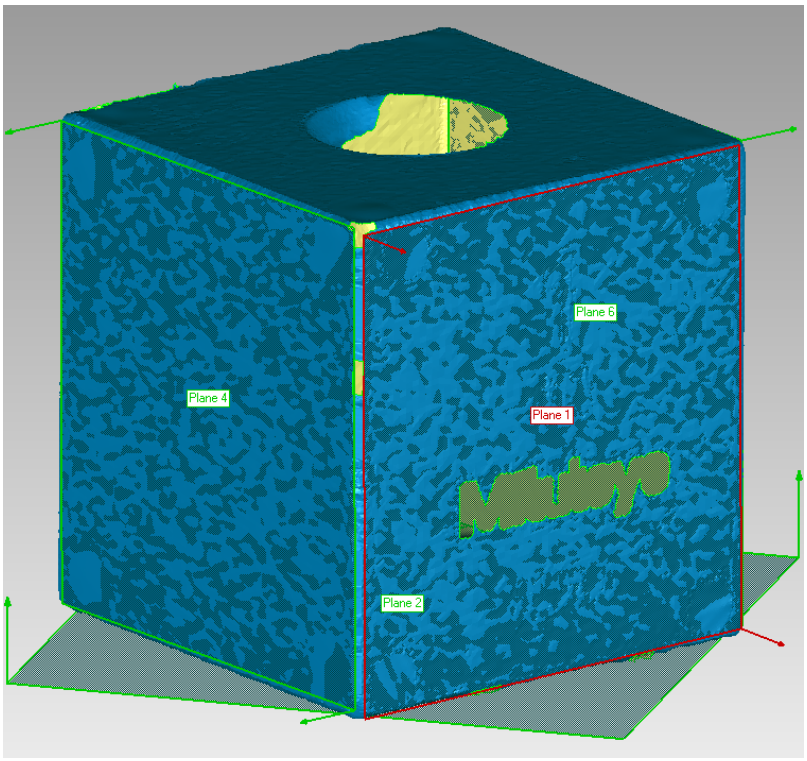

Figure 3.10: Three planes used to locate the CAD data in 3D space, image created using scan data from a 1” gage block acquired using the ATOS system

Once a model was created from the polygon mesh, all discernible features were removed in the creation of the parametric models, leaving only flat surfaces and edges. During the polygonization process, a coordinate axis was automatically created by the ATOS software to determine the X, Y, and Z coordinates for each point. The created coordinate system was based from the sensor's position in the first scan, causing the orientation of the scanned data to be arbitrarily located within the coordinate system. Using Geomagic Studio software, planes were created using a least squares regression

(LRS) of the points that formed the front, left, and bottom surfaces of the polygon mesh. The three planes can be seen in *Figure 3.10*. The polygon mesh was then moved and the newly created bottom plane aligned with the X, Y plane. The left side was aligned with the Y, Z plane and the front aligned with the X, Z plane. *Figure 3.11* illustrates the new position of the gage block based on the coordinate system. With the polygon mesh located in the readjusted orientation, the front, top, and right side of the mesh matched the sides of the Cartesian coordinate system used in parametric modeling packages.

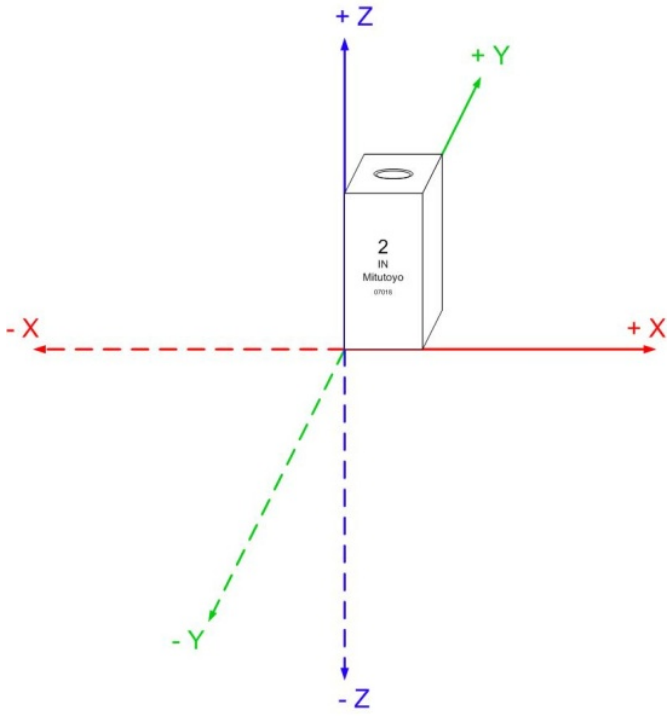

Figure 3.11: Readjusted position of the gage block within the Cartesian coordinate system

Geomagic has a built-in operation to detect and fix small abnormalities within a polygon mesh. Small abnormalities such as small deformations, spikes, high crested edges, self-intersections, and small holes may occur during the polygonization process.

These abnormalities will cause problems when creating a parametric surface from a polygon mesh because the surface model in not continuous where the abnormalities exist. These abnormalities can be seen in *Figure 2.15*, and the resulting polygon mesh after the abnormalities were fixed can be seen in *Figure 2.16*. Larger holes, such as the ones left by the reference points, were filled using Geomagic Studios. To create a patch for the holes, the points surrounding the holes were interpolated using Geomagic to create new points to build the patch.

To reduce the amount of error when creating parametric surfaces, a 1mm wide section was removed from the polygon mesh's edges. A half inch diameter around the gage block's center hole was removed to surround the entire hole. These data were excluded from the polygon mesh to reduce the likelihood that false data, caused by the gage block's rounded edges, were introduced into the final constraint based parametric model. The polygon mesh, after these data were removed, can be seen in *Figure 3.12*.

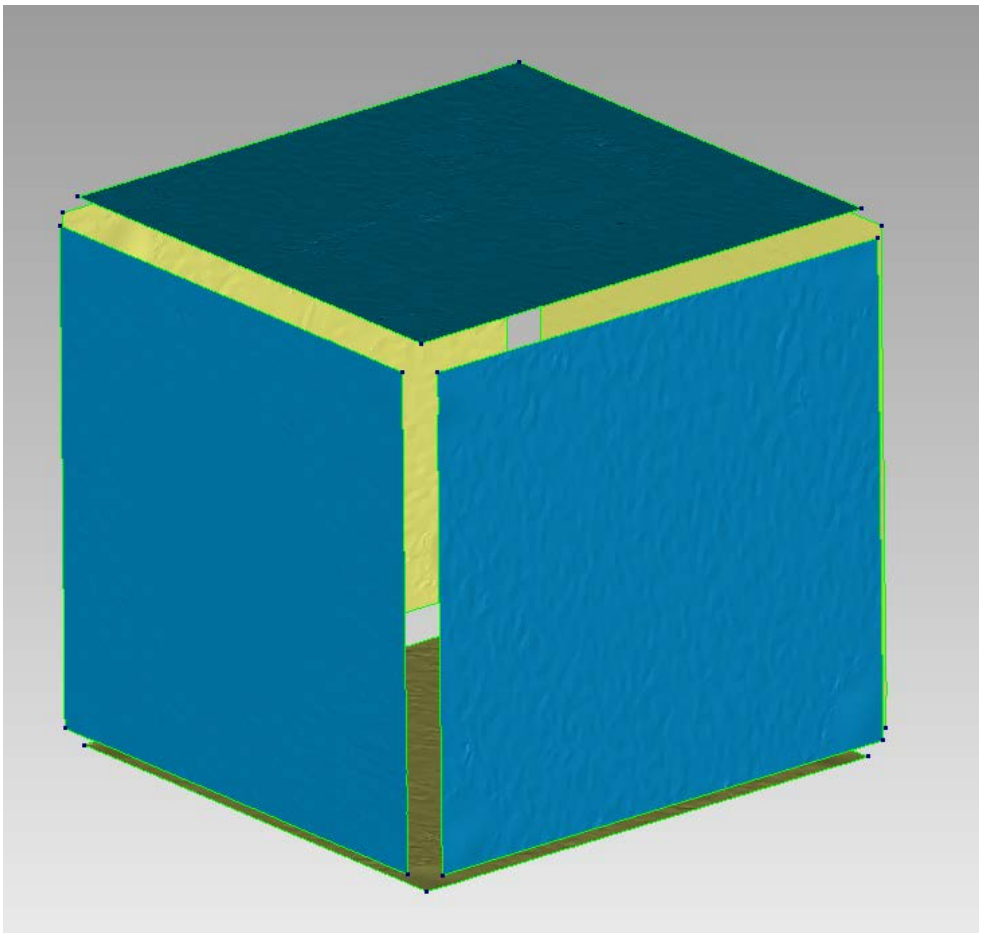

Figure 3.12: Polygon mesh after data were removed from the edges, image created using scan data from a 1” gage block acquired using the ATOS system.

Geomagic uses a parametric surfacing function to detect surface regions and create contour lines along edges. Surfaces are classified as parametric shapes such as planes, spheres, cones, cylinders, extrusions, drafted extrusions, revolves, sweeps, lofts, and free form surfaces. The six regions of the polygon mesh were defined as planes and a contour line formed around each surface. To convert the polygon mesh into a constraint based parametric model, Geomagic Studio used LSR on the points that were defined as planes within the created contours. The LSR determined the best fit plane and created a parametric plane to represent the gage block's surface. The last step in the creation of a

constraint based CAD model was to export the parametric surfaces into a 3D CAD package. Geomagic Studio had the capability to export the surfaces to Pro/Engineer® 5.0 (Pro/E).

Measurement Method

Pro/E is a parametric modeling package that allowed users to create feature based parametric 3D models. For the gage block scan data, Geomagic Studio acts as the user to create parametric surfaces that can be edited within Pro/E. For each parametric model, the six surfaces were extended out until they intersected with the adjacent surfaces. *Figure 3.13* displays the parametric within Pro/E. Points were created at each corner where the three planes intersected, and the measurement function was used to measure the four edges between the top and bottom surfaces (measurement surfaces). *Figure 3.14* illustrates the four edges that were measured.

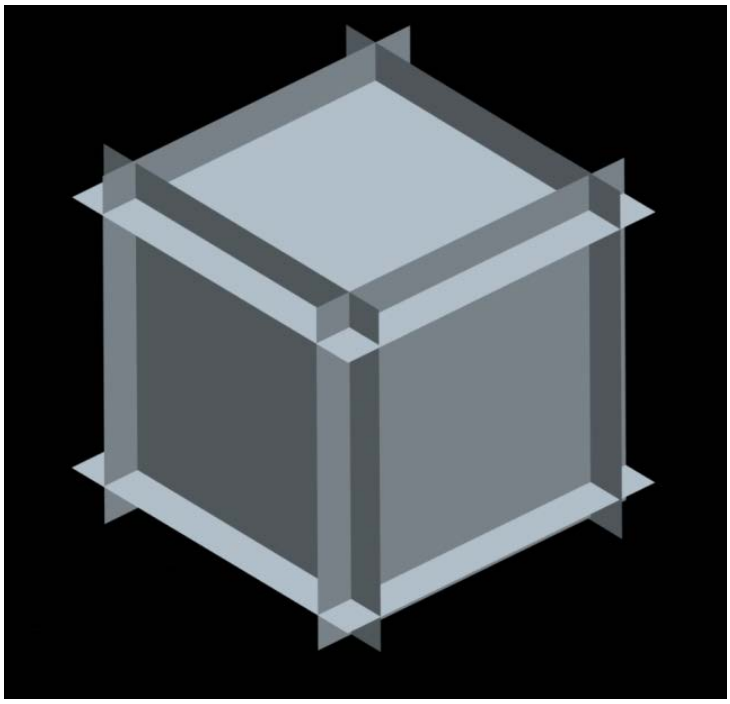

Figure 3.13: Parametric model measured in Pro/Engineer.

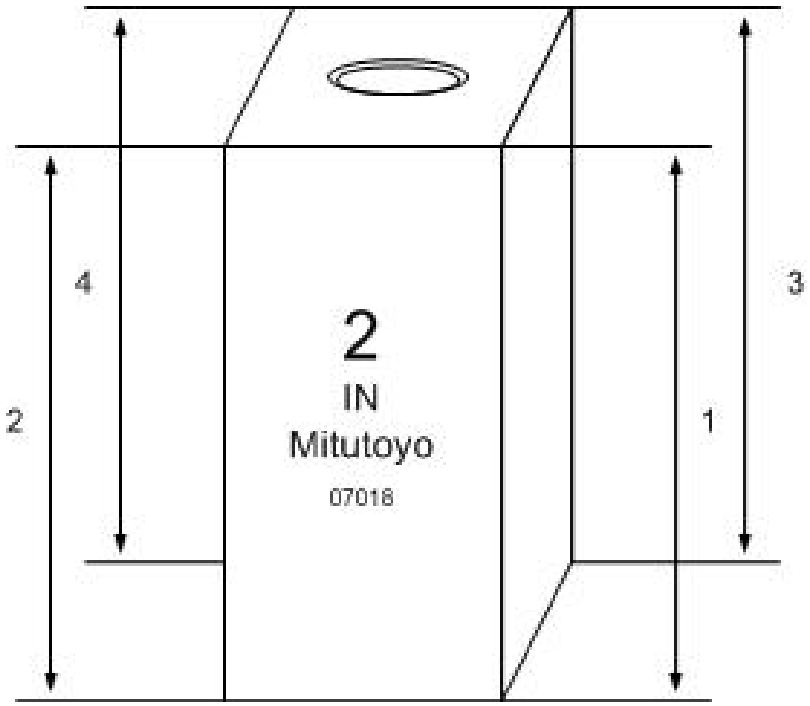

Figure 3.14: Position of the four measurements taken from gage block scan data.

Procedure for Analyzing Data

For the data collected, inferential statistics were used to evaluate the hypotheses presented in Chapter IV. J. Evans states, "Statistical inference is the process of drawing conclusions about unknown characteristics of a population from which data were taken" (J. R. Evans, and W. M. Lindsay, 2005, p. 531). An analysis of variance (ANOVA) and Student t-tests were performed on the data for hypothesis testing.

In hypothesis testing, an alpha value, described by the NIST e-Statistics Handbook (2011) as the amount of risk that the hypothesis could be mistakenly rejected, is used. For the hypotheses in the current study, a .01 α value was chosen, which gave the test a 1% margin of error. To determine if the null hypothesis is retained or rejected, the alpha value is compared to a P-value. The e-Statistics Handbook described the P-value as the probability that a test statistic is at least as extreme as the one observed.

According to the NIST e-Statistics Handbook (2011), limitations exist on the type of data required for the inferential statistics test performed. These limitations required the data to come from a single process, the distributions to be normal, and the data to be uncorrelated over time. The data collected were known to be from a single process and uncorrelated over time, but a test was required to verify if the data was normally distributed. To verify if the data was normally distributed, an Anderson-Darling normality test was conducted on the data. The Anderson-Darling normality test is a hypothesis test that compares the test statistic to a critical value (NIST e-Statistics Handbook 2011).

The NIST e-Statistics Handbook (2011) explained the t-test and how it was used to compare the means of two independent processes. According to the handbook, a t-test is used to test if two means are statistically the same or if one mean is greater or less than the other mean. Using equations 3.1, the *t* statistic can be calculated. Two types of t-tests were used in the current study, a one sample t-test, where the mean of one process was compared to an assumed mean, and the two sample t-test where the means of two independent processes were compared.

$$t = \frac{\bar{Y} - \mu_o}{s/\sqrt{N}} \tag{3.1}$$

D. Schiff (1996) described the ANOVA as a statistical test to identify differences in means and to identify the means that are significantly different. Two types of ANOVAs were performed for the current study: a one-way ANOVA and a general linear model using three factors. Schiff states that the one-way ANOVA “involves data sampled

from two or more populations or treatments, or two or more different levels of factors" (D. Schiff, and R. Agostino, 1996, pp 144-145). According to the NIST e-Statistics Handbook (2011), an ANOVA splits the data into components attributable to the different levels of the factors. For a one-way ANOVA, a single factor with multiple levels and observations. The ANOVA was also used to analyze the general linear model. According to StatSoft, Inc (2011), the general linear model allows for linear transformations or linear combinations of multiple dependent variables. This allowed insight into which factors were and were not related to one another.

CHAPTER 4: ANALYSIS AND RESULTS

The purpose of the current thesis was to characterize the accuracy of constraint-based 3D models. These 3D models were created using Geomagic Studio reverse engineering software and scan data collected by an ATOS system. Chapter IV presents and analyzes the data collected using Pro/E. To analyze the data collected, hypothesis testing was conducted to compare the data and inferential statistics were applied. The statistical tests include one-sample t-tests to compare data with the NIST certified gage blocks, two-sample t-tests to compare edges between the different measurement volumes, a General Linear Model (GLM), and multiple 1-way ANOVA. By assessing these statistical tests, a better understanding of the raw data was developed to characterize the accuracy of the reverse engineering process.

Normal Probability Test

The Anderson-Darling normal probability test is one-sided, with a hypothesis that stated the distribution is normal. The data from each measurement volume were plotted, and the p-values were found to all be greater than the .01 alpha value. The p-values inferred that the distribution of measurements was normally distributed. The normal probability plots can be viewed in *Figure 4.1-4.4.* The data were plotted against theoretical normal distributions. If the data were normally distributed, the points would form a straight line.

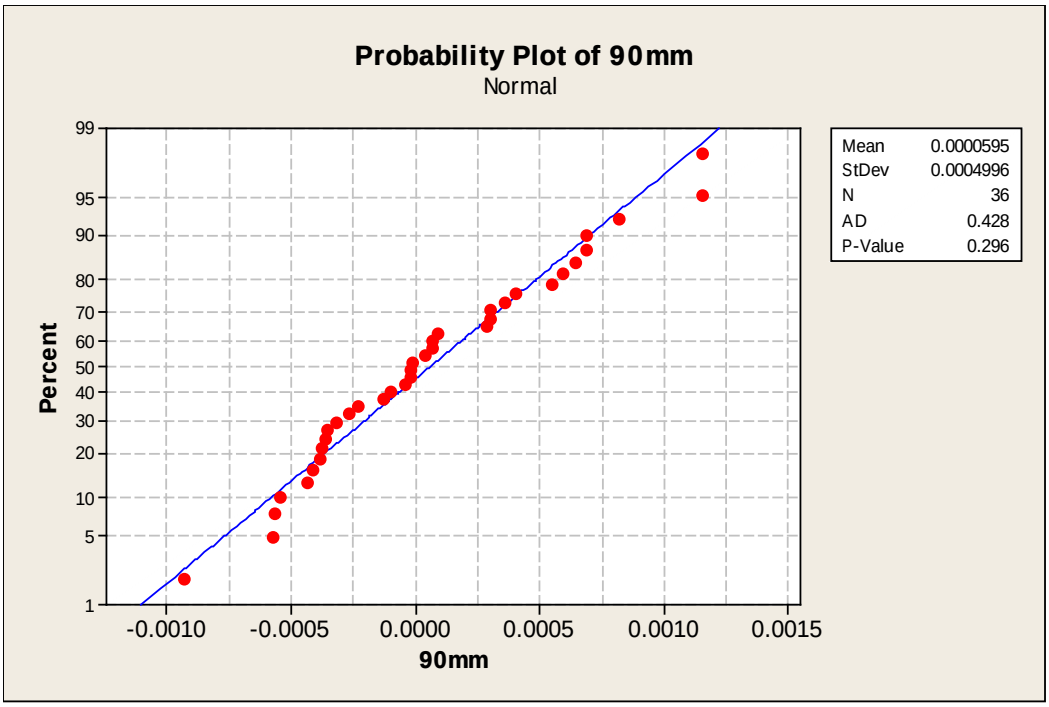

Figure 4.1: Normal probability plot for 90mm measurement volume

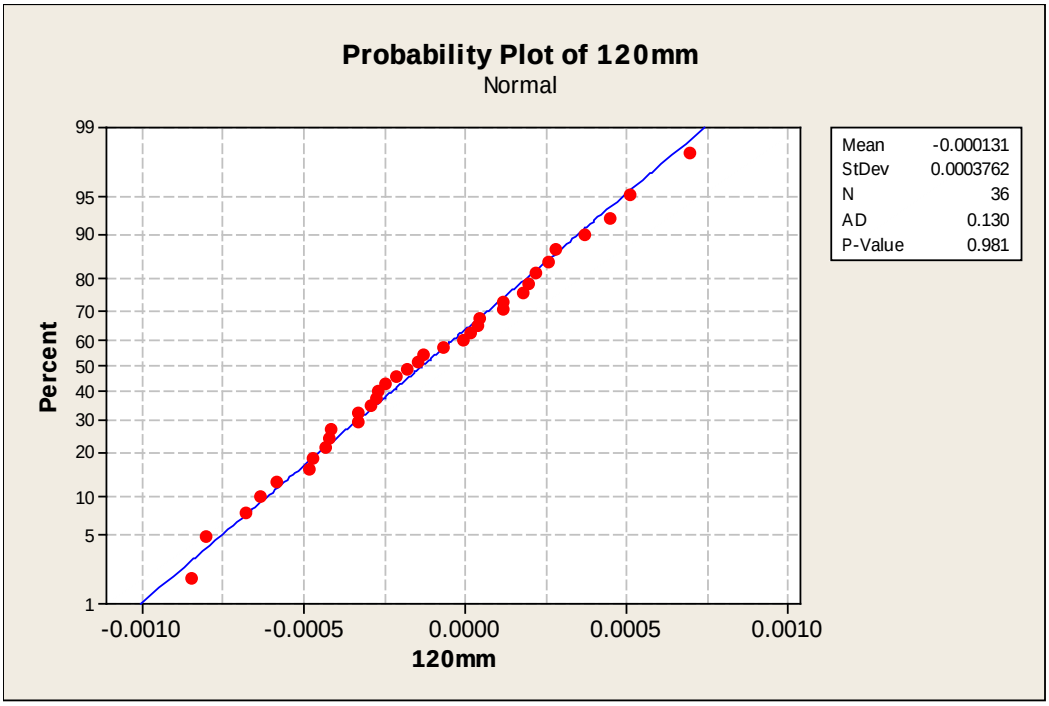

Figure 4.2: Normal probability plot for 120mm measurement volume

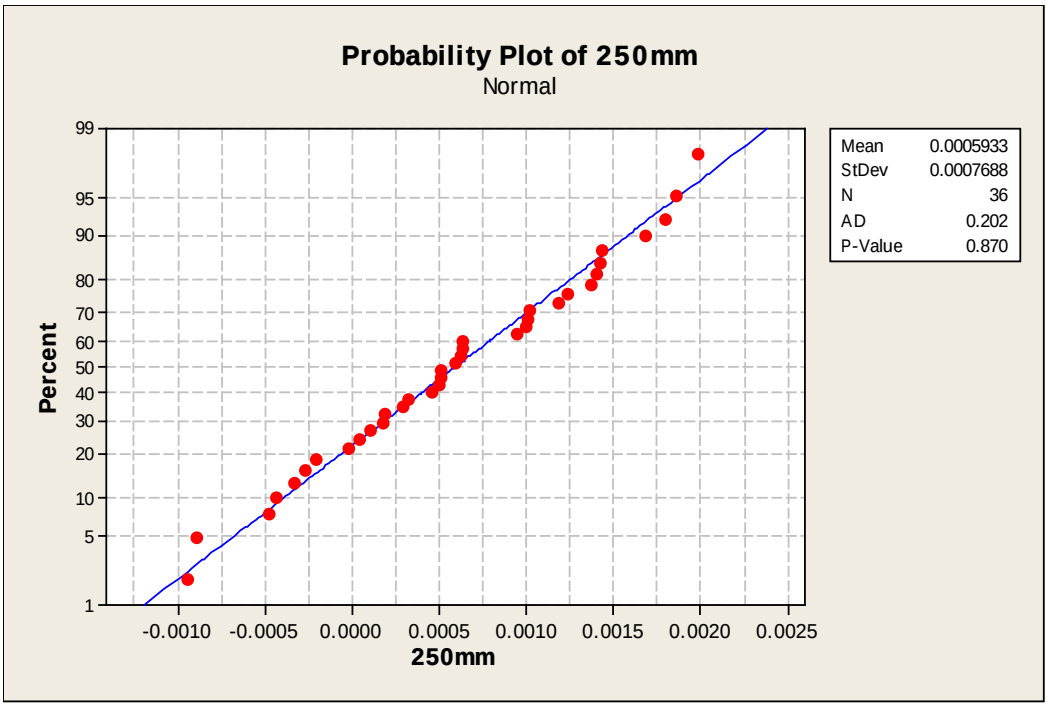

Figure 4.3: Normal probability plot for 250mm measurement volume

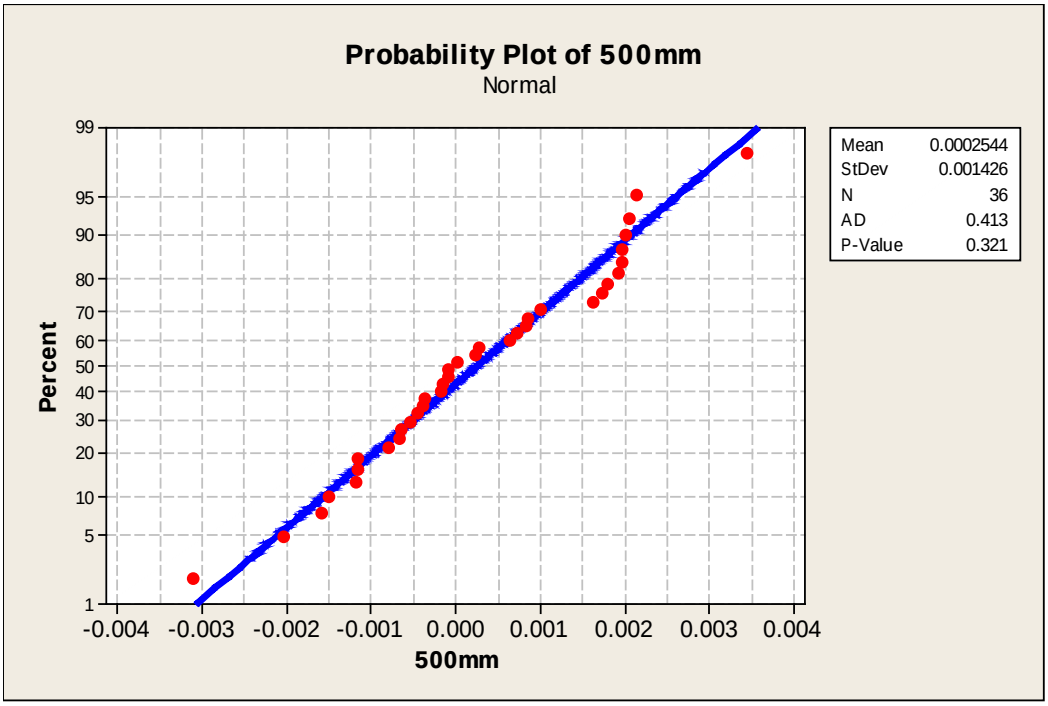

Figure 4.4: Normal probability plot for 500mm measurement volume

Data collected from the measurement process may be viewed in Appendix B. The four measurements collected from each scan were averaged together with the three replicates, resulting in a completed mean for each gage block size for the four measurement volumes. These means, along with other descriptive statistics, are presented in *table 4.1.*

Table 4.1

Descriptive statistics

Measurement Volume	**90mm**			**120mm**		
Gage Block Size	**1.000000**	**2.000000**	**0.500000**	**1.000000**	**2.000000**	**0.500000**
Maximum	1.000690	2.001150	0.499987	1.000120	2.000700	0.500047
Minimum	0.999071	2.000040	0.499431	0.999418	2.000020	0.499152
Range	0.001619	0.001110	0.000556	0.000702	0.000680	0.000895
Mean	0.999961	2.000563	0.499654	0.999763	2.000279	0.499565
Standard deviation	0.000403	0.000361	0.000186	0.000201	0.000199	0.000271

Measurement Volume	**250mm**			**500mm**		
Gage Block Size	**1.000000**	**2.000000**	**0.500000**	**1.000000**	**2.000000**	**0.500000**
Maximum	1.001000	2.001980	0.500636	1.002060	2.002140	0.503443
Minimum	0.999670	2.001010	0.499053	0.998421	1.999460	0.496888
Range	0.001330	0.000970	0.001583	0.003639	0.002680	0.006555
Mean	1.000374	2.001449	0.499957	0.999835	2.001043	0.499886
Standard deviation	0.000413	0.000321	0.000560	0.001268	0.000959	0.001711

One Sample t-test

One sample, two tailed t-tests were performed on the means of the measured length to determine if the means were statistically equal to the NIST certified gage block length. For the one sample t-test, the null hypothesis stated that the sample mean ($\mu_{measured}$) was equal to the true population (μ_{actual}), where the population mean was the NIST specified length for the gage blocks, and the measured mean was the average of the

four measurements and the three replicates for each gage block length under each measurement volume. The null hypothesis for each of the one sample t-tests was:

$$H_O: \mu_{measured} = \mu_{actual}$$

The alternative hypothesis for the one sample t-tests stated that the population mean was not equal to the sample mean. The alternative hypothesis was:

$$H_A: \mu_{measured} \neq \mu_{actual}$$

If the null hypothesis fails to be rejected, then there will be a low variation between the measured observations and the actual certified values; therefore, the mean measured will be equal to the actual NIST certified length. However, if the null hypothesis is rejected, statistical data will show the two means are not equal.

T-tests were performed on the averages from the three different object sizes scanned with the four different measurement volumes. The average was comprised of the four length measurements taken from the three replicates resulting in a total of twelve separate t-tests. A summary of the results from these t-tests can be viewed in *table 4.2*. Appendix C presents the full data from the one sample t-test performed.

Table 4.2

Results from one sample t-test using an alpha of .01

	Variable	N	Mean	StDev	SE Mean	99% CI	T	P
Half Inch	90mm	12	0.499654	0.000186	0.000054	0.499487 0.499820	-6.46	0.000
	120mm	12	0.499565	0.000271	0.000078	0.499322 0.499808	-5.57	0.000
	250mm	12	0.499957	0.000560	0.000162	0.499455 0.500459	-0.26	0.796
	500mm	12	0.499886	0.001711	0.000494	0.498351 0.501420	-0.23	0.821
One Inch	90mm	12	0.999961	0.000403	0.000116	0.999600 1.000323	-0.33	0.745
	120mm	12	0.999763	0.000201	0.000058	0.999583 0.999943	-4.08	0.002
	250mm	12	1.000370	0.000410	0.000120	1.000000 1.000740	3.13	0.010
	500mm	12	0.999835	0.001268	0.000366	0.998698 1.000972	-0.45	0.661
Two Inch	90mm	12	2.000560	0.000360	0.000100	2.000240 2.000890	5.41	0.000
	120mm	12	2.000280	0.000200	0.000060	2.000100 2.000460	4.85	0.001
	250mm	12	2.001450	0.000320	0.000090	2.001160 2.001740	15.660	0.000
	500mm	12	2.001040	0.000960	0.000280	2.000180 2.001900	3.770	0.003

For the one sample t-test, an alpha value of .01 was used. Findings from the twelve t-tests revealed the null hypothesis was retained for the 250mm and 500mm measurement volumes for the half inch object size, and the 90mm and 500mm measurement volumes for the one inch object size. Results where p is less than .01

indicated that a statistically significant difference exists between the measured means compared to the actual mean. Similarly results where the p-value was above .01 indicated non-statistical differences in mean dimensions of actual vs. measured.

The gage blocks had a small tolerance window of less than five micro inches (for the gage blocks' exact specifications, reference Appendix A). One sample t-tests were conducted using actual values of 1.000005 and 0.999995 inches, to cover the upper and lower tolerances of the gage blocks. The first t-tests that were conducted used an actual mean that was five micro inches greater than the NIST certified gage block's size. The second t-tests used an actual mean that was five micro inches less than the NIST certified gage block's size. For the actual means that were greater and less than the NIST certified length, the results found the null hypothesis was retained for the 250mm and 500mm measurement volumes for the half inch object size, and the 90mm and 500mm measurement volumes for the one inch object size. The results from the t-tests are presented in Appendix C. Because the same measurement volumes showed significance from using 1.000005 and 0.999995 as the actual means the deviations in gage block length had no effect on the statistical significance of the t-test.

F-test

F-tests were performed to compare the standard deviations of one measurement volume to the standard deviations of the other three measurement volumes. For the F-test, the null hypothesis stated that standard deviation for two independent measurement volumes were equal for a given object's size. The null hypothesis used for the F-test was:

$$H_0: \sigma_{\text{measurement volume 1}} = \sigma_{\text{measurement volume 2}}$$

The alternative hypothesis for the F-test stated that the standard deviation of the first process was not equal to the standard deviation for the second process. Essentially, the measurements where the null hypothesis was retained showed that the measured gage block dimension matched the nominal value, certified to the NIST standard. The alternative hypothesis was:

$$H_A: \sigma_{\text{measurement volume 1}} \neq \sigma_{\text{measurement volume 2}}$$

The results for each F-test performed are presented in Appendix D. A summary of the results can be viewed in *table 4.3*.The P-value was compared to an alpha value of 0.01, and the null hypothesis rejected for P-values greater than the alpha value. The null hypothesis was rejected for the 90mm vs. 120mm, 90mm vs. 250mm, and 120mm vs. 250mm for both the one and two inch object sizes. Additionally, the null hypothesis was rejected for the 90mm vs. 120mm and 120mm vs. 250mm measurement volumes for the half inch object size. Performing these tests demonstrated that for the cases in which the null hypothesis was rejected, the distributions were said to be unequal. Tests in which the null hypothesis was retained suggested the two standard deviations were equal.

Table 4.3

F-test results

		N	Lower	StDev	Upper	T stat	P-value	
One Inch	**90mm**	12	0.000250	0.000403	0.000895	4.020	0.030	*
	120mm	12	0.000124	0.000201	0.000446			
	90mm	12	0.000250	0.000403	0.000895	0.950	0.936	*
	250mm	12	0.000256	0.000413	0.000918			
	90mm	12	0.000250	0.000403	0.000895	0.100	0.001	
	500mm	12	0.000785	0.001268	0.002815			
	120mm	12	0.000124	0.000201	0.000446	0.240	0.025	*
	250mm	12	0.000256	0.000413	0.000918			
	120mm	12	0.000124	0.000201	0.000446	0.030	0.000	
	500mm	12	0.000785	0.001268	0.002815			
	250mm	12	0.000256	0.000413	0.000918	0.110	0.001	
	500mm	12	0.000785	0.001268	0.002815			
Two Inch	**90mm**	12	0.000223	0.000361	0.000801	3.270	0.061	*
	120mm	12	0.000123	0.000199	0.000443			
	90mm	12	0.000223	0.000361	0.000801	1.270	0.702	*
	250mm	12	0.000198	0.000321	0.000712			
	90mm	12	0.000223	0.000361	0.000801	0.140	0.003	
	500mm	12	0.000593	0.000959	0.002128			
	120mm	12	0.000123	0.000199	0.000443	0.390	0.131	*
	250mm	12	0.000198	0.000321	0.000712			
	120mm	12	0.000123	0.000199	0.000443	0.040	0.000	
	500mm	12	0.000593	0.000959	0.002128			
	250mm	12	0.000198	0.000321	0.000712	0.110	0.001	
	500mm	12	0.000593	0.000959	0.002128			
	90mm	12	0.000115	0.000186	0.000412	0.470	0.226	*
Half Inch	**120mm**	12	0.000168	0.000271	0.000601			
	90mm	12	0.000115	0.000186	0.000412	0.110	0.001	
	250mm	12	0.000347	0.000560	0.001243			
	90mm	12	0.000115	0.000186	0.000412	0.010	0.000	
	500mm	12	0.001059	0.001711	0.003799			
	120mm	12	0.000168	0.000271	0.000601	0.230	0.024	*
	250mm	12	0.000347	0.000560	0.001243			
	120mm	12	0.000168	0.000271	0.000601	0.030	0.000	
	500mm	12	0.001059	0.001711	0.003799			
	250mm	12	0.000347	0.000560	0.001243	0.110	0.001	
	500mm	12	0.001059	0.001711	0.003799			

Two Sample t-test

Two sample t-tests were performed to compare the mean of one measurement volume to each of the means of the other three measurement volumes. For the two sample t-test, the null hypothesis stated that the measured mean for two independent measurement volumes are equal for a given object's size. The null hypothesis used for the two sample t-test was:

$$H_0: \mu_{\text{measurement volume 1}} = \mu_{\text{measurement volume 2}}$$

The alternative hypothesis for the two sample t-test stated that the measured mean of the first process was not equal to the measured mean for the second process. The alternative hypothesis was:

$$H_A: \mu_{\text{measurement volume 1}} \neq \mu_{\text{measurement volume 2}}$$

Twenty- seven two sample t-tests were performed to compare the means of each measurement volume, for all four measurement volumes, for the three object sizes. The results of the two sample t-tests can be viewed in Appendix D; a summary of the results are presented in *table 4.4.* Comparing the p-values to a 0.01 alpha value, the null hypothesis was rejected for the one inch object size at the 120mm vs. 250mm measurement volumes and the two inch object size at the 90mm vs. 250mm and 120mm vs. 250mm measurement volumes. Results where p was less than .01 indicated statistically significant differences existed between the two means measured. Results where the p-value was above 0.01 indicated a non-statistical difference in the means of the two measurement volumes.

Table 4.4:

Results from two sample t-tests.

		N	Mean	StDev	SE Mean	T Stat	P-Value	
One Inch	90mm	12	0.999961	0.000403	0.000120	1.520	0.142	
	120mm	12	0.999763	0.000201	0.000058			
	90mm	12	0.999961	0.000403	0.000120	-2.470	0.022	
	250mm	12	1.000374	0.000413	0.000120			
	90mm	12	0.999961	0.000403	0.000120	0.330	0.748	
	500mm	12	0.999840	0.001270	0.000370			
	120mm	12	0.999763	0.000201	0.000058	-4.600	0.000	*
	250mm	12	1.000374	0.000413	0.000120			
	120mm	12	0.999763	0.000201	0.000058	-0.190	0.850	
	500mm	12	0.999840	0.001270	0.000370			
	250mm	12	1.000374	0.000413	0.000120	1.400	0.185	
	500mm	12	0.999840	0.001270	0.000370			
Two Inch	90mm	12	2.000563	0.000361	0.000100	2.390	0.026	
	120mm	12	2.000279	0.000199	0.000058			
	90mm	12	2.000563	0.000361	0.000100	-6.360	0.000	*
	250mm	12	2.001449	0.000321	0.000093			
	90mm	12	2.000563	0.000361	0.000100	-1.620	0.127	
	500mm	12	2.001043	0.000959	0.000280			
	120mm	12	2.000279	0.000199	0.000058	-10.740	0.000	*
	250mm	12	2.001449	0.000321	0.000093			
	120mm	12	2.000279	0.000199	0.000058	-2.700	0.021	
	500mm	12	2.001043	0.000959	0.000280			
	250mm	12	2.001449	0.000321	0.000093	1.390	0.187	
	500mm	12	2.001043	0.000959	0.000280			
Half Inch	90mm	12	0.499654	0.000186	0.000054	0.940	0.357	
	120mm	12	0.499565	0.000271	0.000078			
	90mm	12	0.499654	0.000186	0.000054	1.780	0.098	
	250mm	12	0.499957	0.000560	0.000160			
	90mm	12	0.499654	0.000186	0.000054	-0.470	0.650	
	500mm	12	0.499890	0.001710	0.000490			
	120mm	12	0.499565	0.000271	0.000078	-2.190	0.040	
	250mm	12	0.499957	0.000560	0.000160			
	120mm	12	0.499565	0.000271	0.000078	-0.640	0.534	
	500mm	12	0.499890	0.001710	0.000490			
	250mm	12	0.499957	0.000560	0.000160	0.140	0.893	
	500mm	12	0.499890	0.001710	0.000490			

* indicates results where $P < \alpha$

General Linear Model

To further analyze the data, a general linear model (GLM) was constructed to compare the analysis of variance for all three factors (main effects) and the interactions between factors. In order to compare data between gage block lengths, the data had to be normalized so that each variable was on the same scale. Normalization of the data was performed by calculating the deviation of the measured length from the actual value. The deviations for each measurement may be viewed in Appendix B. For the GLM, the 144 variables were arranged into a one column matrix and used as the response variable for the GLM. A second matrix contained the design for the GLM using dummy coding for the four individual measurements, the three gage block sizes, and the four measurement volumes. The response matrix and the design matrix can be viewed in Appendix F. The null hypothesis for the ANOVA for the GLM of main effects and interactions stated that the individual cells are statistically equal to all the other cells of the experimental design representing levels within measurement volume, measurement, and object size.

$$H_0: \mu_{ij} = \mu_{ij} \text{ for all ij}$$

Where the alternative hypothesis stated that at least one individual cell is different from the other cells of the experimental design representing levels within measurement volume, measurement, and object size.

$$H_A: \mu_{ij} \neq \mu_{ij} \text{ for at least one or more ij}$$

In this hypothesis, ij representd the variable levels in measurement volume, measurement, and object size. The results of the ANOVA can be viewed in *table 4.5*and a plot of the interactions is shown in *Figure 4.5.*

Table 4.5

Results of ANOVA for general linear model of main effects and interactions

Analysis of Variance for C1, using Adjusted SS for Tests

Source	DF	Seq SS	Adj SS	Adj MS	F	P	
Volume	3	0.0000103	0.0000103	0.0000034	5.80	0.001	*
Measurement	3	0.0000027	0.0000027	0.0000009	1.54	0.210	
Size	2	0.0000306	0.0000306	0.0000153	25.76	0.000	*
Volume*Measurement	9	0.0000034	0.0000034	0.0000004	0.64	0.757	
Volume*Size	6	0.0000032	0.0000032	0.0000005	0.91	0.492	
Measurement*Size	6	0.0000024	0.0000024	0.0000004	0.67	0.672	
Volume*Measurement*Size	18	0.0000062	0.0000062	0.0000003	0.58	0.907	
Error	96	0.0000570	0.0000570	0.0000006			
Total	143	0.0001159					

S = 0.000770537 R-Sq = 50.82% R-Sq(adj) = 26.74%

* indicates results where P < α

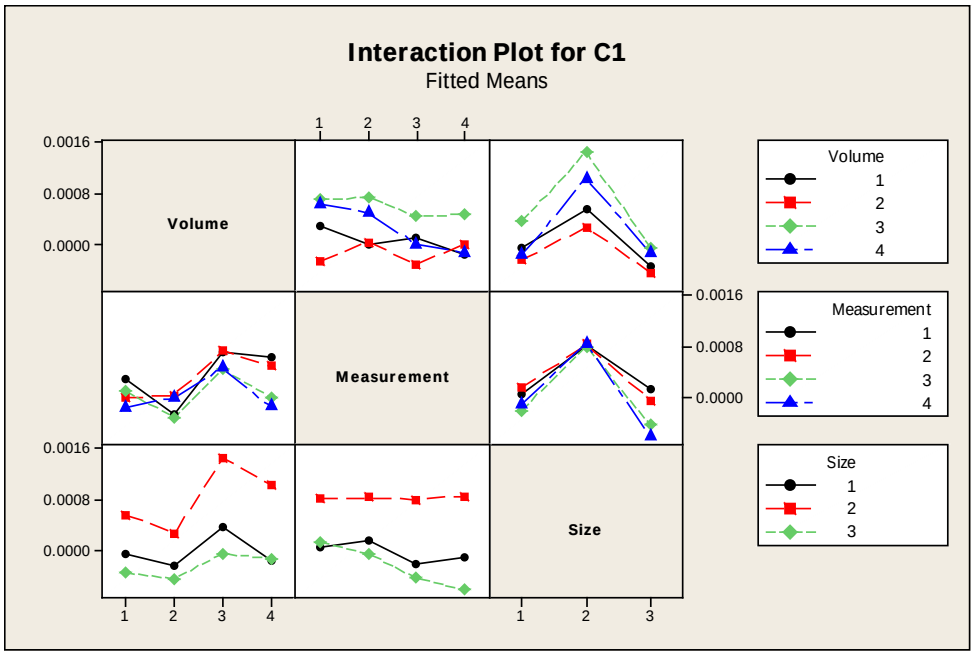

Figure 4.5: Interactions plot for measurement volume, object size and measurement location

Using an alpha value of 0.01, the p-values were compared and a statistical difference was found in the main effects of object size and measurement volume, therefore the null hypothesis was rejected. Although the null hypothesis was rejected, the measurement main effect and all the interactions had a p-value greater than 0.01 indicating non-statistical differences in the means.

Since no significant interactions were found, a second GLM was conducted, this time using only the main effects. The null and alternative hypothesis was assumed to be the same for the second GLM as with the first GLM. The same matrixes were used for the response variable and the dummy coding as were used in the first GLM. These matrixes can be viewed in Appendix C. The results of the ANOVA performed on the GLM, for main effects only can be viewed in *table 4.6.* A plot for the main effects can be viewed in *Figure 4.6*. As with the first GLM, an alpha value of 0.01 was compared to the p-values. A statistical difference was detected in the object size and measurement volume and the null hypothesis was rejected. The measurement once again showed a non-statistical difference.

Table 4.6

Results of ANOVA for general linear model of main effects only

Source	DF	Seq SS	Adj SS	Adj MS	F	P	
Volume	3	0.0000103	0.0000103	0.0000034	6.43	0.000	*
Measurement	3	0.0000027	0.0000027	0.0000009	1.71	0.169	
Size	2	0.0000306	0.0000306	0.0000153	28.57	0.000	*
Error	135	0.0000723	0.0000723	0.0000005			
Total	143	0.0001159					

S = 0.000731571 R-Sq = 37.66% R-Sq(adj) = 33.97%

* indicates results where P < α

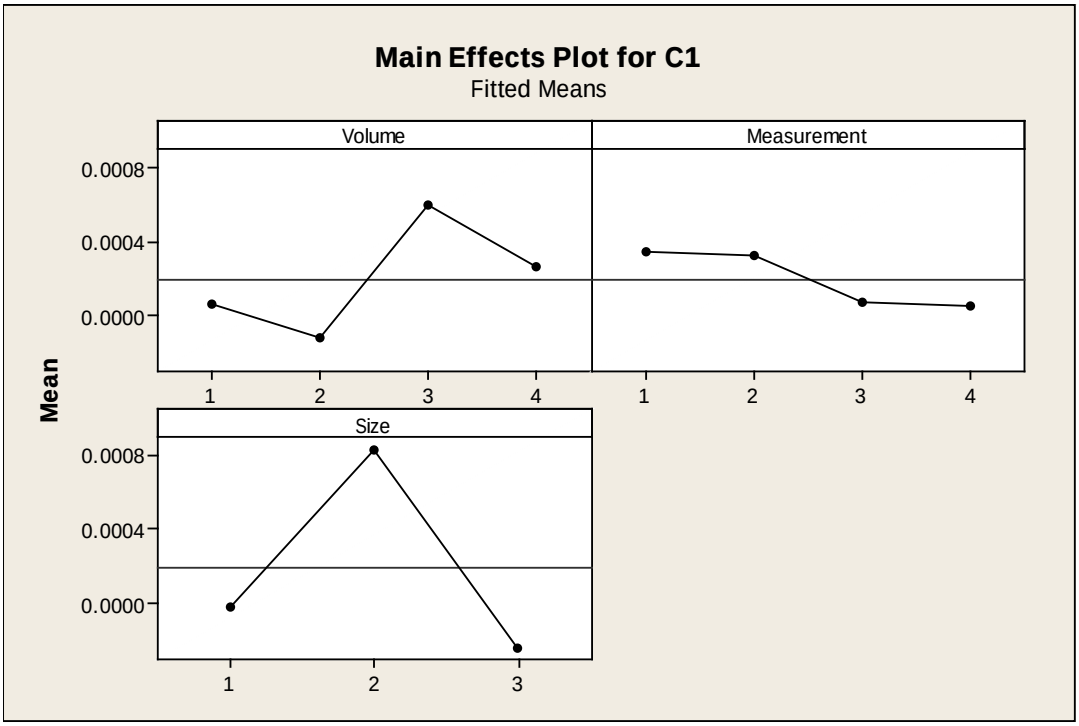

Figure 4.6: Main effects plot from the GLM on the main effects.

To identify patterns within the ANOVA, a Tukey post hoc comparison was conducted. The post hoc comparison will present p-values for the individual levels within each effect. Results of the post hoc comparison are presented in *table 4.7*. Comparisons are presented for measurement volume, measurement, and object size. The post hoc comparison showed that for an alpha of .01, the null hypothesis was rejected for 120mm vs. 250mm measurement volumes, and the one inch vs. two inch and two inch vs. half inch object sizes. Results where p is less than .01 indicated that a statistically significant difference exists between the two factors. Results where the p-value was above 0.01 indicate non-statistical differences in the factors.

The results from the post-hoc comparison test suggested that the statistical significance found by the GLM for measurement volume were between the means for the 120mm volume and 250mm volume. The post hoc comparison showed that the 120mm

measurement volume was statistically different than the 250mm volume. For all other relationships in measurement volume, the post hoc test suggested that no statistical difference existed. Additionally, the statistical significance found by the GLM for object size was between the one inch and two inch, and half inch and two inch gage blocks. The post hoc comparison suggested that the only relationship within object size that was not shown to be statistically different was between the one inch and half inch object sizes.

Table 4.7

Results from Tukey post hoc comparison test

Measurement volume				
	90mm	**120mm**	**250mm**	**500mm**
90mm		0.721	0.211	0.707
120mm			0.001	0.154
250mm				0.25

measurement				
	1	**2**	**3**	**4**
1		0.999	0.416	0.373
2			0.495	0.450
3				1.000

Object Size			
	One Inch	**Two Inch**	**Half Inch**
One Inch		0.000	0.352
Two inch			0.000

Analysis of Variance (ANOVA)

To better understand the relationship between the four measurement volumes, the normalized data were arranged so a one-way ANOVA could be conducted across the four measurement volumes. The new arrangement of data may be viewed in Appendix G along with the results of the ANOVA conducted. The null hypothesis for the ANOVA on measurement volume stated that the means for the four measurement volume are all equal.

$$H_0: \mu_{90mm} = \mu_{120mm} = \mu_{250mm} = \mu_{500mm}$$

The alternative hypothesis for the ANOVA on measurement volume stated that at least one of the four means is not equal. Results from the ANOVA on measurement volume are given in *table 4.8.* A box plot for the data is also provided in *Figure 4.7.* An 0.01 α was used and the null hypothesis rejected, indicating that the four means of the measurement volumes are not statistically equal.

Table 4.8

Results from ANOVA on measurement volume

Source	DF	SS	MS	F	P
Factor	3	0.0000103	0.0000034	4.56	0.004
Error	140	0.0001056	0.0000008		
Total	143	0.0001159			

S = 0.0008684 R-Sq = 8.91% R-Sq(adj) = 6.96%

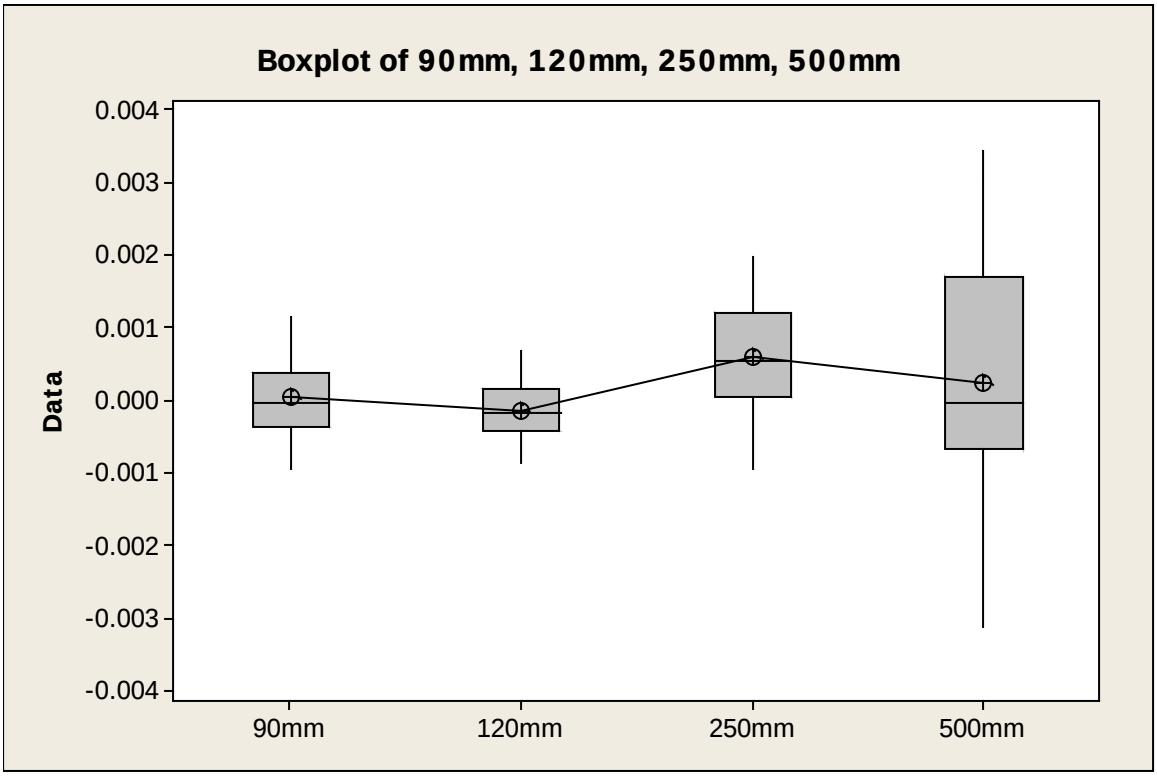

Figure 4.7: Box plot for measurement volume.

An ANOVA was also performed to gather a more detailed understanding between the three object sizes. The normalized data was arranged so a one-way ANOVA could be conducted across the three object sizes. The new arrangement of data may be viewed in appendix G. The null hypothesis for the ANOVA on object size stated that the means for the three sizes were all equal.

$$H_0: \mu_{1"} = \mu_{2"} = \mu_{0.5"}$$

The alternative hypothesis for the ANOVA on object size stated that at least one of the three means is not equal. Results from the ANOVA on object size are given in *table 4.9.* A box plot for the data is also provided in *Figure 4.8.* A 0.01 α was compared

to the p-value. The null hypothesis was rejected, indicating that the three means for the object sizes were not statistically equal.

Table 4.9

Results for ANOVA on object size

Source	DF	SS	MS	F	P
Factor	2	0.0000306	0.0000153	25.27	0.000
Error	141	0.0000853	0.0000006		
Total	143	0.0001159			

S = 0.0007779 R-Sq = 26.39% R-Sq(adj) = 25.34%

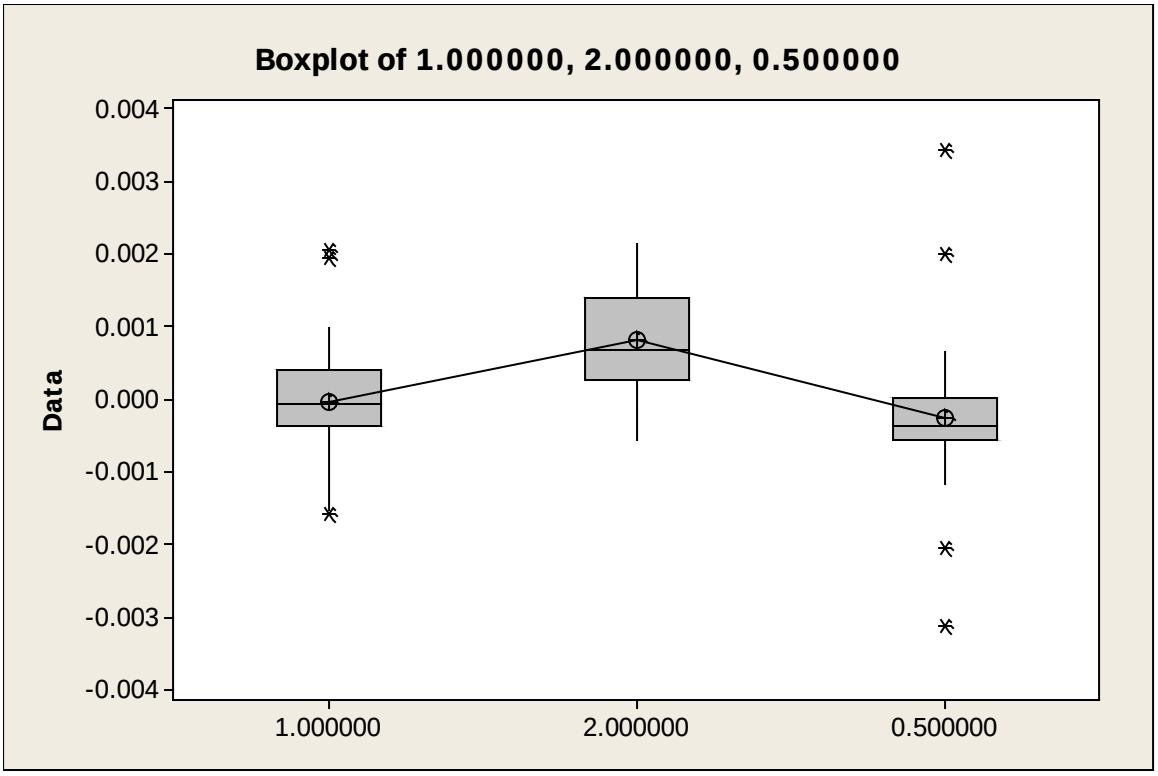

Figure 4.8: Box plot for object size

CHAPTER 5: CONCLUSION AND FUTURE WORK

The purpose of the current study was to characterize the accuracy of a reverse engineering process to develop constraint-based 3D models. These 3D models were created using Geomagic Studio reverse engineering software and scan data collected by an ATOS system. Researchers have shown that calculating the amount of error introduced into constraint-based 3D models can be difficult (F. Chen, G. Brown, & M. Song, 2000). The current study's goal was to characterize the accuracy of the reverse engineering process based on different measurement volumes and object sizes. Chapter V presents the findings based on the methodology and experimentation presented in Chapter IV.

Analysis of Statistical Results

As presented in Chapter IV, statistical testing was conducted to provide a better understanding of how measurement volume, object size, and measurement location affected the accuracy of constraint-based 3D models. Additionally, the amount of deviation from the gage blocks actual size was examined to provide an understanding of the amount of error introduced during the reverse engineering process. Three types of inferential statistical tests were employed to analyze the data collected. One and two sample t-tests were conducted to verify if the measurements performed were statistically different from the specified values of the gage blocks measured. Additionally, two GLMs were implemented to observe differences within or between factors. Two ANOVAs were also created to observe statistical differences between object sizes and measurement volumes.

Discussion of Results from t-tests

Two types of t-test were performed for the current thesis: one-sample t-test, and two-sample t-test. The o-ne sample t-test was performed to evaluate how the increase in measurement volume would affect the accuracy of the reverse engineering process. The two-sample t-test was performed to evaluate how the object size would affect the accuracy of the reverse engineering process.

One sample t-test.

For the twelve t-tests, the null hypothesis was maintained for the half inch gage block using the 250mm and 500mm measurement volumes, and the one inch gage block using the 90mm and 500mm volumes. The null hypothesis failed to be accepted for the remaining eight t-tests. The results suggested that the measured values for the test, in which the null hypothesis failed to be accepted, are not equal to the length of the gage block.

The results of the one-sample t-tests showed the 250mm and 500mm measurement volumes were best to use for the half inch object size, while the 90mm and 500mm measurement volumes are best for the one inch object size. The one sample t-test showed that both measurement volume and object size were factors in the accuracy of the reverse engineering process. From these results, it can be inferred that the 500mm measurement volume was the most accurate, suggesting that as measurement volume increases, the accuracy also increases. The one-sample t-test showed a positive correlation existed between measurement volume and accuracy. These findings conflicted with the findings of Sansoni (1997), who found that as the measurement volume increases, the accuracy decreased.

Although the test suggested that as measurement volume increases, the accuracy also increases, the standard deviation of the results must also be observed when conducting the t-test. *Figure 5.1-5.3* illustrates the normal distributions for each measurement volume. Observing the normal distribution for all three object sizes, the 250mm and 500mm had a higher variance than the 90mm and 120mm. The graph shows that using a larger measurement volume may produce results with a higher deviation from the mean. The normal distribution curves support the argument that Sansoni (1997) suggested. The one-sample t-test also showed that as object size increased, the accuracy would decrease, supporting the finding of Reich (1996), who found that object size was a factor in the accuracy of structured light scanning.

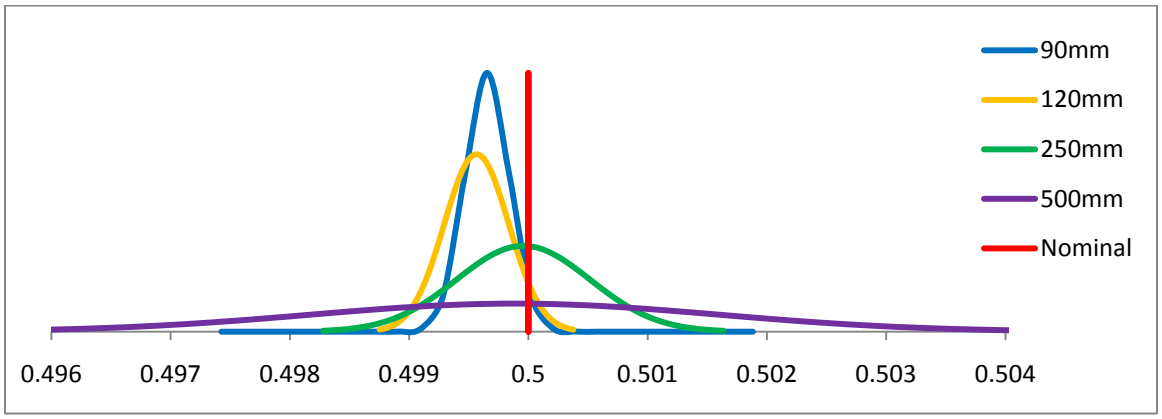

Figure 5.1: Normal distributions for the one inch object size.

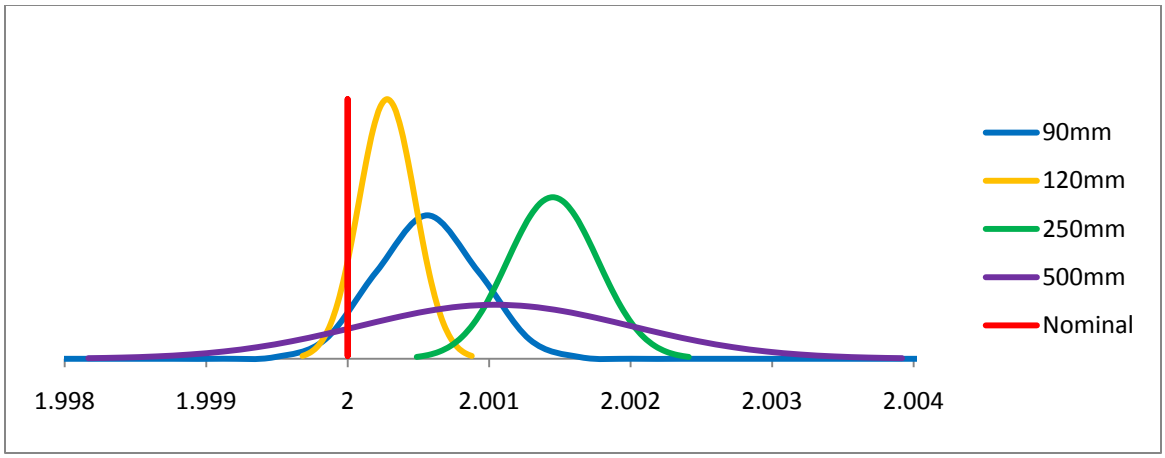

Figure 5.2: Normal distributions for the two inch object size.

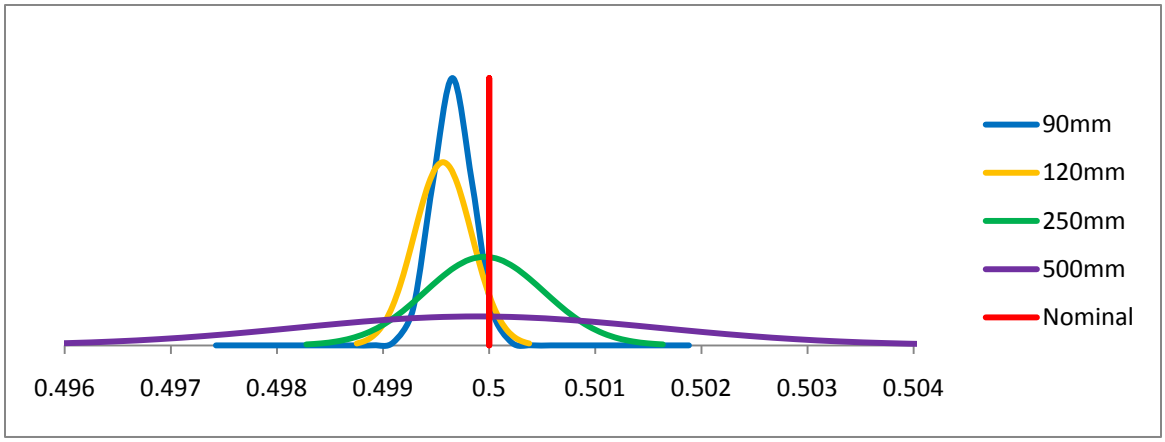

Figure 5.3: Normal distributions for the half inch object size.

Two sample t-test.

For the twenty-seven two sample t-tests, the null hypothesis failed to be accepted for the 90mm vs. 120mm measurement volumes and 120mm vs. 250mm measurement volumes for the one inch gage block. Additionally, the null hypothesis failed to be accepted for the 90mm vs. 120mm; 90mm vs.250mm; 120mm vs. 250mm; and 120mm vs. 500mm for the two inch gage block and the 90mm vs. 120mm; and 120mm vs. 250mm for the half inch gage block. For all other processes, the null hypothesis was

accepted. The results suggested that the means were not equal for the measured values of the 120mm vs. 250mm measurement volumes for the one inch object size, and the 90mm vs. 250mm; and 120mm vs. 500mm for the two inch object size. It must also be noted that the standard deviation increased as measurement volume increased. The two-sample t-test was conducted to develop an understanding of how object size was affected as the size increased. The results showed that a negative correlation existed between object size and accuracy. As object size increased, the accuracy decreased, supporting Reich's (1996) findings that object size was a factor in the accuracy of structured light scanning presented in Chapter II.

GLM Discussion of Results

As presented in Chapter IV, a general linear model was constructed to compare the analysis of variance for all three factors (main effects) and the interactions between these factors (interactions). An ANOVA was used to compare the results of the GLM. The ANOVA was used to determine whether the null hypothesis, which stated the mean of one factor is equal to the means of the other factors for all factors, was accepted or failed to be accepted. An alpha value of 0.01 was used to compare the p-values for the main effects and interactions. For the main effects of measurement volume and object size, the null hypothesis failed to be accepted. Suggesting that both measurement volume and object size have a correlation to accuracy. The interactions between factors showed no correlation along with the measurement location.

To identify patterns within the ANOVA, a Tukey post hoc comparison was conducted. The results from the post hoc comparison suggested that a difference existed between the 120mm volume and 250mm volume. Additionally, the post hoc comparison

found that statistical differences existed between the one inch and two inch, and half inch and two inch gage blocks. The results from the post hoc comparison found that a positive correlation was present between object size and accuracy. The positive correlation implies that larger object sizes will result in a less accurate measurement. The results also suggested that a positive correlation was present between measurement volume and accuracy for the reverse engineering process. The positive correlation implies that larger measurement volumes will result in a less accurate measurement.

The ANOVA revealed a statistically significant difference between the main effects of measurement volume and object size. This finding confirmed the findings of Reich (1996), Chen (2000), and Sansoni (1997), showing that increasing both measurement volume and object size will have an negative effect on the accuracy of the reverse engineering process. The significant difference found between the 120mm and 250mm measurement volumes confirm that as the measurement volume increased, the accuracy will decrease. The post-hoc comparison also found that the statistically significant difference in object size came from the difference between the one inch and two inch sizes and the half inch and two inch sizes. This difference confirms that as the size of the object being measured increases, the accuracy will decrease.

Conclusion

The initial goal of the current study was to characterize the accuracy of a reverse engineering process based on four measurement volumes and three object sizes. *Table 5.1* presents a table with the actual object size ± three standard deviations. *Table 5.1* represents the accuracy that may be expected when reverse engineering an object using the process described in Chapter III. For objects that require high precision greater than

0.005 inches, this is not the best reverse engineering process to follow. However, for processes that do not require high precision, this reverse engineering process is recommended. All reverse engineering projects require a different accuracy tolerance; *table 5.1* should be referenced before choosing the reverse engineering process for the project.

The statistical test found that as measurement volume increased, the deviation from actual decreased. The ATOS User Manual – Software (2008) suggested using the smallest measurement volume possible on parts that require high precision or parts that fit within the measurement volume. Additionally, the statistical test found that as part size increased the deviation for actual decreased. For processes with variable object sizes, it would be best to use the smallest possible to increase accuracy.

Table 5.1

Accuracy table

	90mm	120mm	250mm	500mm
Half Inch	0.500000 ± 0.00056	0.500000 ± 0.00081	0.500000 ± 0.00168	0.500000 ± 0.00513
One Inch	1.000000 ± 0.00121	1.000000 ± 0.00060	1.000000 ± 0.00124	1.000000 ± 0.00016
Two Inch	2.000000 ± 0.00121	2.000000 ± 0.00060	2.000000 ± 0.00096	2.000000 ± 0.00104

Future Work

During scanning, it was noted that the curved corners of the gage block were better defined using the smaller measurement volumes as opposed to the larger measurement volumes. The difference between the curved surface of the 90mm measurement volume and the 500mm measurement volume can be seen in *Figure 5.4*. Although the current study demonstrated that accuracy decreased as measurement volume increased, the study only included surfaces that were flat. For a full

understanding of how the reverse engineering process behaves based on the measurement volumes, a characterization should be done on curved surfaces. Additionally, the current study only characterized the object sizes that fit within all three measurement volumes. A continuation of the current study might include objects of larger sizes. Using larger sizes might provide a better understanding of how object size affects the accuracy of the reverse engineering process. The current study determined that increasing the measurement volume and object size were both factors in the overall accuracy of the reverse engineering process. Further investigation into the reason why these factors were significant is needed to determine the best course of action to take when using higher measurement volumes or object sizes. In addition to the investigation into the factors of object size and measurement volume, an investigation is needed to analyze what specific process within the reverse engineering process causes the greatest source of error.

REFERENCES

Bergmann, D. (1995). New Approach for Automatic Surface Reconstruction with Coded Light. *SPIE*, 2572, 2-9

Bosch, J. A. (Ed.) (1995) *Coordinate Measuring Machines and Systems.* New York, NY.: Marcel Dekker.

Chen, X. Xi, J. Jin, Y. Sun, J (2009) Accurate Calibration for a Camera-Projector Measurement System Based on Structured Light Projection. *Optics and Lasers in Engineering*, 47 310-319

Chen, F. Brown, G. Song, M (2000). Overview of Three-Dimensional Shape Measurement Using Optical Methods. *Optical Engineering*, 39(1) 10-22

De Silva G. M. S. (2002). *Basic Metrology for ISO 9000 Certification*. Boston: Butterworth-Heinemann.

Doiron, T. & Beers, J. S. (2005). The Gauge Block Handbook. Dimensional Metrology Group. Precision Engineering Division. National Institute of Standards and Technology.

Dotson, C. Thompson, R. (2003). *Fundamentals of Dimensional Metrology.* Albany, NY.: Thompson Learning

Evans, J. R. & Lindsay, W. M. (2005) The management and Control of Quality. Eagan, MN, Thomson-West

Farago, F (1968). *Handbood of Dimensional Measurement.* New York: Industrial Press

Fraser, C. S. (1992). Photogrammetric Measurement to One Part in a Million. *Photogrammetric Engineering & Remote Sensing* 58(3), 305-310.

Fu, P. (2008) Reverse Engineering in the Automotive Industry. In V. Raja, & K. J. Fernandes (Eds.), *Reverse engineering: an industrial perspective.* (pp. 141-155) London: Springer-Verlag.

Gesellschaft für Optische Messtechnik (GOM). (2006). *ATOS: Industrial high-end 3D digitizer.*

Gesellschaft für Optische Messtechnik. (2008). *ATOS User Manual – Software* (ATOS v6.1)

Gesellschaft für Optische Messtechnik. (2008). *ATOS User Manual* (ATOS IIe and ATOS IIe SO rev. 01 hardware)

Giesecke, F. (2009). *Technical Drawing.* Upper Saddle River, NJ.: Person Prentice Hall.

Jin, L. (2009). Moire Metrology. In T. Yoshuzawa (ed.), Handbook of Optical Metrology Principles and Applications (pp. 263-280). Boca Raton, FL.: CRC Press.

Karara, H. (1979). *Handbook of non-Topographic Photogrammetry.* Falls Church, VA.: American Society of Photogrammetry

Kochi, N. (2009). Photogrammetry. In T. Yoshuzawa (ed.), Handbook of Optical Metrology Principles and Applications (pp. 511-529). Boca Raton, FL.: CRC Press.

Levoy, M. Rusinliewicz, S. Ginzton, M. Ginsberg, J. Pulli, K. Koller, D.,… Fulk, D (2000). The Digital Michelangelo Project: 3D Scanning of Large Statues. Proceedings of the 27th annual conference on Computer graphics and interactive techniques, *SIGGRAPH* (pp. 131-144). New York, NY, USA: ACM Press/Addison-Wesley.

Linder, W. (2003). *Digital Photogrammetry.* New York, NY.: Springer

Motavalli, S. Shamsaasef, R. (1996) Object-Oriented Modeling of a Feature Based Reverse Engineering System. *Computer Integrated Manufacturing*, 9(5) 354-368

Müller, E. (1995). Fast Three-Dimensional Form Measurement. *Optical Engineering* 34(9), 2754-2756

National Institute of Standards and Technology. (2010). *Report on Special Test* (NIST Test No: 681/280055-10).

NIST/SEMATECH (2011). *e-Handbook of Statistical Methods*. Retrieved from http://www.itl.nist.gov/div898/handbook/

Page, D. (2009). Interferometry. In T. Yoshuzawa (ed.), Handbook of Optical Metrology Principles and Applications (pp. 511-529). Boca Raton, FL.: CRC Press.

Pagés, J. Salvi, J. García, R. & Matabosch C. (2003). Overview of Coded Light Projection Techniques for Automatic 3D Profiling. In *Proceedings ICRA '03 IEEE International Conference: Vol. 1. Robotics and Automation* (p133). Taiwan. Doi: 10.1109/ROBOT.2003.1241585

Pham, D. T. & Hieu, L. C. (2008)Reverse Engineering – Hardware. In V. Raja, & K. J. Fernandes (Eds.), *Reverse engineering: an industrial perspective.* (pp. 33-70) London: Springer-Verlag.

Raja, V. & Fernandes, K. J. (Eds.). (2008). *Reverse engineering: an industrial perspective.* London: Springer-Verlag.

Reich, C. (1996). 3D-Measuremnt of Complex Objects. *Proceedings of SPIE-The International Society for Optical Engineering*. 2787, (pp. 53-61)

Reich, C. (2000). Photogrammetric Matching of Point Clouds for 3D-Measurement of Complex Objects. *SPIE,* 3520, 100-110

Salvi, J. Pagés, J. Batlle, J. (2004). Pattern Codification Strategies in Structured light Systems. *Pattern Recognition*, 37(4), 827-849

Sansoni, G. Corini, S. Rodella, L. Docchio, F. (1997). Three-Dimensional Imaging Based on Gray-Code Light Projection: Characterization of the Measuring Algorithm and Development of a Measuring System for Industrial Applications. *Applied Optics*, 36, 4463-4472

Scharstein, D. Szeliski, R. (2003). High-Accuracy Stereo Depth Maps Using Structured Light. In *CVPR '03 IEEE Computer Society Conference: Vol. 1. Computer Vision and Pattern Recognition.* (pp. 195-202). Madison, WI. Doi: 10.1109/CVPR.2003.1211354

Schiff, D. & D'Agostino, R, B. (1996). Practical Engineering Statistics. New York: John Wiley & Sons, Inc.

Schoonmaker, S. (2003). *The CAD Guidebook A Basic Manual for Understanding and Improving Computer-Aided Design*. Shady Grove, Pennsylvania: Marcel Dekker.

Scott, C. (1998). Introduction to Optics and Optical Imaging. New York: The Institute of Electrical and Electronics Engineering, Inc.

StatSoft, Inc. (2011). *Electronic Statistics Textbook*. Retrieved from: http://www.statsoft.com/textbook/.

Summit, S. (2011, January) Because One Size Doesn't Fit All: Using RTAM to Profoundly Enhance Prosthetics. *Time Compression*. Retrieved From http://www.timecompression.com/articles/because-one-size-doesnt-fit-all-using-rtam-to-profoundly-enhance-prosthetics

Thompson, W. B. Owen, J. C. Germain, J. Stark, S. R. & Henderson, T. C. (1999). Feature-based Reverse Engineering of Mechanical Parts. *IEEE Transactions on Robotics and Automation* 15(1), 57-66

Toogood, R. (2009). *Pro/Engineer Wildfire 5.0 Tutorial.* Mission, KS.: Schoff Development Corporation

Vasilash, G. (2009, May) Creating the 2010 Camaro: A Study in Fast Design. *Time Compression.* Retrieved From http://www.timecompression.com/articles/creating-the-2010-camaro-a-study-in-fast-design

Venuvinod, P. Ma, W. (2004) *Rapid Prototyping – Laser-Based and Other Technologies.* Norwell, Massachusetts: Kluwer Academic Publishers.

Wyant, J. C. (2002). White Light Interferometry. In Caulfield, H. J. (Eds.), Proceedings of SPIE: Vol. 4737. (pp. 98-107)

Yoshuzawa, T. (2009). Handbook of Optical Metrology Principles and Applications. Boca Raton, FL.: CRC Press.

Zhang, Z. (2000). A flexible New Technique for Camera Calibration. *IEEE Transactions on Pattern Analysis and Machine Intelligence* 22(11) 1330-1334

APPENDIX A: DEVIATIONS WITHIN POLYGONIZATION

		One Inch	Two Inch	Half Inch
90mm	A	.011mm	.006mm	.006mm
	B	.005mm	.007mm	.007mm
	C	.005mm	.006mm	.007mm
120mm	A	.007mm	.007mm	.010mm
	B	.009mm	.007mm	.010mm
	C	.007mm	.010mm	.011mm
250mm	A	.008mm	.011mm	.007mm
	B	.007mm	.006mm	.008mm
	C	.007mm	.010mm	.006mm
500mm	A	.009mm	.012mm	.008mm
	B	.011mm	.010mm	.007mm
	C	.010mm	.012mm	.008mm

Mesh Deviation

		One Inch	Two Inch	Half Inch
90mm	**A**	.006mm	.002mm	.002mm
	B	.002mm	.002mm	.002mm
	C	.002mm	.002mm	.002mm
120mm	**A**	.002mm	.003mm	.003mm
	B	.003mm	.003mm	.004mm
	C	.003mm	.003mm	.004mm
250mm	**A**	.008mm	.011mm	.005mm
	B	.003mm	.003mm	.006mm
	C	.004mm	.009mm	.003mm
500mm	**A**	.008mm	.010mm	.008mm
	B	.009mm	.008mm	.007mm
	C	.010mm	.012mm	.008mm

Reference point deviation

APPENDIX B: DATA COLLECTED

Measurement Volume	90mm	90mm	90mm	120mm	120mm	120mm	250mm	250mm	250mm	500mm	500mm	500mm
Gage Block Size	1.000000	2.000000	0.500000	1.000000	2.000000	0.500000	1.000000	2.000000	0.500000	1.000000	2.000000	0.500000
R1 M1	0.999984	2.000640	0.499621	0.999582	2.000260	0.499570	1.000630	2.001800	0.500636	0.998837	1.999910	0.499910
R1 M2	1.000300	2.000360	0.499637	0.999730	2.000510	0.499870	1.000510	2.001980	0.500048	0.999354	2.000280	0.497955
R1 M3	0.999769	2.000690	0.499438	0.999709	2.000450	0.499368	0.999793	2.001680	0.500322	0.998816	1.999460	0.498845
R1 M4	1.000090	2.000400	0.499454	0.999856	2.000700	0.499668	0.999670	2.001860	0.499736	0.999334	1.999820	0.496888
Range	**0.000531**	**0.000330**	**0.000199**	**0.000274**	**0.000440**	**0.000502**	**0.000960**	**0.000300**	**0.000900**	**0.000538**	**0.000820**	**0.003022**
Standard deviation	**0.000221**	**0.000167**	**0.000106**	**0.000112**	**0.000181**	**0.000209**	**0.000489**	**0.000125**	**0.000384**	**0.000299**	**0.000337**	**0.001286**
Average	**1.000036**	**2.000523**	**0.499538**	**0.999719**	**2.000480**	**0.499619**	**1.000151**	**2.001830**	**0.500186**	**0.999085**	**1.999868**	**0.498400**
R2 M1	1.000290	2.001150	0.499734	0.999789	2.000040	0.499516	0.999979	2.001180	0.499524	1.002060	2.001630	0.503443
R2 M2	0.999980	2.000040	0.499987	1.000120	2.000200	0.500047	1.000290	2.001240	0.500595	1.001960	2.001790	0.502006
R2 M3	0.999960	2.001150	0.499431	0.999667	2.000120	0.499195	1.000190	2.001370	0.499106	1.000830	2.000850	0.500648
R2 M4	0.999646	2.000550	0.499567	0.999997	2.000280	0.499727	1.000500	2.001430	0.500174	1.000730	2.001010	0.499205
Range	**0.000644**	**0.001110**	**0.000556**	**0.000453**	**0.000240**	**0.000852**	**0.000521**	**0.000250**	**0.001489**	**0.001330**	**0.000940**	**0.004238**
Standard deviation	**0.000263**	**0.000536**	**0.000239**	**0.000203**	**0.000103**	**0.000358**	**0.000217**	**0.000115**	**0.000663**	**0.000712**	**0.000460**	**0.001817**
Average	**0.999969**	**2.000723**	**0.499680**	**0.999893**	**2.000160**	**0.499621**	**1.000240**	**2.001305**	**0.499850**	**1.001395**	**2.001320**	**0.501326**
R3 M1	1.000690	2.000590	0.499873	0.999530	2.000020	0.499321	1.001000	2.001010	0.500620	0.998421	2.001740	0.499841
R3 M2	0.999685	2.000070	0.499904	0.999936	2.000220	0.499755	1.000510	2.001400	0.500106	0.999552	2.001960	0.499620
R3 M3	1.000070	2.000820	0.499585	0.999418	2.000180	0.499152	1.000950	2.001020	0.499566	0.998496	2.001920	0.500243
R3 M4	0.999071	2.000300	0.499616	0.999824	2.000370	0.499587	1.000460	2.001420	0.499053	0.999631	2.002140	0.500024
Range	**0.001619**	**0.000750**	**0.000319**	**0.000518**	**0.000350**	**0.000603**	**0.000540**	**0.000410**	**0.001567**	**0.001210**	**0.000400**	**0.000623**
Standard deviation	**0.000679**	**0.000328**	**0.000167**	**0.000243**	**0.000144**	**0.000269**	**0.000284**	**0.000228**	**0.000677**	**0.000656**	**0.000164**	**0.000265**
Average	**0.999879**	**2.000445**	**0.499745**	**0.999677**	**2.000198**	**0.499454**	**1.000730**	**2.001213**	**0.499836**	**0.999025**	**2.001940**	**0.499932**

Maximum	**1.000690**	**2.001150**	**0.499987**	**1.000120**	**2.000700**	**0.500047**	**1.001000**	**2.001980**	**0.500636**	**1.002060**	**2.002140**	**0.503443**
Minimum	**0.999071**	**2.000040**	**0.499431**	**0.999418**	**2.000020**	**0.499152**	**0.999670**	**2.001010**	**0.499053**	**0.998421**	**1.999460**	**0.496888**
Range	**0.001619**	**0.001110**	**0.000556**	**0.000702**	**0.000680**	**0.000895**	**0.001330**	**0.000970**	**0.001583**	**0.003639**	**0.002680**	**0.006555**
Standard deviation	**0.000403**	**0.000361**	**0.000186**	**0.000201**	**0.000199**	**0.000271**	**0.000413**	**0.000321**	**0.000560**	**0.001268**	**0.000959**	**0.001711**
Average	**0.999961**	**2.000563**	**0.499654**	**0.999763**	**2.000279**	**0.499565**	**1.000374**	**2.001449**	**0.499957**	**0.999835**	**2.001043**	**0.499886**

Measurement Volume	90mm	90mm	90mm	120mm	120mm	120mm	250mm	250mm	250mm	500mm	500mm	500mm
Gage Block Size	1.000000	2.000000	0.500000	1.000000	2.000000	0.500000	1.000000	2.000000	0.500000	1.000000	2.000000	0.500000
R1 M1	-0.000016	0.000640	-0.000379	-0.000418	0.000260	-0.000430	0.000630	0.001800	0.000636	-0.001163	-0.000090	-0.000090
R1 M2	0.000300	0.000360	-0.000363	-0.000270	0.000510	-0.000130	0.000510	0.001980	0.000048	-0.000646	0.000280	-0.002045
R1 M3	-0.000231	0.000690	-0.000562	-0.000291	0.000450	-0.000632	-0.000207	0.001680	0.000322	-0.001184	-0.000540	-0.001155
R1 M4	0.000090	0.000400	-0.000546	-0.000144	0.000700	-0.000332	-0.000330	0.001860	-0.000264	-0.000666	-0.000180	-0.003112
Range	0.000531	0.000330	0.000199	0.000274	0.000440	0.000502	0.000960	0.000300	0.000900	0.000538	0.000820	0.003022
Std. dev.	0.000221	0.000167	0.000106	0.000112	0.000181	0.000209	0.000489	0.000125	0.000384	0.000299	0.000337	0.001286
Average	0.000036	0.000523	-0.000463	-0.000281	0.000480	-0.000381	0.000151	0.001830	0.000186	-0.000915	-0.000132	-0.001601
R2 M1	0.000290	0.001150	-0.000266	-0.000211	0.000040	-0.000484	-0.000021	0.001180	-0.000476	0.002060	0.001630	0.003443
R2 M2	-0.000020	0.000040	-0.000013	0.000120	0.000200	0.000047	0.000290	0.001240	0.000595	0.001960	0.001790	0.002006
R2 M3	-0.000040	0.001150	-0.000569	-0.000333	0.000120	-0.000805	0.000190	0.001370	-0.000894	0.000830	0.000850	0.000648
R2 M4	-0.000354	0.000550	-0.000433	-0.000003	0.000280	-0.000273	0.000500	0.001430	0.000174	0.000730	0.001010	-0.000795
Range	0.000644	0.001110	0.000556	0.000453	0.000240	0.000852	0.000521	0.000250	0.001489	0.001330	0.000940	0.004238
Std. dev.	0.000263	0.000536	0.000239	0.000203	0.000103	0.000358	0.000217	0.000115	0.000663	0.000712	0.000460	0.001817
Average	-0.000031	0.000722	-0.000320	-0.000107	0.000160	-0.000379	0.000240	0.001305	-0.000150	0.001395	0.001320	0.001325
R3 M1	0.000690	0.000590	-0.000127	-0.000470	0.000020	-0.000679	0.001000	0.001010	0.000620	-0.001579	0.001740	-0.000159
R3 M2	-0.000315	0.000070	-0.000096	-0.000064	0.000220	-0.000245	0.000510	0.001400	0.000106	-0.000448	0.001960	-0.000380
R3 M3	0.000070	0.000820	-0.000415	-0.000582	0.000180	-0.000848	0.000950	0.001020	-0.000434	-0.001504	0.001920	0.000243
R3 M4	-0.000929	0.000300	-0.000384	-0.000176	0.000370	-0.000413	0.000460	0.001420	-0.000947	-0.000369	0.002140	0.000024
Range	0.001619	0.000750	0.000319	0.000518	0.000350	0.000603	0.000540	0.000410	0.001567	0.001210	0.000400	0.000623
Std. dev.	0.000679	0.000328	0.000167	0.000243	0.000144	0.000269	0.000284	0.000228	0.000677	0.000656	0.000164	0.000265
Average	-0.000121	0.000445	-0.000255	-0.000323	0.000198	-0.000546	0.000730	0.001212	-0.000164	-0.000975	0.001940	-0.000068

Maximum	0.000690	0.001150	-0.000013	0.000120	0.000700	0.000047	0.001000	0.001980	0.000636	0.002060	0.002140	0.003443
Minimum	-0.000929	0.000040	-0.000569	-0.000582	0.000020	-0.000848	-0.000330	0.001010	-0.000947	-0.001579	-0.000540	-0.003112
Range	0.001619	0.001110	0.000556	0.000702	0.000680	0.000895	0.001330	0.000970	0.001583	0.003639	0.002680	0.006555
Standard deviation	0.000403	0.000361	0.000186	0.000201	0.000199	0.000271	0.000413	0.000321	0.000560	0.001268	0.000959	0.001711
Average	-0.000039	0.000563	-0.000346	-0.000237	0.000279	-0.000435	0.000373	0.001449	-0.000043	-0.000165	0.001042	-0.000114

APPENDIX C: ONE SAMPLE T-TEST

One-Sample T: 90mm 1, 120mm 1, 250mm 1, 500mm 1

Test of mu = 1 vs not = 1

Variable	N	Mean	StDev	SE Mean	99% CI	T	P
90mm 1	12	0.999961	0.000403	0.000116	(0.999600, 1.000323)	-0.33	0.745
120mm 1	12	0.999763	0.000201	0.000058	(0.999583, 0.999943)	-4.08	0.002
250mm 1	12	1.00037	0.00041	0.00012	(1.00000, 1.00074)	3.13	0.010
500mm 1	12	0.999835	0.001268	0.000366	(0.998698, 1.000972)	-0.45	0.661

One-Sample T: 90mm 2, 120mm 2, 250mm 2, 500mm 2

Test of mu = 2 vs not = 2

Variable	N	Mean	StDev	SE Mean	99% CI	T	P
90mm 2	12	2.00056	0.00036	0.00010	(2.00024, 2.00089)	5.41	0.000
120mm 2	12	2.00028	0.00020	0.00006	(2.00010, 2.00046)	4.85	0.001
250mm 2	12	2.00145	0.00032	0.00009	(2.00116, 2.00174)	15.66	0.000
500mm 2	12	2.00104	0.00096	0.00028	(2.00018, 2.00190)	3.77	0.003

One-Sample T: 90mm .5, 120mm .5, 250mm .5, 500mm .5

Test of mu = 0.5 vs not = 0.5

Variable	N	Mean	StDev	SE Mean	99% CI	T	P
90mm .5	12	0.499654	0.000186	0.000054	(0.499487, 0.499820)	-6.46	0.000
120mm .5	12	0.499565	0.000271	0.000078	(0.499322, 0.499808)	-5.57	0.000
250mm .5	12	0.499957	0.000560	0.000162	(0.499455, 0.500459)	-0.26	0.796
500mm .5	12	0.499886	0.001711	0.000494	(0.498351, 0.501420)	-0.23	0.821

One-Sample T: 90mm 1, 120mm 1, 250mm 1, 500mm 1

Test of mu = 1.00001 vs not = 1.00001

Variable	N	Mean	StDev	SE Mean	99% CI	T	P
90mm 1	12	0.999961	0.000403	0.000116	(0.999600, 1.000323)	-0.38	0.714
120mm 1	12	0.999763	0.000201	0.000058	(0.999583, 0.999943)	-4.17	0.002
250mm 1	12	1.00037	0.00041	0.00012	(1.00000, 1.00074)	3.09	0.010
500mm 1	12	0.999835	0.001268	0.000366	(0.998698, 1.000972)	-0.46	0.652

One-Sample T: 90mm 2, 120mm 2, 250mm 2, 500mm 2

Test of mu = 2.00000 vs not = 2.00000

Variable	N	Mean	StDev	SE Mean	99% CI	T	P
90mm 2	12	2.00056	0.00036	0.00010	(2.00024, 2.00089)	5.36	0.000
120mm 2	12	2.00028	0.00020	0.00006	(2.00010, 2.00046)	4.76	0.001
250mm 2	12	2.00145	0.00032	0.00009	(2.00116, 2.00174)	15.61	0.000
500mm 2	12	2.00104	0.00096	0.00028	(2.00018, 2.00190)	3.75	0.003

One-Sample T: 90mm .5, 120mm .5, 250mm .5, 500mm .5

Test of mu = 0.500005 vs not = 0.500005

Variable	N	Mean	StDev	SE Mean	99% CI	T	P
90mm .5	12	0.499654	0.000186	0.000054	(0.499487, 0.499820)	-6.55	0.000
120mm .5	12	0.499565	0.000271	0.000078	(0.499322, 0.499808)	-5.63	0.000
250mm .5	12	0.499957	0.000560	0.000162	(0.499455, 0.500459)	-0.30	0.773
500mm .5	12	0.499886	0.001711	0.000494	(0.498351, 0.501420)	-0.24	0.814

One-Sample T: 90mm 1, 120mm 1, 250mm 1, 500mm 1

Test of mu = 0.99999 vs not = 0.99999

Variable	N	Mean	StDev	SE Mean	99% CI	T	P
90mm 1	12	0.999961	0.000403	0.000116	(0.999600, 1.000323)	-0.29	0.777
120mm 1	12	0.999763	0.000201	0.000058	(0.999583, 0.999943)	-4.00	0.002
250mm 1	12	1.00037	0.00041	0.00012	(1.00000, 1.00074)	3.17	0.009
500mm 1	12	0.999835	0.001268	0.000366	(0.998698, 1.000972)	-0.44	0.671

One-Sample T: 90mm 2, 120mm 2, 250mm 2, 500mm 2

Test of mu = 2.00000 vs not = 2.00000

Variable	N	Mean	StDev	SE Mean	99% CI	T	P
90mm 2	12	2.00056	0.00036	0.00010	(2.00024, 2.00089)	5.46	0.000
120mm 2	12	2.00028	0.00020	0.00006	(2.00010, 2.00046)	4.94	0.000
250mm 2	12	2.00145	0.00032	0.00009	(2.00116, 2.00174)	15.72	0.000
500mm 2	12	2.00104	0.00096	0.00028	(2.00018, 2.00190)	3.79	0.003

One-Sample T: 90mm .5, 120mm .5, 250mm .5, 500mm .5

Test of mu = 0.499995 vs not = 0.499995

Variable	N	Mean	StDev	SE Mean	99% CI	T	P
90mm .5	12	0.499654	0.000186	0.000054	(0.499487, 0.499820)	-6.36	0.000
120mm .5	12	0.499565	0.000271	0.000078	(0.499322, 0.499808)	-5.50	0.000
250mm .5	12	0.499957	0.000560	0.000162	(0.499455, 0.500459)	-0.23	0.819
500mm .5	12	0.499886	0.001711	0.000494	(0.498351, 0.501420)	-0.22	0.829

APPENDIX D: F-TEST

Test for Equal Variances: 1" 90mm, 1" 120mm

99% Bonferroni confidence intervals for standard deviations

	N	Lower	StDev	Upper
1" 90mm	12	0.0002495	0.0004032	0.0008951
1" 120mm	12	0.0001244	0.0002010	0.0004462

F-Test (Normal Distribution)
Test statistic = 4.02, p-value = 0.030

Levene's Test (Any Continuous Distribution)
Test statistic = 1.82, p-value = 0.191

Test for Equal Variances: 1" 90mm, 1" 250mm

99% Bonferroni confidence intervals for standard deviations

	N	Lower	StDev	Upper
1" 90mm	12	0.0002495	0.0004032	0.0008951
1" 250mm	12	0.0002558	0.0004134	0.0009176

F-Test (Normal Distribution)
Test statistic = 0.95, p-value = 0.936

Levene's Test (Any Continuous Distribution)
Test statistic = 0.09, p-value = 0.772

Test for Equal Variances: 1" 90mm, 1" 500mm

99% Bonferroni confidence intervals for standard deviations

	N	Lower	StDev	Upper
1" 90mm	12	0.0002495	0.0004032	0.0008951
1" 500mm	12	0.0007847	0.0012681	0.0028150

F-Test (Normal Distribution)
Test statistic = 0.10, p-value = 0.001

Levene's Test (Any Continuous Distribution)
Test statistic = 6.62, p-value = 0.017

Test for Equal Variances: 1" 120mm, 1" 250mm

```
99% Bonferroni confidence intervals for standard deviations

           N      Lower      StDev      Upper
1" 120mm  12  0.0001244  0.0002010  0.0004462
1" 250mm  12  0.0002558  0.0004134  0.0009176


F-Test (Normal Distribution)
Test statistic = 0.24, p-value = 0.025


Levene's Test (Any Continuous Distribution)
Test statistic = 3.04, p-value = 0.095
```

Test for Equal Variances: 1" 120mm, 1" 500mm

```
99% Bonferroni confidence intervals for standard deviations

           N      Lower      StDev      Upper
1" 120mm  12  0.0001244  0.0002010  0.0004462
1" 500mm  12  0.0007847  0.0012681  0.0028150


F-Test (Normal Distribution)
Test statistic = 0.03, p-value = 0.000


Levene's Test (Any Continuous Distribution)
Test statistic = 9.91, p-value = 0.005
```

Test for Equal Variances: 1" 250mm, 1" 500mm

```
99% Bonferroni confidence intervals for standard deviations

           N      Lower      StDev      Upper
1" 250mm  12  0.0002558  0.0004134  0.0009176
1" 500mm  12  0.0007847  0.0012681  0.0028150


F-Test (Normal Distribution)
Test statistic = 0.11, p-value = 0.001


Levene's Test (Any Continuous Distribution)
Test statistic = 5.99, p-value = 0.023
```

Test for Equal Variances: 2" 90mm, 2" 120mm

```
99% Bonferroni confidence intervals for standard deviations

           N      Lower      StDev      Upper
 2" 90mm  12  0.0002232  0.0003608  0.0008009
2" 120mm  12  0.0001234  0.0001994  0.0004427


F-Test (Normal Distribution)
Test statistic = 3.27, p-value = 0.061


Levene's Test (Any Continuous Distribution)
Test statistic = 3.05, p-value = 0.094
```

Test for Equal Variances: 2" 90mm, 2" 250mm

```
99% Bonferroni confidence intervals for standard deviations

           N      Lower      StDev      Upper
 2" 90mm  12  0.0002232  0.0003608  0.0008009
2" 250mm  12  0.0001983  0.0003205  0.0007115


F-Test (Normal Distribution)
Test statistic = 1.27, p-value = 0.702


Levene's Test (Any Continuous Distribution)
Test statistic = 0.13, p-value = 0.718
```

Test for Equal Variances: 2" 90mm, 2" 500mm

```
99% Bonferroni confidence intervals for standard deviations

           N      Lower      StDev      Upper
 2" 90mm  12  0.0002232  0.0003608  0.0008009
2" 500mm  12  0.0005931  0.0009586  0.0021280


F-Test (Normal Distribution)
Test statistic = 0.14, p-value = 0.003


Levene's Test (Any Continuous Distribution)
Test statistic = 11.30, p-value = 0.003
```

Test for Equal Variances: 2" 120mm, 2" 250mm

```
99% Bonferroni confidence intervals for standard deviations
```

```
           N      Lower      StDev      Upper
2" 120mm  12  0.0001234  0.0001994  0.0004427
2" 250mm  12  0.0001983  0.0003205  0.0007115


F-Test (Normal Distribution)
Test statistic = 0.39, p-value = 0.131


Levene's Test (Any Continuous Distribution)
Test statistic = 2.01, p-value = 0.170
```

Test for Equal Variances: 2" 120mm, 2" 500mm

```
99% Bonferroni confidence intervals for standard deviations

           N      Lower      StDev      Upper
2" 120mm  12  0.0001234  0.0001994  0.0004427
2" 500mm  12  0.0005931  0.0009586  0.0021280


F-Test (Normal Distribution)
Test statistic = 0.04, p-value = 0.000


Levene's Test (Any Continuous Distribution)
Test statistic = 18.99, p-value = 0.000
```

Test for Equal Variances: 2" 250mm, 2" 500mm

```
99% Bonferroni confidence intervals for standard deviations

           N      Lower      StDev      Upper
2" 250mm  12  0.0001983  0.0003205  0.0007115
2" 500mm  12  0.0005931  0.0009586  0.0021280


F-Test (Normal Distribution)
Test statistic = 0.11, p-value = 0.001


Levene's Test (Any Continuous Distribution)
Test statistic = 12.95, p-value = 0.002
```

Test for Equal Variances: .5" 90mm, .5" 120mm

```
99% Bonferroni confidence intervals for standard deviations

            N      Lower      StDev      Upper
 .5" 90mm  12  0.0001149  0.0001857  0.0004122
.5" 120mm  12  0.0001676  0.0002709  0.0006013


F-Test (Normal Distribution)
Test statistic = 0.47, p-value = 0.226


Levene's Test (Any Continuous Distribution)
Test statistic = 1.57, p-value = 0.223
```

Test for Equal Variances: .5" 90mm, .5" 250mm

```
99% Bonferroni confidence intervals for standard deviations

            N      Lower      StDev      Upper
 .5" 90mm  12  0.0001149  0.0001857  0.0004122
.5" 250mm  12  0.0003465  0.0005600  0.0012431


F-Test (Normal Distribution)
Test statistic = 0.11, p-value = 0.001


Levene's Test (Any Continuous Distribution)
Test statistic = 9.67, p-value = 0.005
```

Test for Equal Variances: .5" 90mm, .5" 500mm

```
99% Bonferroni confidence intervals for standard deviations

            N      Lower      StDev      Upper
 .5" 90mm  12  0.0001149  0.0001857  0.0004122
.5" 500mm  12  0.0010589  0.0017112  0.0037988


F-Test (Normal Distribution)
Test statistic = 0.01, p-value = 0.000


Levene's Test (Any Continuous Distribution)
Test statistic = 8.48, p-value = 0.008
```

Test for Equal Variances: .5" 120mm, .5" 250mm

```
99% Bonferroni confidence intervals for standard deviations

            N      Lower      StDev      Upper
.5" 120mm  12  0.0001676  0.0002709  0.0006013
.5" 250mm  12  0.0003465  0.0005600  0.0012431


F-Test (Normal Distribution)
Test statistic = 0.23, p-value = 0.024


Levene's Test (Any Continuous Distribution)
Test statistic = 5.28, p-value = 0.031
```

Test for Equal Variances: .5" 120mm, .5" 500mm

```
99% Bonferroni confidence intervals for standard deviations

            N      Lower      StDev      Upper
.5" 120mm  12  0.0001676  0.0002709  0.0006013
.5" 500mm  12  0.0010589  0.0017112  0.0037988


F-Test (Normal Distribution)
Test statistic = 0.03, p-value = 0.000


Levene's Test (Any Continuous Distribution)
Test statistic = 7.28, p-value = 0.013
```

Test for Equal Variances: .5" 250mm, .5" 500mm

```
99% Bonferroni confidence intervals for standard deviations

            N      Lower      StDev      Upper
.5" 250mm  12  0.0003465  0.0005600  0.0012431
.5" 500mm  12  0.0010589  0.0017112  0.0037988


F-Test (Normal Distribution)
Test statistic = 0.11, p-value = 0.001


Levene's Test (Any Continuous Distribution)
Test statistic = 3.84, p-value = 0.063
```

APPENDIX E: TWO SAMPLE T-TEST RESULTS

Two-Sample T-Test and CI: 90mm .5, 120mm .5

```
Two-sample T for 90mm .5 vs 120mm .5

            N      Mean     StDev   SE Mean
90mm .5    12  0.499654  0.000186  0.000054
120mm .5   12  0.499565  0.000271  0.000078


Difference = mu (90mm .5) - mu (120mm .5)
Estimate for difference:  0.000089
99% CI for difference:  (-0.000182, 0.000360)
T-Test of difference = 0 (vs not =): T-Value = 0.94  P-Value = 0.358  DF = 19
```

Two-Sample T-Test and CI: 90mm .5, 250mm .5

```
Two-sample T for 90mm .5 vs 250mm .5

            N      Mean     StDev   SE Mean
90mm .5    12  0.499654  0.000186  0.000054
250mm .5   12  0.499957  0.000560   0.00016


Difference = mu (90mm .5) - mu (250mm .5)
Estimate for difference:  -0.000303
99% CI for difference:  (-0.000816, 0.000210)
T-Test of difference = 0 (vs not =): T-Value = -1.78  P-Value = 0.098  DF = 13
```

Two-Sample T-Test and CI: 90mm .5, 500mm .5

```
Two-sample T for 90mm .5 vs 500mm .5

            N      Mean     StDev   SE Mean
90mm .5    12  0.499654  0.000186  0.000054
500mm .5   12   0.49989   0.00171   0.00049


Difference = mu (90mm .5) - mu (500mm .5)
Estimate for difference:  -0.000232
99% CI for difference:  (-0.001775, 0.001311)
T-Test of difference = 0 (vs not =): T-Value = -0.47  P-Value = 0.650  DF = 11
```

Two-Sample T-Test and CI: 120mm .5, 250mm .5

```
Two-sample T for 120mm .5 vs 250mm .5

           N      Mean     StDev   SE Mean
120mm .5  12  0.499565  0.000271  0.000078
250mm .5  12  0.499957  0.000560   0.00016


Difference = mu (120mm .5) - mu (250mm .5)
Estimate for difference:  -0.000392
99% CI for difference:  (-0.000922, 0.000137)
T-Test of difference = 0 (vs not =): T-Value = -2.19  P-Value = 0.045  DF = 15
```

Two-Sample T-Test and CI: 120mm .5, 500mm .5

```
Two-sample T for 120mm .5 vs 500mm .5

           N      Mean     StDev   SE Mean
120mm .5  12  0.499565  0.000271  0.000078
500mm .5  12   0.49989   0.00171   0.00049


Difference = mu (120mm .5) - mu (500mm .5)
Estimate for difference:  -0.000321
99% CI for difference:  (-0.001874, 0.001232)
T-Test of difference = 0 (vs not =): T-Value = -0.64  P-Value = 0.534  DF = 11
```

Two-Sample T-Test and CI: 250mm .5, 500mm .5

```
Two-sample T for 250mm .5 vs 500mm .5

           N      Mean     StDev  SE Mean
250mm .5  12  0.499957  0.000560  0.00016
500mm .5  12   0.49989   0.00171  0.00049


Difference = mu (250mm .5) - mu (500mm .5)
Estimate for difference:  0.000071
99% CI for difference:  (-0.001494, 0.001637)
T-Test of difference = 0 (vs not =): T-Value = 0.14  P-Value = 0.893  DF = 13
```

Two-Sample T-Test and CI: 90mm 1, 120mm 1

```
Two-sample T for 90mm 1 vs 120mm 1

          N      Mean     StDev   SE Mean
90mm 1   12  0.999961  0.000403   0.00012
120mm 1  12  0.999763  0.000201  0.000058


Difference = mu (90mm 1) - mu (120mm 1)
Estimate for difference:  0.000198
99% CI for difference:  (-0.000182, 0.000578)
T-Test of difference = 0 (vs not =): T-Value = 1.52  P-Value = 0.147  DF = 16
```

Two-Sample T-Test and CI: 90mm 1, 250mm 1

```
Two-sample T for 90mm 1 vs 250mm 1

          N      Mean     StDev  SE Mean
90mm 1   12  0.999961  0.000403  0.00012
250mm 1  12  1.000374  0.000413  0.00012


Difference = mu (90mm 1) - mu (250mm 1)
Estimate for difference:  -0.000412
99% CI for difference:  (-0.000884, 0.000060)
T-Test of difference = 0 (vs not =): T-Value = -2.47  P-Value = 0.022  DF = 21
```

Two-Sample T-Test and CI: 90mm 1, 500mm 1

```
Two-sample T for 90mm 1 vs 500mm 1

          N      Mean     StDev  SE Mean
90mm 1   12  0.999961  0.000403  0.00012
500mm 1  12   0.99984   0.00127  0.00037


Difference = mu (90mm 1) - mu (500mm 1)
Estimate for difference:  0.000126
99% CI for difference:  (-0.001031, 0.001283)
T-Test of difference = 0 (vs not =): T-Value = 0.33  P-Value = 0.748  DF = 13
```

Two-Sample T-Test and CI: 120mm 1, 250mm 1

```
Two-sample T for 120mm 1 vs 250mm 1

          N      Mean     StDev   SE Mean
120mm 1  12  0.999763  0.000201  0.000058
250mm 1  12  1.000374  0.000413   0.00012


Difference = mu (120mm 1) - mu (250mm 1)
Estimate for difference:  -0.000610
99% CI for difference:  (-0.001001, -0.000219)
T-Test of difference = 0 (vs not =): T-Value = -4.60  P-Value = 0.000  DF = 15
```

Two-Sample T-Test and CI: 120mm 1, 500mm 1

```
Two-sample T for 120mm 1 vs 500mm 1

          N      Mean     StDev   SE Mean
120mm 1  12  0.999763  0.000201  0.000058
500mm 1  12   0.99984   0.00127   0.00037


Difference = mu (120mm 1) - mu (500mm 1)
Estimate for difference:  -0.000072
99% CI for difference:  (-0.001223, 0.001079)
T-Test of difference = 0 (vs not =): T-Value = -0.19  P-Value = 0.850  DF = 11
```

Two-Sample T-Test and CI: 250mm 1, 500mm 1

```
Two-sample T for 250mm 1 vs 500mm 1

          N      Mean     StDev  SE Mean
250mm 1  12  1.000374  0.000413  0.00012
500mm 1  12   0.99984   0.00127  0.00037


Difference = mu (250mm 1) - mu (500mm 1)
Estimate for difference:  0.000538
99% CI for difference:  (-0.000621, 0.001698)
T-Test of difference = 0 (vs not =): T-Value = 1.40  P-Value = 0.185  DF = 13
```

Two-Sample T-Test and CI: 90mm 2, 120mm 2

```
Two-sample T for 90mm 2 vs 120mm 2

          N      Mean     StDev   SE Mean
90mm 2   12  2.000563  0.000361   0.00010
120mm 2  12  2.000279  0.000199  0.000058


Difference = mu (90mm 2) - mu (120mm 2)
Estimate for difference:  0.000284
99% CI for difference:  (-0.000061, 0.000629)
T-Test of difference = 0 (vs not =): T-Value = 2.39  P-Value = 0.029  DF = 17
```

Two-Sample T-Test and CI: 90mm 2, 250mm 2

```
Two-sample T for 90mm 2 vs 250mm 2

          N      Mean     StDev   SE Mean
90mm 2   12  2.000563  0.000361   0.00010
250mm 2  12  2.001449  0.000321  0.000093


Difference = mu (90mm 2) - mu (250mm 2)
Estimate for difference:  -0.000886
99% CI for difference:  (-0.001280, -0.000491)
T-Test of difference = 0 (vs not =): T-Value = -6.36  P-Value = 0.000  DF = 21
```

Two-Sample T-Test and CI: 90mm 2, 500mm 2

```
Two-sample T for 90mm 2 vs 500mm 2

          N      Mean     StDev  SE Mean
90mm 2   12  2.000563  0.000361  0.00010
500mm 2  12  2.001043  0.000959  0.00028


Difference = mu (90mm 2) - mu (500mm 2)
Estimate for difference:  -0.000479
99% CI for difference:  (-0.001359, 0.000401)
T-Test of difference = 0 (vs not =): T-Value = -1.62  P-Value = 0.127  DF = 14
```

Two-Sample T-Test and CI: 120mm 2, 250mm 2

```
Two-sample T for 120mm 2 vs 250mm 2

          N      Mean     StDev   SE Mean
120mm 2  12  2.000279  0.000199  0.000058
250mm 2  12  2.001449  0.000321  0.000093


Difference = mu (120mm 2) - mu (250mm 2)
Estimate for difference:  -0.001170
99% CI for difference:  (-0.001484, -0.000856)
T-Test of difference = 0 (vs not =): T-Value = -10.74  P-Value = 0.000  DF = 18
```

Two-Sample T-Test and CI: 120mm 2, 500mm 2

```
Two-sample T for 120mm 2 vs 500mm 2

          N      Mean     StDev   SE Mean
120mm 2  12  2.000279  0.000199  0.000058
500mm 2  12  2.001043  0.000959   0.00028


Difference = mu (120mm 2) - mu (500mm 2)
Estimate for difference:  -0.000763
99% CI for difference:  (-0.001641, 0.000115)
T-Test of difference = 0 (vs not =): T-Value = -2.70  P-Value = 0.021  DF = 11
```

Two-Sample T-Test and CI: 250mm 2, 500mm 2

```
Two-sample T for 250mm 2 vs 500mm 2

          N      Mean     StDev   SE Mean
250mm 2  12  2.001449  0.000321  0.000093
500mm 2  12  2.001043  0.000959   0.00028


Difference = mu (250mm 2) - mu (500mm 2)
Estimate for difference:  0.000407
99% CI for difference:  (-0.000472, 0.001286)
T-Test of difference = 0 (vs not =): T-Value = 1.39  P-Value = 0.187  DF = 13
```

APPENDIX F: General Linear Model

		90mm (1)	120mm (2)	250mm (3)	500mm (4)
One Inch (1)	Measurement 1	-0.000016	-0.000418	0.000630	-0.001163
		0.000290	-0.000211	-0.000021	0.002060
		0.000690	-0.000470	0.001000	-0.001579
	Measurement 2	0.000300	-0.000270	0.000510	-0.000646
		-0.000020	0.000120	0.000290	0.001960
		-0.000315	-0.000064	0.000510	-0.000448
	Measurement 3	-0.000231	-0.000291	-0.000207	-0.001184
		-0.000040	-0.000333	0.000190	0.000830
		0.000070	-0.000582	0.000950	-0.001504
	Measurement 4	0.000090	-0.000144	-0.000330	-0.000666
		-0.000354	-0.000003	0.000500	0.000730
		-0.000929	-0.000176	0.000460	-0.000369
Two Inch (2)	Measurement 1	0.000640	0.000260	0.001800	-0.000090
		0.001150	0.000040	0.001180	0.001630
		0.000590	0.000020	0.001010	0.001740
	Measurement 2	0.000360	0.000510	0.001980	0.000280
		0.000040	0.000200	0.001240	0.001790
		0.000070	0.000220	0.001400	0.001960
	Measurement 3	0.000690	0.000450	0.001680	-0.000540
		0.001150	0.000120	0.001370	0.000850
		0.000820	0.000180	0.001020	0.001920
	Measurement 4	0.000400	0.000700	0.001860	-0.000180
		0.000550	0.000280	0.001430	0.001010
		0.000300	0.000370	0.001420	0.002140
Half Inch (3)	Measurement 1	-0.000379	-0.000430	0.000636	-0.000090
		-0.000266	-0.000484	-0.000476	0.003443
		-0.000127	-0.000679	0.000620	-0.000159
	Measurement 2	-0.000363	-0.000130	0.000048	-0.002045
		-0.000013	0.000047	0.000595	0.002006
		-0.000096	-0.000245	0.000106	-0.000380
	Measurement 3	-0.000562	-0.000632	0.000322	-0.001155
		-0.000569	-0.000805	-0.000894	0.000648
		-0.000415	-0.000848	-0.000434	0.000243
	Measurement 4	-0.000546	-0.000332	-0.000264	-0.003112
		-0.000433	-0.000273	0.000174	-0.000795
		-0.000384	-0.000413	-0.000947	0.000024

	Volume	Measurement	Size
-0.000016	1	1	1
0.000290	1	1	1
0.000690	1	1	1
0.000300	1	2	1
-0.000020	1	2	1
-0.000315	1	2	1
-0.000231	1	3	1
-0.000040	1	3	1
0.000070	1	3	1
0.000090	1	4	1
-0.000354	1	4	1
-0.000929	1	4	1
-0.000418	2	1	1
-0.000211	2	1	1
-0.000470	2	1	1
-0.000270	2	2	1
0.000120	2	2	1
-0.000064	2	2	1
-0.000291	2	3	1
-0.000333	2	3	1
-0.000582	2	3	1
-0.000144	2	4	1
-0.000003	2	4	1
-0.000176	2	4	1
0.000630	3	1	1
-0.000021	3	1	1
0.001000	3	1	1
0.000510	3	2	1
0.000290	3	2	1
0.000510	3	2	1
-0.000207	3	3	1
0.000190	3	3	1
0.000950	3	3	1
-0.000330	3	4	1
0.000500	3	4	1
0.000460	3	4	1
-0.001163	4	1	1
0.002060	4	1	1
-0.001579	4	1	1
-0.000646	4	2	1

0.001960	4	2	1
-0.000448	4	2	1
-0.001184	4	3	1
0.000830	4	3	1
-0.001504	4	3	1
-0.000666	4	4	1
0.000730	4	4	1
-0.000369	4	4	1
0.000640	1	1	2
0.001150	1	1	2
0.000590	1	1	2
0.000360	1	2	2
0.000040	1	2	2
0.000070	1	2	2
0.000690	1	3	2
0.001150	1	3	2
0.000820	1	3	2
0.000400	1	4	2
0.000550	1	4	2
0.000300	1	4	2
0.000260	2	1	2
0.000040	2	1	2
0.000020	2	1	2
0.000510	2	2	2
0.000200	2	2	2
0.000220	2	2	2
0.000450	2	3	2
0.000120	2	3	2
0.000180	2	3	2
0.000700	2	4	2
0.000280	2	4	2
0.000370	2	4	2
0.001800	3	1	2
0.001180	3	1	2
0.001010	3	1	2
0.001980	3	2	2
0.001240	3	2	2
0.001400	3	2	2
0.001680	3	3	2
0.001370	3	3	2
0.001020	3	3	2

0.001860	3	4	2
0.001430	3	4	2
0.001420	3	4	2
-0.000090	4	1	2
0.001630	4	1	2
0.001740	4	1	2
0.000280	4	2	2
0.001790	4	2	2
0.001960	4	2	2
-0.000540	4	3	2
0.000850	4	3	2
0.001920	4	3	2
-0.000180	4	4	2
0.001010	4	4	2
0.002140	4	4	2
-0.000379	1	1	3
-0.000266	1	1	3
-0.000127	1	1	3
-0.000363	1	2	3
-0.000013	1	2	3
-0.000096	1	2	3
-0.000562	1	3	3
-0.000569	1	3	3
-0.000415	1	3	3
-0.000546	1	4	3
-0.000433	1	4	3
-0.000384	1	4	3
-0.000430	2	1	3
-0.000484	2	1	3
-0.000679	2	1	3
-0.000130	2	2	3
0.000047	2	2	3
-0.000245	2	2	3
-0.000632	2	3	3
-0.000805	2	3	3
-0.000848	2	3	3
-0.000332	2	4	3
-0.000273	2	4	3
-0.000413	2	4	3
0.000636	3	1	3
-0.000476	3	1	3

0.000620	3	1	3
0.000048	3	2	3
0.000595	3	2	3
0.000106	3	2	3
0.000322	3	3	3
-0.000894	3	3	3
-0.000434	3	3	3
-0.000264	3	4	3
0.000174	3	4	3
-0.000947	3	4	3
-0.000090	4	1	3
0.003443	4	1	3
-0.000159	4	1	3
-0.002045	4	2	3
0.002006	4	2	3
-0.000380	4	2	3
-0.001155	4	3	3
0.000648	4	3	3
0.000243	4	3	3
-0.003112	4	4	3
-0.000795	4	4	3
0.000024	4	4	3

Dummy coded matrix

General Linear Model: C1 versus Volume, Measurement, Size

Factor	Type	Levels	Values
Volume	fixed	4	1, 2, 3, 4
Measurement	fixed	4	1, 2, 3, 4
Size	fixed	3	1, 2, 3

Analysis of Variance for C1, using Adjusted SS for Tests

Source	DF	Seq SS	Adj SS	Adj MS	F	P
Volume	3	0.0000103	0.0000103	0.0000034	5.80	0.001
Measurement	3	0.0000027	0.0000027	0.0000009	1.54	0.210
Size	2	0.0000306	0.0000306	0.0000153	25.76	0.000
Volume*Measurement	9	0.0000034	0.0000034	0.0000004	0.64	0.757
Volume*Size	6	0.0000032	0.0000032	0.0000005	0.91	0.492
Measurement*Size	6	0.0000024	0.0000024	0.0000004	0.67	0.672
Volume*Measurement*Size	18	0.0000062	0.0000062	0.0000003	0.58	0.907
Error	96	0.0000570	0.0000570	0.0000006		
Total	143	0.0001159				

S = 0.000770537 R-Sq = 50.82% R-Sq(adj) = 26.74%

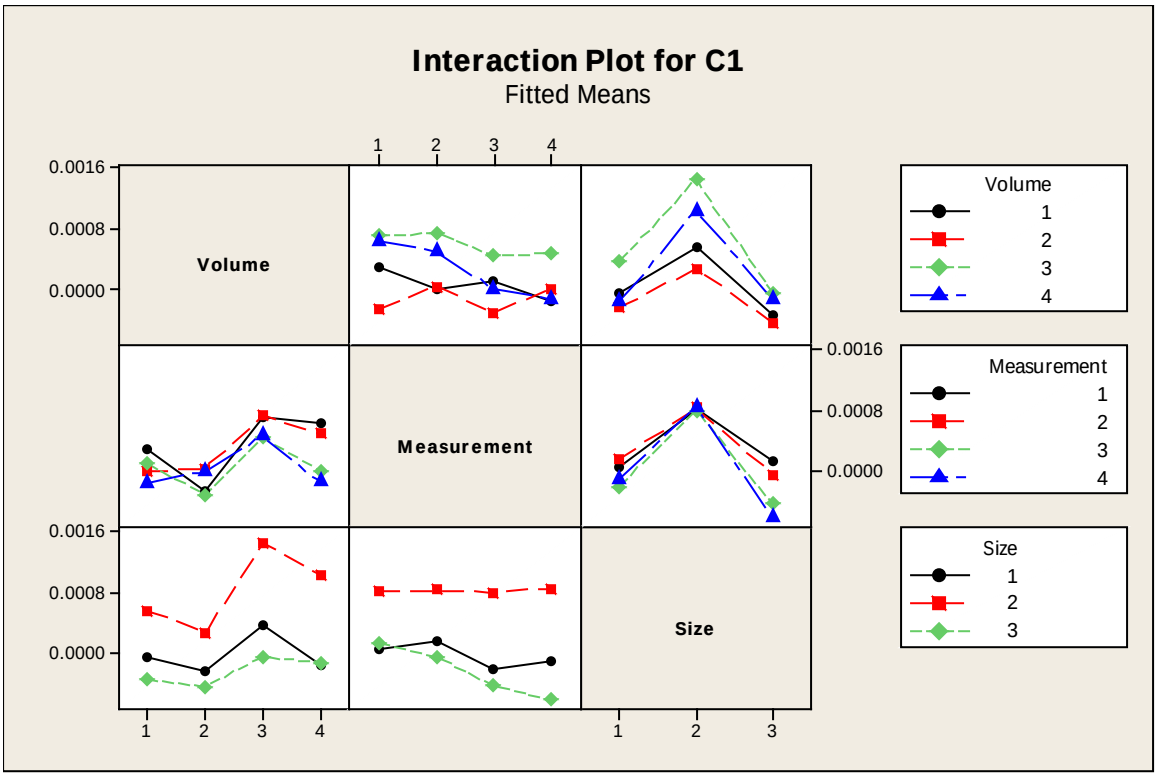

Interactions plot

General Linear Model: C1 versus Volume, Measurement, Size

Factor	Type	Levels	Values
Volume	fixed	4	1, 2, 3, 4
Measurement	fixed	4	1, 2, 3, 4
Size	fixed	3	1, 2, 3

Analysis of Variance for C1, using Adjusted SS for Tests

Source	DF	Seq SS	Adj SS	Adj MS	F	P
Volume	3	0.0000103	0.0000103	0.0000034	6.43	0.000
Measurement	3	0.0000027	0.0000027	0.0000009	1.71	0.169
Size	2	0.0000306	0.0000306	0.0000153	28.57	0.000
Error	135	0.0000723	0.0000723	0.0000005		
Total	143	0.0001159				

S = 0.000731571 R-Sq = 37.66% R-Sq(adj) = 33.97%

Unusual Observations for C1

Obs	C1	Fit	SE Fit	Residual	St Resid	
38	0.002060	0.000193	0.000183	0.001867	2.64	R
39	-0.001579	0.000193	0.000183	-0.001772	-2.50	R
41	0.001960	0.000169	0.000183	0.001791	2.53	R
45	-0.001504	-0.000087	0.000183	-0.001417	-2.00	R
134	0.003443	-0.000025	0.000183	0.003468	4.90	R
136	-0.002045	-0.000049	0.000183	-0.001996	-2.82	R
137	0.002006	-0.000049	0.000183	0.002055	2.90	R
142	-0.003112	-0.000319	0.000183	-0.002793	-3.94	R

R denotes an observation with a large standardized residual.

Least Squares Means for C1

	Mean	SE Mean
Volume		
1	0.000060	0.000122
2	-0.000131	0.000122
3	0.000593	0.000122
4	0.000254	0.000122
Measurement		
1	0.000344	0.000122
2	0.000320	0.000122
3	0.000063	0.000122
4	0.000050	0.000122
Size		
1	-0.000017	0.000106
2	0.000834	0.000106
3	-0.000235	0.000106

Tukey 99.0% Simultaneous Confidence Intervals
Response Variable C1
All Pairwise Comparisons among Levels of Volume
Volume = 1 subtracted from:

Volume	Lower	Center	Upper
2	-0.000738	-0.000191	0.000357
3	-0.000014	0.000534	0.001081
4	-0.000353	0.000195	0.000742

```
Volume  -----+---------+---------+---------+-
2          (--------*--------)
3                    (--------*--------)
4               (--------*--------)
        -----+---------+---------+---------+-
          -0.00060   0.00000   0.00060   0.00120


Volume = 2  subtracted from:

Volume      Lower    Center     Upper  -----+---------+---------+---------+-
3        0.000177  0.000724  0.001272                   (--------*--------)
4       -0.000162  0.000385  0.000933              (--------*---------)
                                       -----+---------+---------+---------+-
                                         -0.00060   0.00000   0.00060   0.00120


Volume = 3  subtracted from:

Volume      Lower     Center     Upper
4       -0.000886  -0.000339  0.000209

Volume  -----+---------+---------+---------+-
4       (--------*--------)
        -----+---------+---------+---------+-
          -0.00060   0.00000   0.00060   0.00120


Tukey Simultaneous Tests
Response Variable C1
All Pairwise Comparisons among Levels of Volume
Volume = 1  subtracted from:

        Difference       SE of           Adjusted
Volume    of Means  Difference  T-Value   P-Value
2        -0.000191    0.000172   -1.105    0.6872
3         0.000534    0.000172    3.096    0.0126
4         0.000195    0.000172    1.130    0.6715


Volume = 2  subtracted from:

        Difference       SE of           Adjusted
Volume    of Means  Difference  T-Value   P-Value
3         0.000724    0.000172    4.200    0.0003
4         0.000385    0.000172    2.235    0.1191


Volume = 3  subtracted from:

        Difference       SE of           Adjusted
Volume    of Means  Difference  T-Value   P-Value
4        -0.000339    0.000172   -1.965    0.2064


Tukey 99.0% Simultaneous Confidence Intervals
Response Variable C1
All Pairwise Comparisons among Levels of Measurement
Measurement = 1  subtracted from:

Measurement      Lower     Center     Upper
2           -0.000571  -0.000024  0.000523
```

```
3            -0.000828  -0.000280  0.000267
4            -0.000841  -0.000294  0.000253

Measurement    -+---------+---------+---------+-----
2                    (-----------*------------)
3              (-------------*-------------)
4              (-------------*------------)
               -+---------+---------+---------+-----
             -0.00080  -0.00040  -0.00000   0.00040


Measurement = 2  subtracted from:

Measurement      Lower     Center     Upper
3            -0.000804  -0.000256  0.000291
4            -0.000817  -0.000270  0.000277

Measurement    -+---------+---------+---------+-----
3               (-------------*------------)
4               (------------*-------------)
               -+---------+---------+---------+-----
             -0.00080  -0.00040  -0.00000   0.00040


Measurement = 3  subtracted from:

Measurement      Lower     Center     Upper
4            -0.000561  -0.000014  0.000534

Measurement    -+---------+---------+---------+-----
4                    (-------------*------------)
               -+---------+---------+---------+-----
             -0.00080  -0.00040  -0.00000   0.00040


Tukey Simultaneous Tests
Response Variable C1
All Pairwise Comparisons among Levels of Measurement
Measurement = 1  subtracted from:

             Difference       SE of           Adjusted
Measurement    of Means  Difference  T-Value   P-Value
2             -0.000024    0.000172   -0.139    0.9990
3             -0.000280    0.000172   -1.626    0.3675
4             -0.000294    0.000172   -1.705    0.3252


Measurement = 2  subtracted from:

             Difference       SE of           Adjusted
Measurement    of Means  Difference  T-Value   P-Value
3             -0.000256    0.000172   -1.487    0.4482
4             -0.000270    0.000172   -1.566    0.4017


Measurement = 3  subtracted from:

             Difference       SE of            Adjusted
Measurement    of Means  Difference   T-Value   P-Value
4             -0.000014    0.000172  -0.07877    0.9998


Tukey 99.0% Simultaneous Confidence Intervals
```

```
Response Variable C1
All Pairwise Comparisons among Levels of Size
Size = 1  subtracted from:

Size      Lower     Center     Upper  ---------+---------+---------+-------
2      0.000408   0.000850  0.001293                          (-----*----)
3     -0.000660  -0.000218  0.000225             (----*-----)
                                     ---------+---------+---------+-------
                                           -0.00080   0.00000   0.00080


Size = 2  subtracted from:

Size      Lower     Center      Upper  ---------+---------+---------+-------
3     -0.001511  -0.001068  -0.000626  (-----*----)
                                      ---------+---------+---------+-------
                                            -0.00080   0.00000   0.00080


Tukey Simultaneous Tests
Response Variable C1
All Pairwise Comparisons among Levels of Size
Size = 1  subtracted from:

      Difference       SE of           Adjusted
Size    of Means  Difference  T-Value   P-Value
2       0.000850    0.000149    5.694    0.0000
3      -0.000218    0.000149   -1.459    0.3139


Size = 2  subtracted from:

      Difference       SE of           Adjusted
Size    of Means  Difference  T-Value   P-Value
3      -0.001068    0.000149   -7.153    0.0000
```

APPENDIX G: ANOVA RESULTS

Rep/Measurement	Size	90mm	120mm	250mm	500mm
R1 M1	**1.000000**	-0.000016	-0.000418	0.000630	-0.001163
R1 M2	**1.000000**	0.000300	-0.000270	0.000510	-0.000646
R1 M3	**1.000000**	-0.000231	-0.000291	-0.000207	-0.001184
R1 M4	**1.000000**	0.000090	-0.000144	-0.000330	-0.000666
R2 M1	**1.000000**	0.000290	-0.000211	-0.000021	0.002060
R2 M2	**1.000000**	-0.000020	0.000120	0.000290	0.001960
R2 M3	**1.000000**	-0.000040	-0.000333	0.000190	0.000830
R2 M4	**1.000000**	-0.000354	-0.000003	0.000500	0.000730
R3 M1	**1.000000**	0.000690	-0.000470	0.001000	-0.001579
R3 M2	**1.000000**	-0.000315	-0.000064	0.000510	-0.000448
R3 M3	**1.000000**	0.000070	-0.000582	0.000950	-0.001504
R3 M4	**1.000000**	-0.000929	-0.000176	0.000460	-0.000369
R1 M1	**2.000000**	0.000640	0.000260	0.001800	-0.000090
R1 M2	**2.000000**	0.000360	0.000510	0.001980	0.000280
R1 M3	**2.000000**	0.000690	0.000450	0.001680	-0.000540
R1 M4	**2.000000**	0.000400	0.000700	0.001860	-0.000180
R2 M1	**2.000000**	0.001150	0.000040	0.001180	0.001630
R2 M2	**2.000000**	0.000040	0.000200	0.001240	0.001790
R2 M3	**2.000000**	0.001150	0.000120	0.001370	0.000850
R2 M4	**2.000000**	0.000550	0.000280	0.001430	0.001010
R3 M1	**2.000000**	0.000590	0.000020	0.001010	0.001740
R3 M2	**2.000000**	0.000070	0.000220	0.001400	0.001960
R3 M3	**2.000000**	0.000820	0.000180	0.001020	0.001920
R3 M4	**2.000000**	0.000300	0.000370	0.001420	0.002140
R1 M1	**0.500000**	-0.000379	-0.000430	0.000636	-0.000090
R1 M2	**0.500000**	-0.000363	-0.000130	0.000048	-0.002045
R1 M3	**0.500000**	-0.000562	-0.000632	0.000322	-0.001155
R1 M4	**0.500000**	-0.000546	-0.000332	-0.000264	-0.003112
R2 M1	**0.500000**	-0.000266	-0.000484	-0.000476	0.003443
R2 M2	**0.500000**	-0.000013	0.000047	0.000595	0.002006
R2 M3	**0.500000**	-0.000569	-0.000805	-0.000894	0.000648
R2 M4	**0.500000**	-0.000433	-0.000273	0.000174	-0.000795
R3 M1	**0.500000**	-0.000127	-0.000679	0.000620	-0.000159
R3 M2	**0.500000**	-0.000096	-0.000245	0.000106	-0.000380
R3 M3	**0.500000**	-0.000415	-0.000848	-0.000434	0.000243
R3 M4	**0.500000**	-0.000384	-0.000413	-0.000947	0.000024

Data arrangement for ANOVA on measurement volume

One-way ANOVA: 90mm, 120mm, 250mm, 500mm (Measurement Volume)

```
Source   DF         SS         MS     F      P
Factor    3  0.0000103  0.0000034  4.56  0.004
Error   140  0.0001056  0.0000008
Total   143  0.0001159

S = 0.0008684   R-Sq = 8.91%   R-Sq(adj) = 6.96%

                                 Individual 99% CIs For Mean Based on
                                 Pooled StDev
Level   N        Mean      StDev  ---+---------+---------+---------+------
90mm   36   0.0000595  0.0004996       (--------*---------)
120mm  36  -0.0001310  0.0003762  (---------*--------)
250mm  36   0.0005933  0.0007688                    (---------*--------)
500mm  36   0.0002544  0.0014263           (--------*---------)
                                 ---+---------+---------+---------+------
                                 -0.00040   0.00000   0.00040   0.00080

Pooled StDev = 0.0008684

Tukey 95% Simultaneous Confidence Intervals
All Pairwise Comparisons

Individual confidence level = 98.97%

90mm subtracted from:

            Lower      Center      Upper
120mm  -0.0007231  -0.0001905  0.0003421
250mm   0.0000012   0.0005338  0.0010664
500mm  -0.0003377   0.0001949  0.0007275

       --------+---------+---------+---------+-
120mm          (------*-------)
250mm                    (-------*------)
500mm               (-------*------)
       --------+---------+---------+---------+-
            -0.00070   0.00000   0.00070   0.00140

120mm subtracted from:

            Lower     Center      Upper
250mm   0.0001917  0.0007243  0.0012569
500mm  -0.0001472  0.0003854  0.0009180

       --------+---------+---------+---------+-
250mm                     (------*-------)
500mm                (-------*------)
       --------+---------+---------+---------+-
            -0.00070   0.00000   0.00070   0.00140

250mm subtracted from:

            Lower      Center      Upper
500mm  -0.0008715  -0.0003389  0.0001938

       --------+---------+---------+---------+-
500mm        (------*-------)
       --------+---------+---------+---------+-
            -0.00070   0.00000   0.00070   0.00140
```

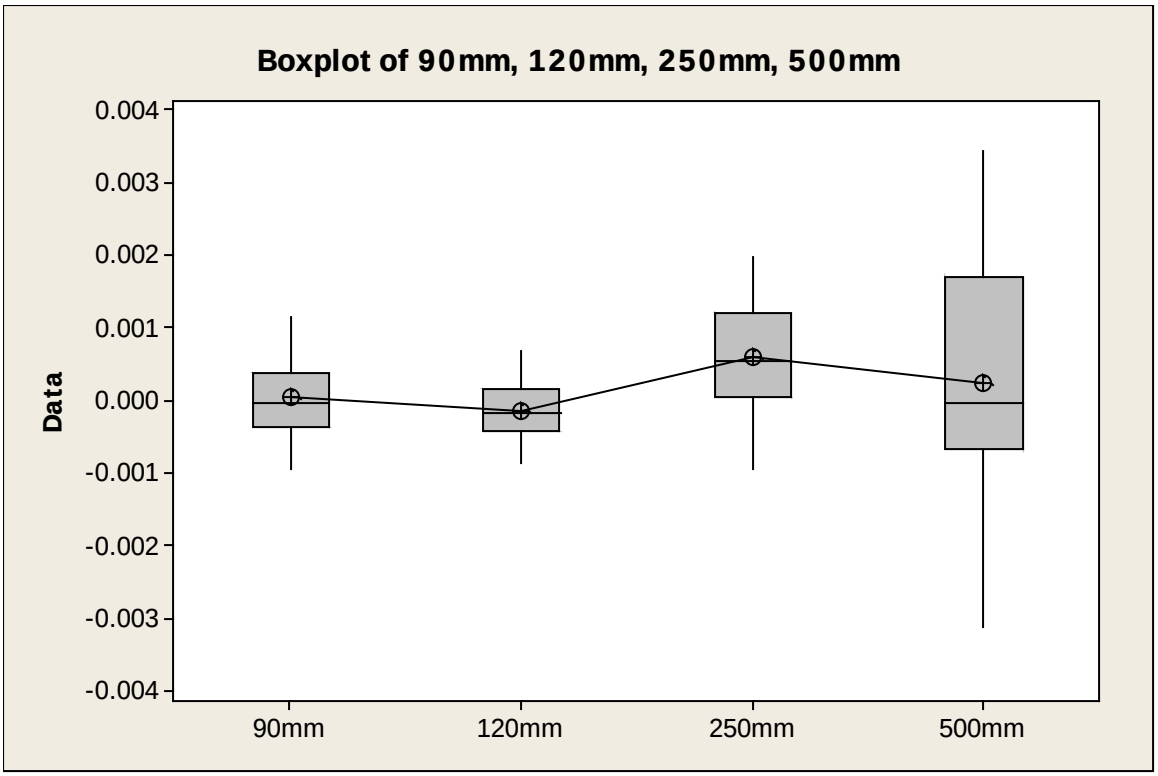

Boxplot for measurement volume

Measurement/rep	Volume	1.000000	2.000000	0.500000
R1 M1	90mm	-0.000016	0.000640	-0.000379
R1 M2	90mm	0.000300	0.000360	-0.000363
R1 M3	90mm	-0.000231	0.000690	-0.000562
R1 M4	90mm	0.000090	0.000400	-0.000546
R2 M1	90mm	0.000290	0.001150	-0.000266
R2 M2	90mm	-0.000020	0.000040	-0.000013
R2 M3	90mm	-0.000040	0.001150	-0.000569
R2 M4	90mm	-0.000354	0.000550	-0.000433
R3 M1	90mm	0.000690	0.000590	-0.000127
R3 M2	90mm	-0.000315	0.000070	-0.000096
R3 M3	90mm	0.000070	0.000820	-0.000415
R3 M4	90mm	-0.000929	0.000300	-0.000384
R1 M1	120mm	-0.000418	0.000260	-0.000430
R1 M2	120mm	-0.000270	0.000510	-0.000130
R1 M3	120mm	-0.000291	0.000450	-0.000632
R1 M4	120mm	-0.000144	0.000700	-0.000332
R2 M1	120mm	-0.000211	0.000040	-0.000484
R2 M2	120mm	0.000120	0.000200	0.000047
R2 M3	120mm	-0.000333	0.000120	-0.000805
R2 M4	120mm	-0.000003	0.000280	-0.000273
R3 M1	120mm	-0.000470	0.000020	-0.000679
R3 M2	120mm	-0.000064	0.000220	-0.000245
R3 M3	120mm	-0.000582	0.000180	-0.000848
R3 M4	120mm	-0.000176	0.000370	-0.000413
R1 M1	250mm	0.000630	0.001800	0.000636
R1 M2	250mm	0.000510	0.001980	0.000048
R1 M3	250mm	-0.000207	0.001680	0.000322
R1 M4	250mm	-0.000330	0.001860	-0.000264
R2 M1	250mm	-0.000021	0.001180	-0.000476
R2 M2	250mm	0.000290	0.001240	0.000595
R2 M3	250mm	0.000190	0.001370	-0.000894
R2 M4	250mm	0.000500	0.001430	0.000174
R3 M1	250mm	0.001000	0.001010	0.000620
R3 M2	250mm	0.000510	0.001400	0.000106
R3 M3	250mm	0.000950	0.001020	-0.000434
R3 M4	250mm	0.000460	0.001420	-0.000947
R1 M1	500mm	-0.001163	-0.000090	-0.000090
R1 M2	500mm	-0.000646	0.000280	-0.002045
R1 M3	500mm	-0.001184	-0.000540	-0.001155
R1 M4	500mm	-0.000666	-0.000180	-0.003112
R2 M1	500mm	0.002060	0.001630	0.003443
R2 M2	500mm	0.001960	0.001790	0.002006
R2 M3	500mm	0.000830	0.000850	0.000648
R2 M4	500mm	0.000730	0.001010	-0.000795
R3 M1	500mm	-0.001579	0.001740	-0.000159
R3 M2	500mm	-0.000448	0.001960	-0.000380
R3 M3	500mm	-0.001504	0.001920	0.000243
R3 M4	500mm	-0.000369	0.002140	0.000024

One-way ANOVA: 1.000000, 2.000000, 0.500000 (Object size)

```
Source   DF         SS         MS      F      P
Factor    2  0.0000306  0.0000153  25.27  0.000
Error   141  0.0000853  0.0000006
Total   143  0.0001159

S = 0.0007779   R-Sq = 26.39%   R-Sq(adj) = 25.34%



Level      N        Mean      StDev
1.000000  48  -0.0000168  0.0007217
2.000000  48   0.0008335  0.0006956
0.500000  48  -0.0002346  0.0009003

          Individual 99% CIs For Mean Based on Pooled StDev
Level       -+---------+---------+---------+--------
1.000000         (-----*-----)
2.000000                       (-----*-----)
0.500000    (-----*-----)
            -+---------+---------+---------+--------
          -0.00050   0.00000   0.00050   0.00100

Pooled StDev = 0.0007779


Tukey 95% Simultaneous Confidence Intervals
All Pairwise Comparisons

Individual confidence level = 98.08%


1.000000 subtracted from:

               Lower      Center      Upper
2.000000   0.0004742   0.0008503  0.0012264
0.500000  -0.0005940  -0.0002179  0.0001582

          --------+---------+---------+---------+-
2.000000                       (----*---)
0.500000            (---*----)
          --------+---------+---------+---------+-
               -0.00080   0.00000   0.00080   0.00160


2.000000 subtracted from:

               Lower      Center       Upper
0.500000  -0.0014443  -0.0010682  -0.0006921

          --------+---------+---------+---------+-
0.500000  (----*---)
          --------+---------+---------+---------+-
               -0.00080   0.00000   0.00080   0.00160
```

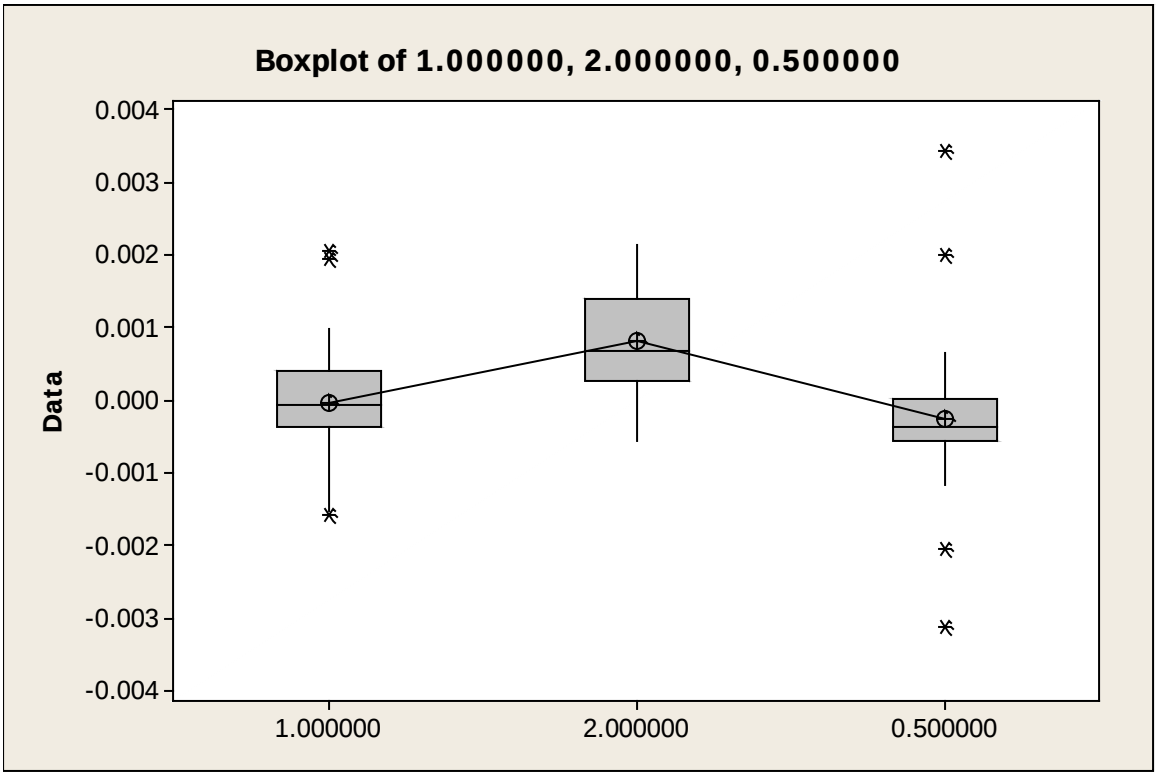

Boxplot for object size.